OPTIMAL DESIGN OF A KINESTHETIC HAPTIC DEVICE MECHANISM FOR ENHANCING ITS IMPEDANCE CHARACTERISTICS

A Thesis Submitted to
the Graduate School of Engineering and Sciences of
İzmir Institute of Technology
in Partial Fulfillment of the Requirements for the Degree of

MASTER OF SCIENCE

in Mechanical Engineering

by
İbrahimcan GÖRGÜLÜ

July 2018
İZMİR

We approve the thesis of **İbrahimcan GÖRGÜLÜ**

Examining Committee Members:

_____

Assoc. Prof. Dr. Mehmet İsmet Can DEDE
Department of Mechanical Engineering
İzmir Institute of Technology

_____

Prof. Dr. Serhan ÖZDEMİR
Department of Mechanical Engineering
İzmir Institute of Technology

_____

Assist. Prof. Dr. Fatih Cemal CAN
Department of Mechatronics Engineering
İzmir Kâtip Çelebi University

9 July 2018

_____

Assoc. Prof. Dr. Mehmet İsmet Can DEDE
Supervisor,
Department of
Mechanical Engineering
İzmir Institute of Technology

_____

Assoc. Prof. Dr. Gökhan KİPER
Co-supervisor,
Department of
Mechanical Engineering
İzmir Institute of Technology

_____

Prof. Dr. Metin TANOĞLU
Head of the Department of
Mechanical Engineering

_____

Prof. Dr. Aysun SOFUOĞLU
Dean of the Graduate School of
Engineering and Sciences

ACKNOWLEDGMENTS

I want to thank my mother and siblings for their patience and understanding when I was unable to spare time for them due to my long period of studies.

I owe a debt of gratitude to my supervisors Dr. Mehmet İsmet Can DEDE and Dr. Gökhan KİPER for their patience, guidance, and support throughout this thesis study and for their confidence in me.

I would like to sincerely thank my colleagues in IZTECH Robotics Lab. for their support and friendship, Barış TANER, Emre UZUNOĞLU, Çağhan KİRİŞÇİ, Osman Nuri ŞAHİN, Emir MOBEDİ, Gizem ATEŞ, Oğulcan IŞITMAN, Orhan AYİT, Görkem KARABULUT, and Furkan KÜÇÜKOĞLU. I also would like to thanks my friends, Özgün KÖSE, Erdi SAYAR, and Hüseyin DİNÇ for giving me moral support and encouraging me to advance.

This thesis is a milestone of my scientific journey.

ABSTRACT

OPTIMAL DESIGN OF A KINESTHETIC HAPTIC DEVICE MECHANISM FOR ENHANCING ITS IMPEDANCE CHARACTERISTICS

In this work, the optimal design of modified version of 3 degrees of freedom R-CUBE mechanism has been studied in order to develop a high-performance haptic device mechanism. A high-performance haptic mechanism is achieved by having high transparency and high-frequency range. These two properties are determined by the mechanical impedance of the mechanism. Hence, to increase the quality of a haptic mechanism, its mechanical impedance performance must be enhanced. This refers to have low inertia, low friction, high back-drivability, high force output, high structural stiffness, and high manipulability for the mechanism. All these properties are designated by kinematic, stiffness, and dynamic properties of the mechanism. Hence, as a first step of this thesis, kinematic, stiffness and dynamic models of the mechanism are analytically procured. The analytical model of stiffness is achieved via the virtual joint method. Then, in order to obtain the objective function for the design procedure, performance metrics affecting the above-mentioned properties are reviewed and produced. Since these metrics have common parameters such as link lengths and the cross-section area of the links, there is a highly non-linear and contradictory relationship between the metrics. In order to deal with the non-linearity and to determine the global optimum design, an evolutionary optimization method, genetic algorithm, is preferred. The optimization time is reduced by investigating the most critical poses of the workspace and reducing the performance metrics to simpler forms. The link lengths and the cross-section areas are optimized. Carbon fiber tubes are used as links. The Pareto-front solution set is obtained as a result of the optimization procedure.Finally, an optimal solution is proposed and evaluated for the design of this modified R-CUBE mechanism to be used in haptic applications.

ÖZET

EMPEDANS KARAKTERİSTİKLERİNİN İYİLEŞTİRİLMESİ İÇİN OPTİMAL KİNESTETİK HAPTİK CİHAZ TASARIMI

Bu çalışmada, yüksek performanslı bir haptik cihaz mekanizması geliştirmek için 3 serbestlik dereceli R-CUBE mekanizmasının yeni bir sürümünün en-iyilenmiş tasarımı incelenmiştir. Yüksek performanslı bir haptik mekanizması, yüksek geçirgenlik ve yüksek frekans aralığı ile sağlanabilir. Bu iki özellik mekanizmanın mekanik empedansı ile belirlenir. Bu nedenle, bir haptik mekanizmanın kalitesini artırmak için mekanik empedans performansı artırılmalıdır. Bu, düşük eylemsizliğe, düşük sürtünmeye, yüksek geri-sürülebilirliğe, yüksek kuvvet çıkışına, yüksek yapısal direngenliğe ve mekanizma için yüksek manipüle edilebilirliğe sahip olmak demektir. Bütün bu özellikler, mekanizmanın kinematik, direngenlik ve dinamik özellikleri ile belirlenir. Bu nedenle bu tezin ilk adımı olarak, mekanizmanın kinematik, direngenlik ve dinamik modelleri analitik olarak elde edildi. Analitik direngenlik modeli, sanal mafsal yöntemi ile elde edildi. Daha sonra, tasarım prosedürü için amaç fonksiyonunu elde etmek amacıyla, yukarıda bahsedilen özellikleri etkileyen performans ölçütleri gözden geçirildi ve oluşturuldu. Uzuv boyutları ve uzuvların kesit alanı gibi ortak parametrelere sahip olduklarından, bu metrikler arasında son derece doğrusal olmayan ve çelişkili bir ilişki vardır. Doğrusal olmayan sorunla baş edebilmek ve genel en-iyilenmiş tasarımı belirleyebilmek için, evrimsel bir en iyileştirme yöntemi olan genetik algoritma tercih edildi. Çalışma alanının en kritik pozlarının incelenmesi ve performans metriklerinin daha basit şekle indirgenmesiyle en-iyileştirme süresi azaltıldı. Uzuv boyutları ve kesit alanları en-iyileştirildi. Uzuv olarak karbon fiber tüpler kullanıldı. Pareto çözüm seti, en iyileştirme sürecinin bir sonucu olarak elde edildi. Son olarak, haptik uygulamalarda kullanılacak olan yeni R-CUBE mekanizması için en-iyilenmiş çözüm belirlendi ve değerlendirildi.

This thesis is dedicated to my mother Hatice Görgülü who have always supported and encouraged me during the challenges of my studies.

TABLE OF CONTENTS

LIST OF FIGURES

LIST OF TABLES

CHAPTER 1

INTRODUCTION

A human-being has five type of sensations to perceive the environment. These are vision, hearing, smell, taste, and touch. By the help of any of these senses or the combination of them human interacts with the objects in its environment and perceives the surroundings by making use of information received from the sensory organs and neurons. Photo-receptor cell sensory neurons generate electrical information of light for vision. Olfactory sensory neurons identify the smell of the tiny molecules and transmit the data to the brain through the neurons. Taste receptors recognize the molecules which interact with the saliva in the oral cavity. Sound waves travel through the surrounding material untill they reach the ear and vibrates the auditory receptors through the tiny bones in ears. Lastly, physical interactions with the environment which generates mechanical stimuli are captured by the mechanoreceptors located in the skin.

Among the whole senses, the sensation of touch is the most deductive sense to analyze the reality and differs due to its physical feedback from the environment. While the vision and smell collect most of the data about the objects in the environment, without the sense of touch, the objects have no difference than a virtual image in the brain. In order to survive and advance, the human-being has to interact with the environment and the full grasp of it is vital to achieving the objectives. Shape, texture, temperature, and weight are the physical properties which are needed to obtain the full grasp of nature. Only then, the human can comprehend and control the objects in the surrounding. Handmade items, painting on a canvas or sculptures are some examples which require the sense of touch to craft (Kern, 2009).

The sense of touch is constructed upon two types of sensors. Tactile (or the cutaneous) and kinesthetic sensors. Tactile sensors are located in the skin to sense the skin interactions like texture, temperature, pain, pressure etc. Kinesthetic sensors, on the other hand, are located in muscles, tendons, and joints. They are developed to sense the force and torque acting on the body and the location of the limbs. While the tactile interaction is sensitive to tiny details of the touched object, kinesthetic interaction is a rough interaction compared to tactile interaction. A blind person uses his tactile sensors to read the braille alphabet. A surgeon, in other respects, manipulates his muscles by making use of the feedback information taken from the kinesthetic sensors during surgery.

1.1. Haptic Interaction

Scientist are always amazed by the human sensory system and wanted to duplicate them. They have developed cameras, microphones and sensors which are sensitive to pressure, force, and torque in order to digitize and analyze the natural information. Later, they started to imitate the nature with the analyzed data. They have composed the digital data to recreate the sensed natural information by using the monitors and speakers for vision and sound. Yet, the recreation of the forces and torques was problematic due to the complexity of the data. With the advances in robotics, the difficulties to generate the force/torque information are overcome gradually but steadily. They have constructed devices to imitate the force and torque and named these devices as haptic devices.

Haptic is a term which is derived from the Greek word "haptios" which has the meaning of touch. With that respect, a haptic device is a device which generates the touch sensation in order to reflect it to the user. These the devices receives the digital touch information from the computer and converts it into the physical stimuli. The process is a haptic interaction process. A flowchart for haptic interaction is shown in Figure 1.1.
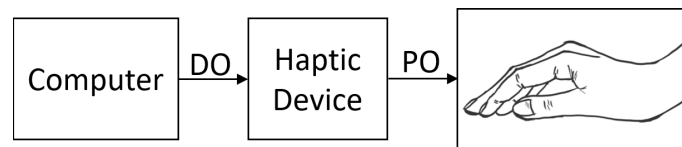
Figure 1.1. Active haptic interaction flow chart. DO: Digital Output, PO: Physical Output.

As shown, an active haptic interaction requires the existence of a computer, a haptic device, and a user. As presented in the Figure, haptic interaction system can be divided into human haptics, computer haptics, and machine haptics (El Saddik, 2007). Human haptics studies on the perception of the human of the touch sensation. Computer haptics refers to the generation of haptic information such as force, motion, vibration etc. Machine haptics refers to mechanical haptic devices which are the interfaces connects the human and the computer.

There are also passive haptic interactions to get feedback from the environment. For instance, little bumps on the 'J' and 'F' keys of a keyboard enable the user to position his/her index finger with passive haptic interaction as in the braille alphabet. However, this kind of interactions is beyond the scope of this thesis.

1.2. Haptic Applications

Users need the haptic devices to enhance the perception of realism in teleoperation of virtual reality interactions. Hence, they may have better experience and control over the applications. From entertainment to medical applications, haptic devices have a wide range of application. Although for some fields, haptic feedback is an additional feature like the vibrators in joysticks of game consoles, it is a necessity for dangerous operations where human risks his life. Training simulators for surgeons on a virtual patient without risking a real patient's health, radioactive material disposal by using teleoperated robots, and controlling the unmanned vehicles in a battlefield are some examples where haptics feedback is needed for an accurate control. Depending on the application type, a haptic interaction can be divided into virtual reality application, teleoperation application, and cooperative applications.

Virtual reality applications are mainly oriented around entertainment and education. Holding and throwing a virtual ball, shooting with guns to virtual targets, and wheeling a race car in a video game are some examples where haptic feedback is used. For the education field, flight simulators and training of dentistry tools are typical examples.

Teleoperation applications are also referred to as telepresence since human interacts with the remote environment via robots. In order to control the slave robots, haptic master interfaces are used. Manipulating a robot arm in a space station from the surface, doing surgery on a patient from a different location, and controlling the bomb defusion robot over a distance are some teleoperation scenarios which require haptic interaction.

A cooperative application is an assistive application to the operator. Exoskeletons help the user to lift heavy weights which are normally impossible to lift. Laparoscope attached to haptic interface prevents the surgeon to approach vital organs and tissues during the surgery. Arm rehabilitation robots with haptic interfaces either helps to move the limbs of the patient for physiotherapy to reteach to move them or generates resistive force to enhance the muscle performance.

1.3. Classification of Haptic Devices

Haptic devices can be divided into groups according to their control type, interaction type, structure type. Hence, while defining the type of a haptic device, each group is stated.

First grouping can be done according to the type of haptic interaction. Similar to the sense of touch, haptic devices can also be divided into two groups as tactile and kinesthetic haptic devices. Obviously, tactile type of haptic devices interacts with skin to generate the stimuli for the user. Kinesthetic devices generate force/torque for the muscle of the user. Tactile haptic devices are generally small and operate at high frequencies. Vibrators and pin arrays are some examples of the tactile type haptic devices. Kinesthetic haptic devices are low-frequency devices with large footprints. These devices are mostly used as manipulators for motion and force generation. Some examples of tactile and kinesthetic haptic devices are given in Figure 1.2.
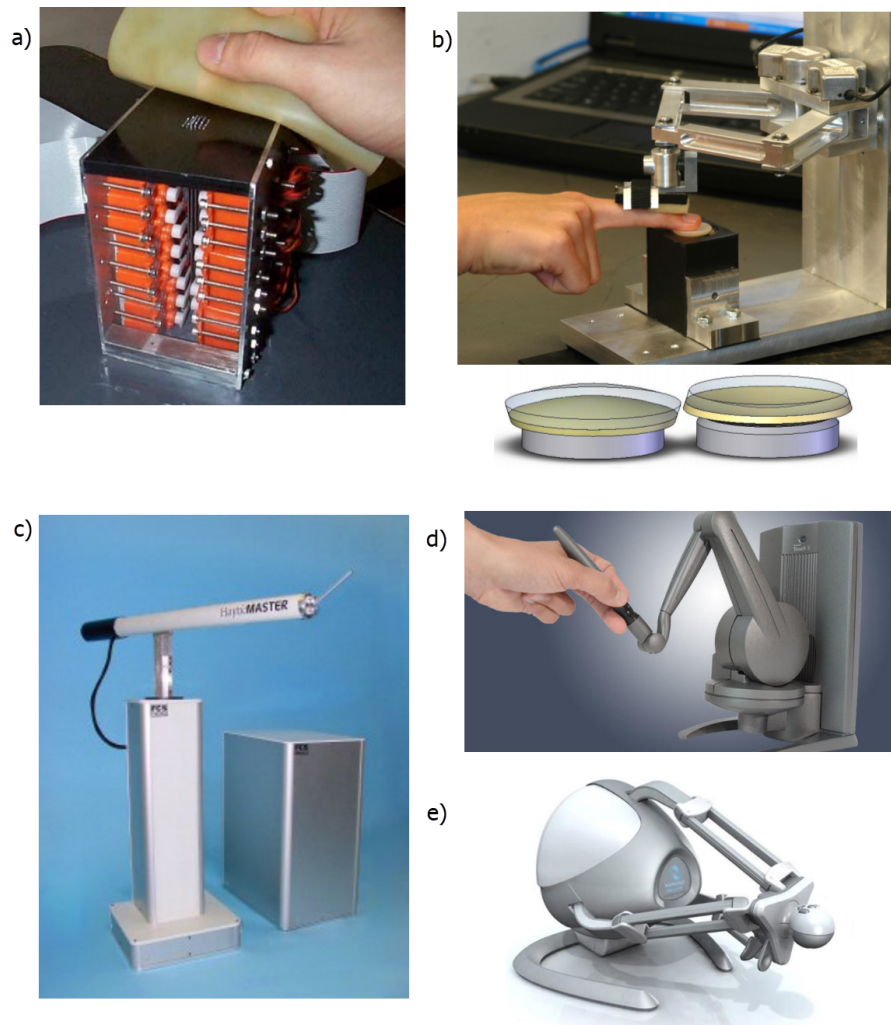
Figure 1.2. Tactile devices: a)Tactile pin array (Source: Wagner et al. (2002)). b)T-Pad tactile texture (Source: Winfield et al. (2007)). Kinesthetic devices: c)Haptic master 3DoF force reflecting haptic device (Source: Lab (2018)). d)6 DoF force reflecting haptic device (Source: 3D SYSTEMS (2018)). e)3 DoF force reflection (Source: Novint (2011)).

Haptic devices are also grouped as the ground-based and the body-fixed devices. Ground-based devices are fixed to the ground and mostly used as master devices for tele-operation and virtual interaction. Body fixed devices such as exoskeletons have high mobility and generally used for assistive operations like lifting weights. Figure 1.3 gives haptic device examples.
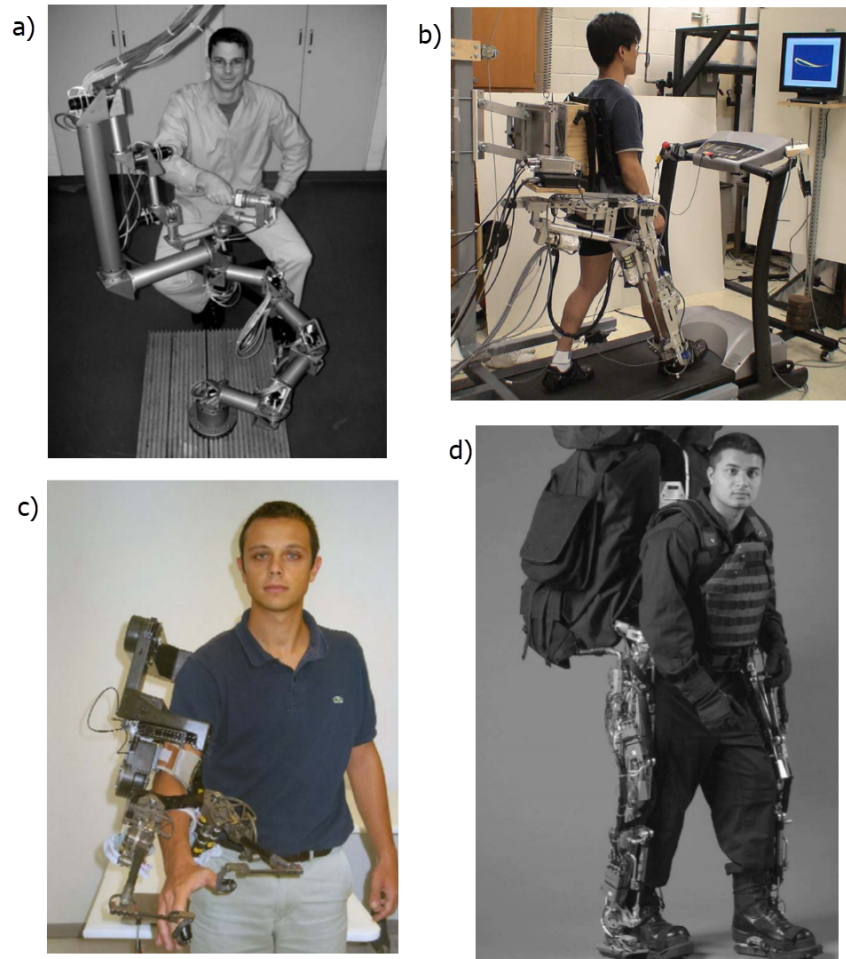
Figure 1.3. Ground-based devices: a)Hyper-redundant haptic interface (Source: Ueberle et al. (2004)). b)Leg exoskeleton ALEX (Source: Banala et al. (2009)). c)Arm exoskeleton (Source: Frisoli et al. (2005)). Body-fixed device: d)Lower extremity exoskeleton (BLEEX) (Source: Zoss et al. (2006)).

The input/output type of the haptic devices designates if the device is an impedance or admittance type of device. Impedance type of haptic devices measures the motion input from the user and exerts force/torque to the user. In admittance type, force/torque inputs are measured and the motion control is achieved. Due to the difference in input and output types, the transmission system of the devices differs. Direct drive or low trans-

mission ratio is used in impedance type haptic devices while in admittance type devices, high reduction between the actuator and linkages of the mechanism can be used. Since the impedance type of haptic devices has low reduction ratio, back-drivability is high and inertia has to be low. Two examples are shown in Figure 1.4.
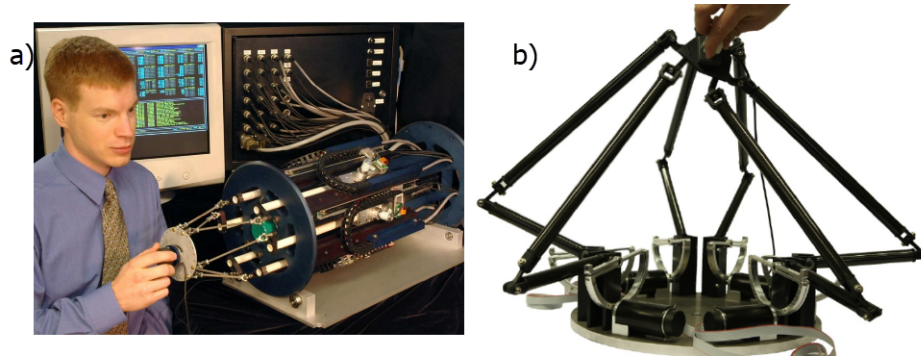
Figure 1.4. a) Admitance type Cobotic hand controller (Source: Faulring et al. (2006)). b)Impedance type 6DoF haptic interface (Source: Ergin and Peer (2013)).

In terms of control methodology, haptic devices might be open or closed loop haptic devices. The closed-loop control type haptic devices have a sensor to measure the desired output. The closed-loop sensor might be force/torque sensor for an impedance type or encoder for an admittance type for position sensing. Open-loop control type has no sensor to measure the output but may have a sensor for input by the user. The type of the sensor is determined by the type of the input/output. Open and closed-loop control block diagram with admittance and impedance type of haptic devices are shown in Figure 1.5.

Due to the variety of the classifications, a haptic device is described by stating each of the classes. For instance, Novint (2011) in Figure 1.2 is a kinesthetic, ground-based, impedance type haptic device with open-loop control. The classification gives detailed information of the type of haptic device to deduce the general properties of it.

1.4. Performance of Haptic Devices

Day by day, the need for research on haptic devices increases. The need is not only for a better experience on the application but also to have better control on it. However, due to the variety of the application areas and the type of haptic interactions, there are

6
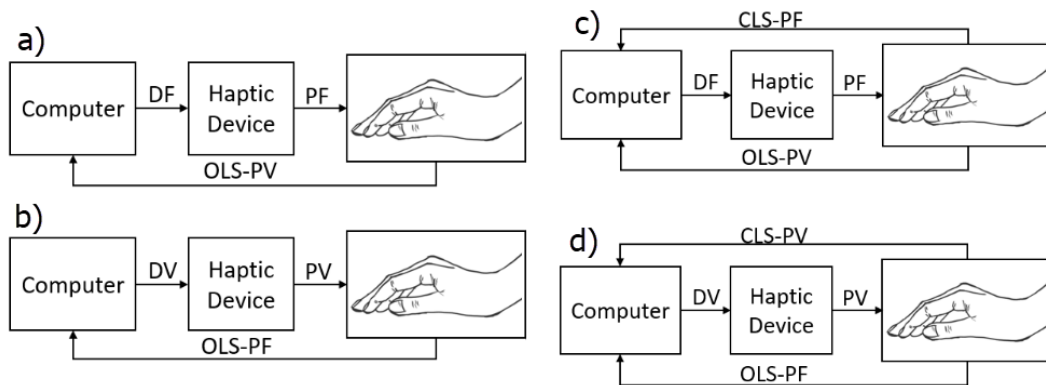
Figure 1.5. Haptic control types: a)Impedance Type Open-Loop System (OLS). b)Admittance Type OLS. c)Impedance Type CLS. d)Admittance Type Closed-Loop System (CLS). Digital Velocity (DV), Digital Force (DF), Physical Velocity (PV), Physical Force (PF)

various haptic devices which highly differ from each other. The reason is that the type of haptic application designates the limitations of the haptic device.

The quality of the haptic interaction depends on the information flow between the computer and the human during their cooperative action. Information flow quality and its rate of flow is mainly determined by the sub-parts of the haptic device. Haptic devices are composed by electrical-electronic, electro-mechanical, and mechanical components. Electrical-electronic components are the integrated circuits, and microprocessors. This is where the control algorithm is run. Electro-mechanical parts are the actuator or semi-actuators and sensors and they convert the electrical information to physical information and physical to electrical. The mechanical part contains the joints and links which compose the mechanism. This part enables the connection between the human and the electro-mechanic parts. Although the mechanical part is the last ring on the haptic device chain, is also the most important part since the impedance and the frequency ranges (which are the two main performance metrics) are mainly determined in the mechanical part. Hence, this thesis focuses on the performance of the mechanical part.

Since the haptic devices have mechanical components, they obey to physical laws of nature. Their compliance, dynamics, and maximum operating range depending on the dimensions and the number of the parts used to construct the haptic device. For instance, admittance type devices have high transmission ratio which makes them more rigid compared to impedance type. However, rigidity comes with a cost in low dynamic performance. As another example, open loop control has a sensorless design compared to

closed-loop control which makes it cheaper and simple. Yet, the sensorless design brings lack of accuracy in force. Figure 1.6 shows the relation between admittance/impedance and open/closed loop control.
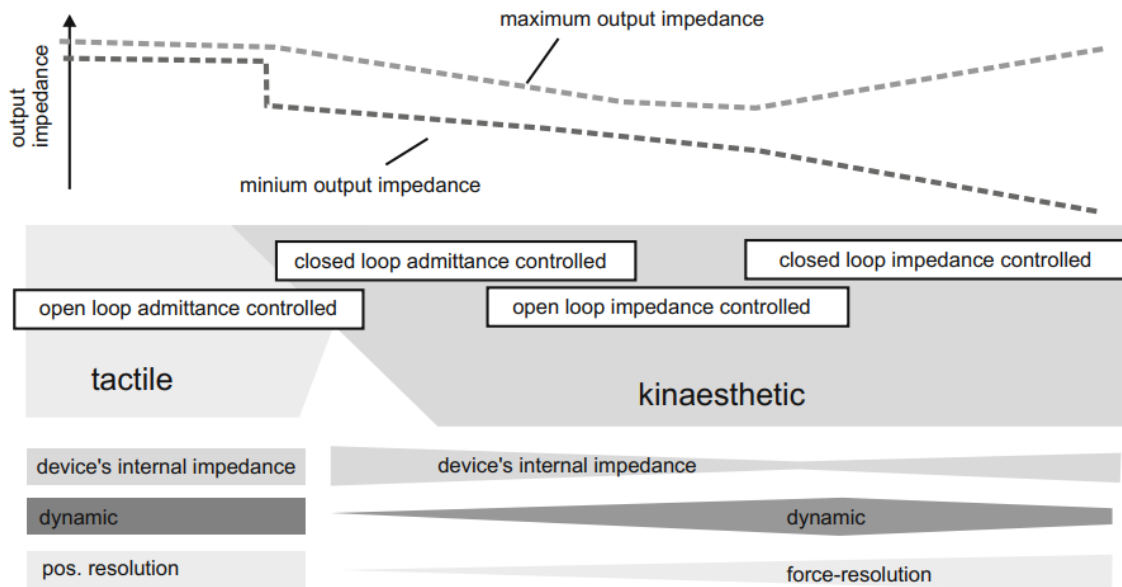
Figure 1.6. Comparison of haptic device characteristics with respect to control types.
(Source: Kern 2009)

The tactile type devices are generally admittance type devices. Their sizes are small compared to kinesthetic ones. They also have small workspaces but they have good positioning resolution. Due to the small amount of inertia, they have very good dynamic properties. Yet, they are not back-drivable and have a high internal impedance which causes high resistance to input motion. The variety between their maximum and minimum output impedance (also can be referred as force capability) is small which shows that they have a precise mathematical model and easy to control. Therefore, even open loop control can be successfully used for tactile type haptic devices.

Kinesthetic type devices, on the other hand, greatly differs from the tactile ones in terms of mechanical properties. They can be either admittance or impedance type. Admittance type has high internal impedance. Due to their rigid structure, they lack dynamic performance in high-frequency motion. It is not easy to back-drive them without damaging the device. Hence, a closed loop control is needed where a force sensor is attached to the device. In impedance type of devices, internal impedance of the device (mechanical impedance of the manipulator) reduces dynamic range and force resolution increases. With the good model knowledge of the device, open control loop may be used. The re-

duction in internal impedance, however, also reduces possible maximum force output. Increasing the internal impedance makes the mechanism closer to admittance but helps to increase the force range. The effect of increased internal impedance can be compensated via a closed loop control.

Another performance criterion for a haptic device is the transparency which is the ratio of the desired and the real impedance. If the ratio is 1 then the desired impedance is accurately reflected to the user. Hence, all the design studies of haptic devices aim to have the transparency ratio close to 1. Assuming that the device has sufficient electrical-electronic and electro-mechanical parts, the transparency ratio can be made closer to 1 if the device has the following properties;

- Sufficient number of degree of freedom
- Sufficient size of the workspace
- High dexterity and manipulability
- Isotropic workspace
- Low inertia
- Low friction
- Back-drivability (low minimum impedance)
- High force output (high maximum impedance)
- High structural stiffness
- High positioning resolution
- Low backlash or zero backlash
- Singularity-free workspace
- High acceleration capability
- High-frequency range

Yet, some of these properties contradict with each other such as low inertia prevents high structural stiffness.

1.5. Thesis Objective and Motivation

It has already stated that the design and the performance of haptic devices depend on the requirements of the haptic application. An ideal haptic device has high-performance which enables it to cover all frequency ranges with infinite impedance capability. Yet, increase in the frequency range (better dynamics) causes loss in impedance performance (maximum-minimum force) which is briefly explained in Section 1.4. Hence,

a single haptic device cannot satisfy all requirements of an application. A high performance haptic device design, thus, is a challenging process which result in comparing and optimizing the aforementioned properties due to the needs.

The challenge can be explained by a single degree of freedom manipulator with a single link and a rotary actuator. In order to have a high workspace, the length of the link must be increased. Increased link length, however, decreases the resolution of positioning and force. On the other hand, long links are flexible with the forces applied on them. Hence, such a link will cause a loss in transparency. Increasing the cross section area of the link makes it stiffer. Yet, this also increases the inertia of the link which decreases the frequency range and increases the minimum impedance. Hence, the design problem is an optimization problem due to the contradictive relationships between design parameters.

The motivation of this thesis is to investigate all the performance metrics of kinematics, dynamics, and stiffness and propose an objective function to enhance the mechanical impedance characteristics of the manipulator. There are several studies on optimization of haptic device manipulators. Yet, most of them do not consider all of the performance metrics simultaneously. The current literature is mainly oriented around kinematic optimization without considering the stiffness and dynamics (Vulliez and Zeghloul, 2016; Lambert and Herder, 2015; Li et al., 2012; Lopes et al., 2012). Even in the papers which includes the stiffness performance metrics, they do not evaluate the dynamics of the device (Ahmad et al., 2014; Gao et al., 2010). There are few studies which consider all performance metric simultaneously (Zhao et al., 2011; Gosselin et al., 2005). Therefore, the thesis is devoted to the design of a haptic device manipulator considering all performance metrics.

As a case study, the main aim of the selected design is to produce a general purpose desktop type haptic device. Hence, the ergonomy, footprint and long period of usage are considered during the design process.

Due to the nonlinear relationship between the performance metrics, evolutionary optimization algorithms are used. The adopted methods are multi-objective genetic algorithm solution algorithm in MATLAB. The previous works in the literature mainly uses single objective function and gives weight to each performance metric (Ahmad et al., 2014; López M. et al., 2012; Kang et al., 2012). Here, the Pareto-front solution set is obtained by the multi-objective genetic algorithm.

In the literature, the general tendency is to use a parallel manipulator as haptic manipulators. In this study, a simplified version of R-CUBE parallel mechanism is used as the case study for optimal design as a haptic manipulator. The reasons to choose the

R-CUBE mechanism, (1) it has already been as haptic manipulator by Bilgincan et al. (2010) and named HIPHAD (HIgh Precision HAptic Device) and (2) it has decoupled motion capability unlike the general parallel mechanisms used in literature which provides design flexibility for working on each serial chain independently.

Carbon fiber links are preferred for link construction since it is a lightweight material and has relatively better mechanical properties which results in high strength to weight ratio. Another benefit of using composite material is to obtain an extra design parameter which is the orientation of the plies of the composite material. According to the conducted literature survey, there is no contribution on the modeling of the stiffness of the manipulator by using composite material and implementing it into the design problem for parallel manipulators.

The objective of the thesis is to optimize the design of R-CUBE parallel mechanism which has 3 translational degrees of freedom according to the following criteria:

1. Having dexterous, singularity free and isotropic workspace with the size of $(120 \times 120 \times 120)$ mm^3.
2. Low inertia and high back-drivability to minimize the minimum impedance.
3. High structural stiffness to maximize the maximum impedance.
4. High positioning resolution for equal force distribution throughout the workspace.
5. High-frequency range to reflect various haptic sensations to the user.
6. Ergonomic design for long period of usage.

1.6. Main Contributions

1. A systematic procedure is proposed in designing a haptic device manipulator.
2. The stiffness model is enhanced to be more accurate and computationally efficient compared the previous version of the R-CUBE (Taner and Dede, 2017).
3. R-CUBE mechanism is modified and simplified. This also speeds up the computation of stiffness matrix in real-time control.
4. In addition to external wrenches applied by the user is included in the stiffness model.
5. It is shown that stiffness and dynamic performance metrics can be simplified to reduce the computation time of optimization algorithms.
6. A compact haptic device manipulator is designed as a case study for the optimization algorithms worked out in this thesis.

1.7. Thesis Outline

This thesis comprises 8 chapters. In Chapter 2, design parameters are investigated that affect the performance of a haptic device. Chapter 3 literature survey is conducted to comprehend which design domains are used in the design and how they are used. Chapter 4 is written to present the mathematical representations of performance metrics and to highlight the physical meaning of implementing the design procedure. Chapter 5 describes the detailed modeling of kinematic, stiffness and dynamic models of the manipulator. In Chapter 6, performance metrics are obtained using the designated models in Chapter 5 and the objective function is constructed. In Chapter 7, results of the optimization are exhibited. In Chapter 8, conclusions are given, outcomes of the thesis are discussed, and future works are addressed.

CHAPTER 2

DESIGN DOMAINS OF A HAPTIC MANIPULATOR

A kinesthetic haptic device is an interface which acquires the pose of the human's related body part and reflects force information to the user in order to interact with a VR simulation or manipulate a remote device in case of a teleoperation scenario. This interaction occurs with a force/motion exchange between the user and haptic interface. The quality of this interaction determines the quality of perception of realism. This quality can be maximized by a well-designed haptic interface. Yet, the perception cannot be a design parameter to evaluate the haptic interface since the sensation of perception changes from person to person (Samur, 2012).

Instead, the force/torque fidelity of the haptic interface is more appropriate as the performance metric. Moreover, the fidelity of haptic interface has the major effect on the quality of overall haptic interaction compared to personal perception. The fidelity for a robot manipulator can be its positioning and velocity performance since those are the desired outputs. In this sense, the fidelity of a haptic interface is the accuracy of force reflection which is its desired output. The performance metric of the fidelity, which compares the actual output forces and desired output forces, is called transparency. The transparency indicates the percentage of the reflection of the desired forces by the computer to the user.

The transparency is affected by a number of design parameters (i.e. information transmission rate, resolution, mass, and stiffness). Some of these parameters are related with each other. Changing one parameter yields an impact on the other parameters. For instance, high stiffness is desired for high force rendering but increased stiffness generally results in high inertia which is undesired. Thus, all design parameters should be considered and adjusted simultaneously during the design procedure. A high-quality haptic interface generally is a resultant of well-optimized design parameters.

In this section, the performance metrics of a haptic interface are presented leading to the definition of the design parameters which affect the performance. It is necessary to know what the performance metrics are in order to define design parameters.

2.1. Haptic Device Performance Metrics

Although there are many haptic interfaces developed up to now, there is not a single categorization method. A categorization can be made based on their haptic interaction types, manipulator types, actuation types, control types and so on. Because of this fact, the evaluation methods are specific to that haptic interface. In this regard, a comparison between haptic interfaces is not straightforward and should be reduced to common evaluation terms (Samur, 2012).

For many systems, the evaluation has been done depending on relation of their outputs and inputs. For haptic interfaces, the comparison should be done according to their inputs given to the system by the user and outputs. This relationship between force and motion is a dynamic relationship and it is related to the so-called 'impedance'. The impedance simply implies the resistance of the system to the motion. This dynamic relationship is represented as;

$$Z(\omega) = \frac{F(\omega)}{v(\omega)} \tag{2.1}$$

where Z is the impedance, F is the force output, v is the measured speed, and ω is the frequency of the motion and torque for an impedance-type device. The impedance-type haptic interface exhibits a reaction force to a measured speed at its end-effector.

Although the impedance reflects the performance of a haptic interface, it does not answer the question of how well the desired force is reflected. Because in the end, haptic interface is a force-reflecting device, thus, it should be evaluated according to force reflection performance and this performance is not independent of impedance. This force reflection performance is called 'transparency' and shown as;

$$T = \frac{Z_{out}(\omega)}{Z_{in}(\omega)} \tag{2.2}$$

where Z_{out} is the actual impedance output and Z_{in} is the desired impedance input to the haptic interface. For a perfectly transparent haptic interface, any desired impedance input can be simulated by the haptic interface and 100% transparency or T=1 is the desired performance criterion for a haptic device. However, in reality, perfect transparency cannot be achieved.

In reality, there are numerous ways of physical interactions between human and his/her environment. For instance, while interacting with a wall, high forces with respect to small displacements are felt whereas squeezing a softball requires lower force for interaction. The diversity in these interactions calls for a wider impedance range to be

displayed by the haptic device. A wide impedance range for haptic interfaces is desired to render the wide dynamic ranges of physical interactions. The impedance range concept is called "Z-Width" introduced by Colgate and Brown (1994) which is presented in Equation 2.3 and shown in Figure 2.1. Z-width should be as wide as possible for the haptic interface to correctly render the large variations of impedance. Increasing the Z-Width is not easy and requires an optimal design in terms of mechanics, electro-mechanics, and control. To increase the Z-Width the factors affecting the Z-Width must be clearly understood.

$$Z_{width} = Z_{max} - Z_{min} \qquad (2.3)$$
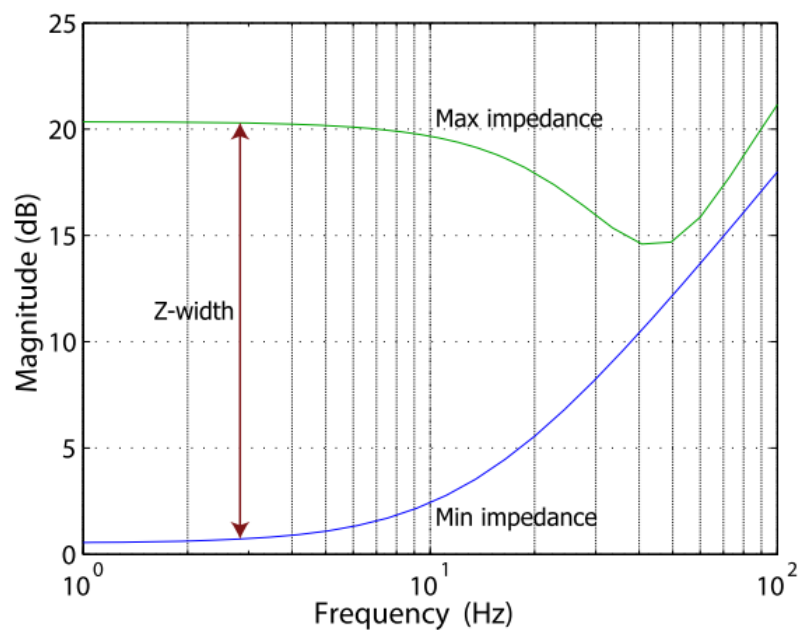
Figure 2.1. Minimum and maximum Impedance with respect to frequency range.
(Source: Samur 2012)

2.2. Factors Affecting Z-Width

Samur (2012) has categorized the haptic system properties into three groups as unpowered, powered and controlled system properties. Pure structural and mechanical properties of the manipulator where no actuation system are included are stated as un-powered system properties. In this group, the capabilities of the manipulator alone are investigated. The powered system properties include actuation and sensing capabilities

are the manipulator. The capability of the robotic system in the absence of a control algorithm is on the focal point in the powered system properties. Finally, by adding a control algorithm to increase Z-Width, the overall robotic system properties can be investigated. By investigating each group, the properties affecting Z-Width can be revealed.

2.2.1. Unpowered System Properties

Unpowered system properties can be categorized as kinematics, elastostatics, and dynamics. Kinematics is the most dominant factor for a manipulator because if a manipulator cannot achieve the desired motion, it is meaningless to evaluate the other two properties. Kinematic properties can be listed as workspace, the degree of freedom, structure, and dexterity.

The haptic interface reflects forces to the operator. It is achieved by the active DoF in Cartesian space. The passive DoF in Cartesian space is not driven actively to deliver force but included in manipulator as spherical wrist to enhance the manipulation easiness of the user. These definitions are the result of the kinematic structure and the topology of the manipulator.

The topology or the structure of the manipulator is determined by the shape of the workspace or vice-versa and required DoF. Thus, selecting a suitable workspace shape for required work is vital since it also determines the manipulator type. For haptic manipulators, for instance, a continuous workspace with regular shapes is the desired for good perception.

Workspace is the space where the end-effector of the manipulator can reach in and therefore, it is one of the most crucial parameters in the definition of kinematic capabilities. The kinematic parameters of the manipulator i.e. link lengths are generally selected based on the size of the workspace. Depending on the design objective, it should be dexterous at a certain level (Kumar and Waldron, 1981). The workspace should be away from any mechanical singularities where manipulator momentarily loses one of its degree of freedom. This is especially crucial for haptic systems since the human moves the end-effector to any location and singularity cannot be avoided by control.

Elastostatics (stiffness) is the second dominant factor in manipulator properties. It basically determines the load capacity of the manipulator. Therefore, the elastostatic property is highly related to the maximum impedance.

Stiff manipulators are less compliant, thus, the end-effector position can be accurately measured from the joints with forward kinematics and higher forces can properly

be reflected at the end effector. The stiffness depends on the link lengths, the cross-section area of the link and the material. In reality, there is no infinitely stiff material. Thus, a stiffness matrix containing the stiffness model of the manipulator,might be useful in order to control the manipulator with higher precision.

Dynamic property reveals itself while the manipulator in motion. Moving links with mass and moment of inertia creates the dynamic effects. Therefore, most of the time dynamics is not a design parameter but a result of kinematics and elastostatics. Although it is a result of other parameters, it has a significant effect on minimum impedance and frequency range. Yet, it is still possible to implement it in design procedure by using dynamic performance metrics with iterative solutions. However, it is also possible to include the dynamics along with the kinematics and elastostatics. Dynamics can also be used to control the manipulator to enhance its performance. All unpowered system metrics are listed in Table 2.1.

Table 2.1. Unpowered System Properties.
(Source: Samur 2012)

Type	Category	Metric
Kinematics	Workspace	Reachable
		Dexterous
	Number of Degree of Freedom	Passive
		Active
	Dexterity	Manipulability
		Condition Number
Elastostatics		Structural Stiffness
Dynamics		Structural Dynamics
		Acceleration Radius

2.2.2. Powered System Properties

The powered system properties are mainly about actuation and sensing capabilities. For any kinesthetic haptic device, the output force is limited by the maximum force/-torque generated by the actuator. In the case of a electric motor (i.e. DC motor), there are two maximum torques which are the stall torque and maximum continuous torque. The stall torque can be applied for a short amount of time due to excessive heat accumulation. During the motion, the dynamic range of the actuator which is the ratio of maximum continuous torque to minimum torque which indicates the friction at the bearings should

be high for high impedance range. The dynamic range is a dominant factor while defining the force bandwidth of the haptic device. Other factors depend on the instrumental capabilities such as motor's time constant.

Table 2.2. Powered System Properties.
(Source: Samur 2012)

Type	Category	Metric	
Actuation	Static	Peak Force	Continious Force
		Minimum Force	Hysteresis
		Sensitivity	Force Resolution
		Dynamic Range	
	Frequency Response	Force Bandwith	Frequency Range
		Amplifier Bandwith	Force Fidelity
		Output Impedance	
	Step Response	Rise Time	Overshoot
		Settling Time	Force Accuracy
		Force Precision	
	Impulse Response	Peak Speed	Peak Acceleration
		Structural Deformation Rate	
Sensing	Static	Sensitivity	Position Resolution
		Hysteresis	Dynamic Range
		Accuracy	Precision
	Frequency Response	Sensor Bandwith	

The other parameters which become apparent when the system is actuated are the dead zone, sensitivity, and minimum force. The dead zone is the result of stiction and Coulomb friction. Just before the actuator starts to rotate, this is the first force offset to overcome. This friction is the sum of all joint frictions including the actuator. Thus, high-quality joints which have low friction should be on the spec of the designer. However, low friction may cause stability problems in controlled system due to low energy dissipation. Sensitivity is the amount of torque change for a single incremental input to the actuator. In order to reflect small changes in force, the sensitivity should be high. Resolution is the minimum increment in torque that is generated by the actuator. The minimum force, which is also referred as the back drive force, is the measure of how small forces can be reflected by the haptic device. On free motion, since there is no force desired, this value should be zero. However, the friction or breakaway force gives a force offset to haptic device by increasing the minimum allowable force boundary. If all above parameters are

chosen wisely, the optimum force fidelity for the haptic device can be achieved.

The position resolution is another important parameter for simulating stiff and smooth surface interaction. Most of the time this parameter is defined by the encoder and the actuator resolution. Designers seek higher sensor resolution to solve the quantization problems. In addition, the encoder resolution affects the quality of velocity and acceleration derivation. High-resolution results in better derivation and fewer ripples on the motion data. In the case of analog sensors, the analog to the digital conversion resolution gains the importance. The powered system properties are listed in Table 2.2.

2.2.3. Controlled System Properties

Controlled system is where overall the potential of the haptic device is revealed. Without the control, haptic device is just a pile of links, joints, sensors, and actuators. Thus, the Z-Width of the device can be extended by proper control at this stage. The minimum and the maximum impedance define the boundaries of Z-Width. Until now, powered and unpowered system parameters are the limiting factors of the Z-width. Friction, back drivability, inertia, and dexterity determine the minimum impedance. Stiffness, maximum continuous torque, dexterity are the factors on the performance of maximum impedance. Sampling rates and dynamic range play the main role on the maximum achievable frequency. Minimum impedance can be lowered by calculating the friction and using it in control. Controlled system properties are shown in Table 2.2.3.

Table 2.3. Controlled System Properties.
(Source: Samur 2012)

Type	Metric
Impedance	Minimum Impedance
	Maximum Impedance
	Z-Width
	Transparency
Control Bandwidth	Impedance Control Bandwidth

2.3. Conclusion

In this Chapter, factors affecting Z-Width and transparency were briefly listed. The impedance (also the transparency) reveals at control stage. It is true that control has a huge impact on the overall performance of the haptic device. With a good controller, almost any manipulator can be converted into a haptic device. However, even the best-designed controller cannot surpass the mechanical limitations of the haptic device. Therefore, increasing the transparency must start at the design stage of the manipulator. This thesis study focuses on the unpowered system domain including kinematics, stiffness, and dynamic optimization of the manipulator since they have the largest influence on impedance. The aim is to increase the Z-Width and the operational frequency.

CHAPTER 3

PREVIOUS WORKS ON DESIGN OF HAPTIC DEVICES

Every manipulator can be evaluated in terms of performance of kinematics, stiffness, and dynamics. In order to have a high-performance manipulator, it must have the best performance in these three domains. Yet, the problem is that all three cannot be maximized simultaneously due to the coupled relation between each other. A simple example can be given between the kinematic and stiffness requirements. A manipulator should have a stiff design so that it can precisely follow a desired trajectory. On the other hand, the stiff design requires short links which reduces the overall workspace and endangers the achievement of the trajectory due to the lack of maximum reach. Another example may be the relationship between the stiffness and dynamics. In terms of dynamics, low inertial properties are desired so that the manipulator may have a high response rate and consumes fewer energy thanks to its lightweight structure. Yet, as the amount of material is reduced, the stiffness of the manipulator reduces also. These two examples show that the relationships between the kinematics, stiffness, and dynamics are highly contradictory. The only solution to achieve the best possible design is optimizing the kinematics, stiffness, and dynamics through the performance metrics. However, in order to derive the performance metrics, the topology must be defined first. Later, the objectives are clarified and the optimization method is specified. In this Chapter, a literature review is included which specifically focuses on the design of haptic manipulators to reveal the design parameters of a haptic device.

3.1. Manipulator Type

Determining the manipulator type is one of the very first steps in the design of a haptic manipulator. The performance of the haptic manipulator is limited by the topology. Therefore, choosing architecture as the suitable manipulator type is extremely important. Manipulators can be classified into three types according to their kinematic structure: serial, parallel and hybrid. Each has its own advantages and disadvantages.

Serial manipulators have a large workspace size and manipulability yet their stiffness and dynamic performances are limited. Parallel manipulators exhibit high stiffness

Table 3.1. Comparison of Manipulator Types in terms of Haptics

	Serial Manipulator	Parallel Manipulator	Hybrid Manipulator
Workspace	Large	Small-Complex	Medium-Complex
Forward Kinematic Computation	Easy	Difficult	Difficult
Inverse Kinematic Computation	Difficult	Easy	Medium
Dexterity of Workspace	High	Low	Medium
Kinematic Uniformity of Workspace	Low	High	Medium
Kinematic Singularities	High	Low	Medium
Number of Moving Actuators	High	Non or Low	Medium
Positioning Resolution	Low	High	Medium
Force Resolution	Low	High	Medium
Maximum Impedance Capability	Low	High	Medium
Minimum Impedance Capability	Low	High	Medium
Stiffness	Low	High	Medium
Stiffness Model Computation	Easy	Difficult	Difficult
Inertia	High	Low	Medium
Dynamic Model Computation	Easy	Difficult	Difficult
Acceleration Capability	Low	High	Medium
Frequency Range	Low	High	Medium
Accuracy	Low	High	Medium
Ergonomic	High	Low	Medium

performance and can operate at high frequencies but their workspace is limited. Hybrid manipulators combine these two manipulators to eliminate the drawbacks of each other. The hybrid combination can be a parallel manipulator on top of a serial one or vice versa. This choice of manipulator structure depends on the type of the work which will be conducted with the manipulator.

Table 3.2. Some impedance type of haptic devices and their manipulator types. DoF I/O indicates possible number of DoF input(I) by the user and the number of actuated DoF output(O)

Reference	Device	Type	DoF I/O
3D SYSTEMS (2018)	Touch	Serial	6/3
	Touch X	Serial	6/3
	Phantom® Premium 1.0	Serial	6/6
	Phantom® Premium 1.5	Hybrid	6/6
	Phantom® Premium 3.0	Hybrid	6/6
MPB (2018)	Freedom-6S	Hybrid	6/6
	Freedom-7S	Hybrid	7/6
Haption (2018)	Virtuose$^{\text{TM}}$ 6D	Serial	6/6
	Virtuose$^{\text{TM}}$ 6D TAO	Serial	6/6
	Virtuose$^{\text{TM}}$ 3D	Serial	6/3
	Virtuose$^{\text{TM}}$ 6D Desktop	Serial	6/6
	Virtuose$^{\text{TM}}$ 3D Desktop	Serial	6/3
Systems (2018)	Cyber Force	Serial	6/3
Dimensions (2018)	omega.3	Parallel	3/3
	omega.6	Hybrid	6/3
	omega.7	Hybrid	7/3
	delta.3	Parallel	3/3
	delta.6	Hybrid	6/6
	sigma.7	Hybrid	7/7
QUANSER (2018)	HD^2	Parallel	6/6
Novint (2011)	Falcon	Parallel	3/3

Patel and George (2012) have compared the advantages and disadvantages of parallel manipulators over serial ones. Parallel manipulators have lower inertia, higher stiffness, better resolution, lower backlash and better dynamic characteristics compared to serial manipulators. They can carry higher loads at higher bandwidths. The actuators of parallel mechanisms can be located on the fixed ground to reduce the inertial effects. Generally, they do not contain singularities in the workspace. Joint errors are not additive, unlike the serial manipulators. A comparative chart is shown in Table 3.1

Although in terms of impedance parallel manipulators have better properties for

Table 3.3. Impedance type of haptic devices and their manipulator types developed by scientists. DoF I/O indicates possible number of DoF input(I) by the user and the number of actuated DoF output(O)

Reference	Device	Type	DoF I/O
Vulliez and Zeghloul (2016)	Delthaptic	Parallel	6/6
Agboh et al. (2016)	-	Parallel	6/6
Peng et al. (2015)	-	Parallel	2/2
Lambert and Herder (2015)	-	Hybrid	7/7
Qin et al. (2015)	-	Hybrid	6/6
Ahmad et al. (2014)	-	Parallel	6/6
Ergin and Peer (2013)	-	Parallel	6/6
Li et al. (2012)	-	Hybrid	8/8
Arata et al. (2011)	DELTA-4 (DELTA-R)	Hybrid	7/7
Zhao et al. (2011)	-	Hybrid	6/3
Bilgincan et al. (2010)	HIPHAD	Hybrid	6/3
Faulring et al. (2006)	Cobotic Hand Controller	Parallel	6/6
Chablat and Wenger (2006)	-	Hybrid	6/6
Lee and Kim (2006)	-	Parallel	6/6
Sabater et al. (2005)	Magister-p	Parallel	6/3
Gosselin et al. (2005)	-	Parallel	6/6
Gosselin et al. (2005)	-	Hybrid	6/5
Borro et al. (2004)	LHIfAM	Serial	6/6
Sabater et al. (2004)	-	Parallel	6/6
Birglen et al. (2002)	SHaDe	Parallel	3/3
Lee et al. (2001)	-	Parallel	6/6
Yoon and Ryu (2001)	-	Parallel	6/6
Tsumaki et al. (1998)	-	Hybrid	6/6
Iwata (1993)	-	Parallel	6/6

haptic applications, the active links of the parallel manipulators have restricted for rotational motions. In addition, the range of this rotational motion is limited. This is why hybrid manipulators are preferred over parallel ones. Hybrid manipulators have advantages regarding both parallel and serial manipulators. In general configuration of a hybrid manipulator there is a parallel manipulator that has a mobile platform and a serial mechanism on top of it. This serial manipulator generally has rotational DoF for wrist motion is to achieve higher manipulability.

The haptic manipulators are examined for commercial and non-commercial use. Companies prefer to use serial manipulators since it is easy to model, manufacture, and calibrate them. From the aspect of the end user, ergonomic usage for a long period of time

and having larger workspace are more important. Parallel manipulators are generally preferred for high-end applications where precision and accuracy is much more important than the workspace and manipulability. Hybrid manipulators combine the usage of comfort and high performance.

Some commercial impedance type of haptic manipulators are listed in Table 3.2. When this table examined, it can be seen that most of the commercial haptic devices use serial manipulator as haptic manipulator due to the necessity of a large workspace and dexterity. In Table 3.3 some non-commercial haptic devices are listed. They use either parallel or hybrid manipulators.

3.2.   Design Optimization Considering Unpowered System Properties

As expressed in the previous Chapter, the unpowered system properties are determined by three three main properties of the manipulator: kinematics, stiffness, and dynamics. Among them, the kinematics is the most studied property in the literature since it does not only identify the motion but it also contains the information which determines the stiffness and the dynamics performance. Since the mechanical stiffness depends on link lengths and the configuration of the manipulator, the kinematics is one of the dominant factors which determines it. Similarly, kinematics is a part of the dynamics.

Kinematics contains the required information to generate motion data such as link lengths, the range of joint angles/strokes, and orientation of the bodies. This information is used to derive the forward and the inverse kinematics to evaluate the kinematic performance metrics. Forward kinematics is used to determine the size and the location of the workspace. By making use of link lengths and joint angles the volume of the workspace is computed and the shape of the workspace is determined. The inverse kinematic solution, on the other hand, is used to determine the configuration (assembly mode) and the placement of the passive links. The choice of the configuration is vital to avoid collision between the links. Also, the change in configuration depends on the limitations of the joints which is designated via inverse kinematics.

Kinematic information is used to locate the end effector in different poses. However, in transition between two poses, the configuration change may occur or a singular pose may be in the transition path. To analyze the motion, the kinematics in velocity level is derived by taking the time derivative of the kinematics formulated in position level. As a result, the mapping between the joint space velocity and the task space velocity is achieved via the Jacobian matrix. Since the Jacobian matrix establishes such a relation

between the joint and task space, it has been the backbone of all performance metrics.

In kinematics domain performance analyses, there are two main performance metrics which makes use of the Jacobian matrix, the manipulability, and the condition number. Manipulability decribes the ease of the motion which is introduced by Yoshikawa (1985b). This metrics is the measure of closeness to a singular pose and a measure of back-drivability. In many cases, singularity is required to be avoided. In terms of haptics, however, even getting close to a singular pose minimizes the back-drivability. Hence, this measure is very important for haptic manipulators. Condition number, on the other hand, is a measure of the motion resolution at the end effector (Salisbury and Craig, 1982). In standard manipulators, positioning resolution is a measure of precision. In haptics, the position resolution is highly dependent on force resolution since the force/torque transmission between the actuators and end-effector is related with the kinematics.

Stiffness is the measure of compliant displacement ratio of the manipulator under external wrenches. The compliant displacements affect the positioning precision and accuracy of the end-effector, adversely. Since the positioning quality is also the measure of force quality, elasticity is not desired in haptic manipulators. In addition to quality and accuracy, only very stiff manipulators can render high forces in haptic applications. This property makes the stiffness a determining factor of maximum impedance performance. As the stiffness or maximum impedance increases the magnitude of the maximum force that can be rendered by the manipulator increases.

In the evaluation of minimum impedance, it is desired to have no force felt by the user at the end effector during free motion. Even though the actuators are not powered and the weight of the manipulator is compensated, the dynamic forces are generated when the motion is supplied to manipulator by the user. Hence, the dynamic performance metrics are the measures for the minimum impedance performance. In addition, dynamics constrains the motion capability of the manipulator. Due to the limited output power of the actuators against inertial effects, the desired motion may not be achieved. Hence, it is desired to minimize the inertia of the manipulator to enhance the dynamic performance.

Dynamics and stiffness properties designate the maximum frequency range of the manipulator since the frequency is determined by the relation between the stiffness and inertia. As this range increases, the variety of the forces which can be rendered also increases. Hence, both subject must be on the focal point of the design. Yet, all design procedures must be conducted under the constraints such as described workspace, singularity and/or geometric limitations. Table 3.4 shows used performance metrics and their constraints in the literatue on design of haptic device.

Table 3.4. List of Literature on Performance Metrics. CN: Condition Number, W: Workspace, FC: Force Capability, SN: Stiffness, AC: Acceleration Capability, IN: Inertia, S: Singularity, G: Geometric, P: Payload, CD: Compliant Displacement

Reference	Performance Metrics	Constraints
Vulliez and Zeghloul (2016)	CN, W	S, W, G
Lambert and Herder (2015)	CN	S, W, G
Ahmad et al. (2014)	CN, W, FC, SN	S, G
Ergin and Peer (2013)	CN, W, AC, FC	S, G
Li et al. (2012)	CN	S, G
Lopes et al. (2012)	CN	Single Pose
López M. et al. (2012)	CN, FC	S
Kang et al. (2012)	CN, W	S, G
Zhao et al. (2011)	CN, W, FC, SN, IN	S
Ergin et al. (2011)	CN, FC, IN	S, W
Khan et al. (2011)	CN, FC, W	S, W
Hung and Na (2011)	CN, FC, W	S
Yoon et al. (2010)	CN, W	S, W
Gao et al. (2010)	CN, SN	S
Unal et al. (2008)	CN, IN	S, G
Unal and Patoglu (2008)	CN, IN	S, W, G
Lee and Kim (2006)	CN, FC	S, W, G
Barbosa et al. (2005)	CN	S, G
Gosselin et al. (2005)	CN, W, FC, SN, IN	S, W, P, CD
Gosselin et al. (2005)	W, FC	S, G
Lee and Lee (2003)	CN	S, W, G
Birglen et al. (2002)	CN, W	S
Ueberle and Buss (2002)	CN, FC	S
Stocco et al. (2001)	CN	S
Lee et al. (2001)	CN, FC, W	S, G
Yoon and Ryu (2001)	CN, FC	S, W
Salcudean and Stocco (2000)	CN	S, W

3.3. Optimization Algorithms

In Section 3.2, it can be deduced that the design of the haptic manipulator requires optimization of multiple performance metrics. The design problem, however, is challenging to be solved directly due to the contradictive and nonlinear relation between the performance metrics. For instance, enhancing the stiffness performance may be achieved with links that have larger cross-section area yet this causes loss in dynamic performance because of increased mass-inertia. Hence, the design problem of the manipulator is an optimization problem. Because of the nonlinear relationship between the metrics, con-

ventional solution methods result in local optimal solutions depending on the initial design point. For obtaining the global optima, evolutionary solution algorithms such as the genetic algorithm or particle swarm optimization are preferred. Artificial intelligence methods like neural-networks are also used in the literature. Sometimes, both methods are combined to reduce the duration of optimization process such as the neuro-genetic algorithm. Some designers prefer to use culling algorithm to discard the non-optimal solution sets.

Another problem of optmization is the construction of the objective function. Multi-objective optimization either can be conducted on a single objective function or multiple objective functions. In single objective function method, performance metrics are summed up in a single equation and depending on the importance of the metric they are assigned different weighting coefficients. The method is simple and fast, yet obtained results are generally local optimal solutions. Other methods require the construction of objective functions each having a single performance metric. The resultant of the method is multiple solutions called Pareto-front solution sets. For n number of objective functions, Pareto-front solutions represent the solution curves, surfaces, or hypersurfaces. The benefit of the Pareto-Front approach is that it provides the detailed design solutions to the designer. Table 3.5 shows the optimization methods used in the literature of haptic device design.

3.4. Comments on the State of the Art in Optimal Design of Haptic Devices

Most of the studies in the literature focus on kinematic optimization. In terms of actuator torques and end-effector force output, kinematics information is used in the mapping role between the joint and task space. However, impedance performance must be on the focal point of the design but there are only few studies on elasto-dynamic performance enhancement which focuses on the impedance performance. In addition, the evaluation of frequency range (or the natural frequency) of the manipulator generally is omitted.

The common purpose of the design is to designate the link lengths and maximum/minimum joint angles. Hence, the dimensional synthesis of cross-sectional profile of the links is not studied enough. In addition, the link materials are generally chosen as isotropic materials such as steel and aluminum. Links made of composite materials are almost never studied and there is no record found on the design of fiber orientation

Table 3.5. Preferred Solution Algorithms and Methods

Reference	Solution Algorithm	Method
Vulliez and Zeghloul (2016)	Genetic Algorithm	Pareto Front
Ahmad et al. (2014)	Genetic Algorithm	Weighted Sum
Ergin and Peer (2013)	Neural Network Genetic Algorithm	Pareto Front
Lopes et al. (2012)	Genetic Algorithm Neuro-Genetic Algorithm	Pareto Front
López M. et al. (2012)	-	Weighted Sum
Kang et al. (2012)	Genetic Algorithm	Weighted Sum
Ergin et al. (2011)	Culling Algorithm	Pareto Front
Khan et al. (2011)	Genetic Algorithm	Weighted Sum
Hung and Na (2011)	-	Weighted Sum
Yoon et al. (2010)	Genetic Algorithm	Weighted Sum
Unal et al. (2008)	Culling Algorithm	Pareto Front
Unal and Patoglu (2008)	Genetic Algorithm	Pareto Front
Lee and Kim (2006)	Genetic Algorithm	Weighted Sum
Barbosa et al. (2005)	Genetic Algorithm Neuro-Genetic Algorithm	Pareto Front
Birglen et al. (2002)	-	Weighted Sum
Stocco et al. (2001)	Culling Algorithm	-
Lee et al. (2001)	Genetic Algorithm	Weighted Sum

alignment of the links. The thesis is dedicated to focus on the solution of these issues.

3.5. Methodology That is Followed in This Thesis

In this thesis, initially, the mathematical formulations of performance metrics are investigated including their physical meaning to construct the objective functions. In order to use the performance metrics in the objective functions, kinematic, stiffness, and dynamic models of the manipulator are required.

A modified version of R-CUBE mechanism which was first proposed by Li et al. (2005) is chosen as a case study which is shown in Figure 3.1. The manipulator comprises a decoupled mechanism so each serial chain is only responsible for the motion of one of the degree of freedom. The reason to choose this manipulator is that each serial chain is the same and hence, one chain can be designed to represent all of the mechanism. It has only revolute joints which is good for low cost and back-drivability and larger
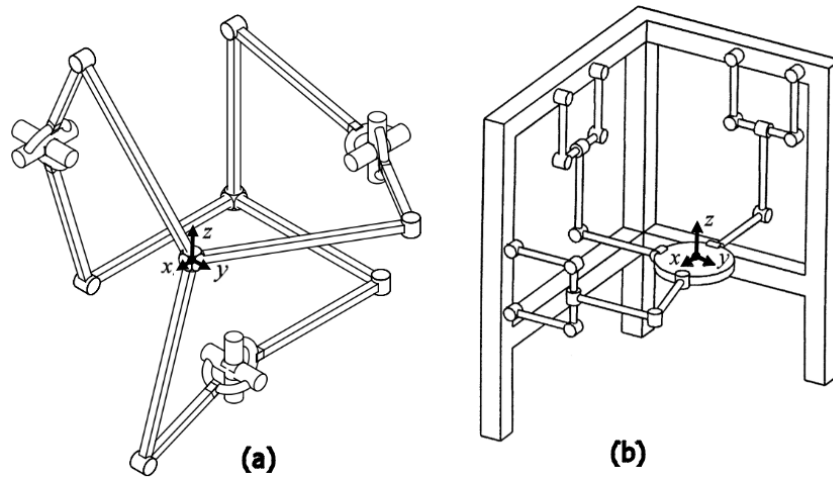
Figure 3.1. a) Modified R-CUBE Mechanism. b) Original R-CUBE Mechanism by
(Li et al., 2005).

workspace to footprint ratio. Its forward and inverse kinematics are relatively easier to compute compared to general parallel mechanisms. This enhances the computation time of stiffness model and makes it easier to work with for control purposes. It has a cubic and symmetric workspace which makes it better in terms of ergonomic usage and mapping in between the workspaces.

First, forward and inverse kinematics are obtained for R-CUBE manipulator. Position level kinematics are verified via a CAD program (SolidWorks). The kinematic model in velocity and acceleration level are validated in MATLAB environment using the Sim mechanics model of the manipulator. In order to prevent the dimensional inconsistency in kinematic performance metrics, the kinematic equations are synthesized as dimensionless.

Then, the stiffness model is procured by using the virtual joint method and programmed in MATLAB. The stiffness model for a single link structure with composite material is verfied in MATLAB, ADAMS and ANSYS software programs. Next, the stiffness models for all serial chains and the whole manipulator are formulated and validated in MATLAB and ANSYS.

Afterwards, dynamic model of the manipulator is obtained via the virtual work method. Verification is conducted via the model constructed by using Sim mechanics blocks in MATLAB.

Performance metrics are applied making use of all models and simplified for the critical poses of the manipulator in order to reduce the optimization process. Using the metrics, multiple objective functions are constructed where each function is formed by a

single performance metric. The multi-objective genetic algorithm in MATLAB is used as solution algorithm and Pareto-front solution set is obtained. Prescribed workspace, singular poses, and ergonomy conditions are used as constraints. The optimization process is divided into two steps. First, the link lengths and maximum deviation angles of active links are determined as the result of optimization. Next, thickness and the composite material angles are determined.

Then, the selection of the optimum solution is done in accordance with the natural frequency outputs of the solutions. Since the highest frequency denotes the stiffest manipulator with minimum possible dynamics. The flow chart of the methodolgy is shown in Figure 3.2.
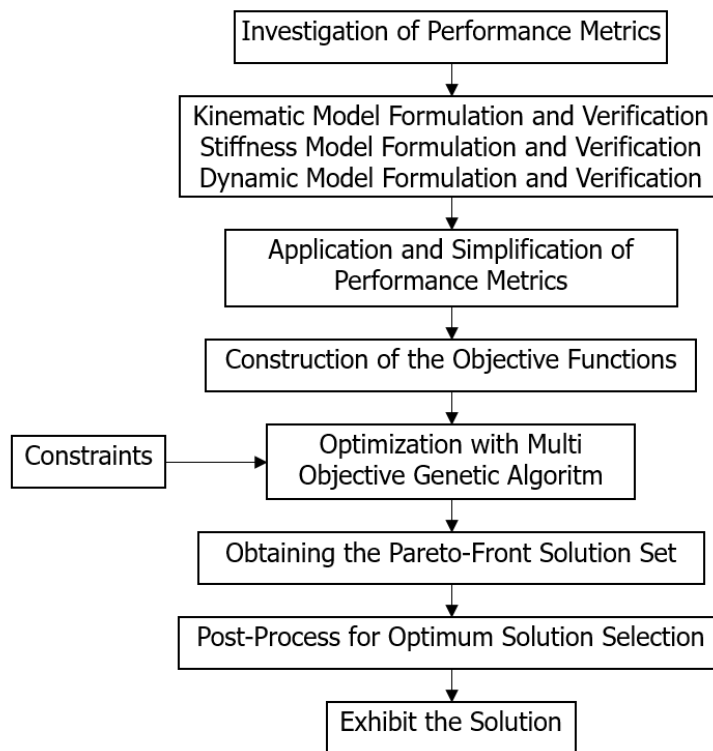
Figure 3.2. The flow chart of the methodology.

3.6. Conclusion

In this Chapter, a literature review is conducted to determine the performance metrics and optimization method used for haptic manipulator design. The literature review is only limited to the haptic mechanisms. General robot manipulator designs are

excluded. It has been shown that the majority have focused on kinematic optimization by excluding the stiffness and dynamics performances. It is true that the kinematic effect the stiffness and dynamic performance, however, the most critical metrics are stiffness and dynamics since the impedance performance directly determined by these 2 domains. Therefore, even in kinematic synthesis, the effect of stiffness and dynamics on impedance performance must be included in the dimensional synthesis.

CHAPTER 4

UNPOWERED PERFORMANCE METRICS OF HAPTIC DEVICES

In this section, unpowered performance metrics are investigated. First, kinematic performance metrics are discussed. For these metrics, the importance of the use of the dimensionally homogeneous Jacobian matrix is highlighted. Then, stiffness modeling methods are reviewed. Links with the composite material are considered for stiffness model. Virtual joint method is adopted for developing stiffness performance metrics. Finally, dynamic performance metrics are reviewed and explained.

4.1. Motion Related Design Parameters

In the literature, kinematic performance metrics are always the core of the design. The main reason of this is that kinematics affects all of the performance metrics including the stiffness and dynamics. Stiffness is a kinematic pose-dependent property. Dynamic effects are also configuration-dependent and additionally affected by the link velocities which are also dependent on the kinematic architecture of the device. The relation between the actuator velocities/torques and the end-effector velocities/forces is ruled by the kinematic architecture of the manipulator. Therefore, in the previous works, researchers have usually neglected the stiffness and dynamic performance metrics of the manipulator in the optimization process.

In this section, kinematic performance metrics are reviewed. The actuator and end-effector torque/force relations by carrying out the static equilibrium analysis is denoted. Dimensionally homogeneous Jacobian matrix is introduced to be used in formulating the performance metrics. The condition number which is the resolution of positioning and force output is exhibited. In order to avoid the singularities, manipulability index is highlighted.

4.1.1. Workspace

Workspace is the space where end-effector can reach. The general tendency in design objective for workspace is to enlarge it while preserving the dexterity, especially for parallel manipulators. A design objective approach for dexterous workspace maximization is to limit the maximum link lengths or/and joint ranges and find the dimensions of the maximum dexterous workspace with predefined performance critics. In other design objective, the workspace is prescribed and dimensional properties of the manipulator are optimized which will increase the dexterity of the workspace.

The size of the workspace is evaluated by computing its area, volume, or maximum reach of the serial chain. If it is possible to denote the workspace in analytical form, area or volume may be used as the performance metric. Yet, for some manipulators (especially the serial ones) evaluation of difference between the maximum and minimum reach is sufficient since the area in between is the workspace. Although both approaches are valid to be used as the workspace performance metrics, computation of the difference of maximum and minimum reach is easier. The volume of the workspace is not always represented analytically. Hence, discrete methods are used in such cases which is time-consuming. Maximum reach, however, corresponds to a single discrete point in the workspace. Therefore, it is more suitable for the optimization process. The performance metrics for workspace is given in the following Equation set;

$$W_v = max(V) \tag{4.1}$$

$$W_r = max(\|\bar{r}_p\|) - min(\|\bar{r}_p\|) \tag{4.2}$$

where W_v and W_r denote the workspace performance metrics, V is the volume, and $\bar{r}_p$ is the position vector of the end effector. $\|.\|$ is the Euclidean norm operation. W_v evaluates the volume and W_r computes the norm of maximum reach vector of the workspace.

The problem with this design objective is maximum workspace occurs when the arms are fully folded or fully expanded. Those poses are where the manipulator is close to unstable conditions. The boundary of the workspace is where the manipulability approaches the singularity. In addition, there is a risk that the manipulator may change its configuration during operation. Hence, design objective should be chosen as the dexterous workspace in which there is no such risky regions. To do that, generally, two metrics, manipulability and condition number, are used. These metrics are highly related to the velocity and force ellipsoids of the end-effector.

4.1.2. Force and Velocity Ellipsoids

Performance metrics of a manipulator are represented by scalar values. In general, it is sufficient to evaluate the manipulator with numerical results, yet it is always not easy to conclude the physical interpretation of them. This is important for the designer to understand what kind of performance the manipulator exhibits.

The force and velocity ellipsoids provide a graphical illustration of the velocity and force/torque performance of the manipulator. The ellipsoid denotes the mapping quality between the task and joint space of the manipulator. Both ellipsoids use the eigenvalue and eigenvectors of the Jacobian matrix. This illustration gives a physical understanding of how the interaction that occurs between the task and joint spaces.

In order to obtain the Jacobian matrix, the forward kinematics should be formulated first. The forward kinematic equations are defined as follows;

$$\bar{r} = \bar{f}(\bar{q}) \tag{4.3}$$

$$r_n = f_n(q_1, q_2, ..., q_m) \tag{4.4}$$

$$\bar{r} = \begin{bmatrix} r_1 & r_2 & ... & r_n \end{bmatrix}^T \tag{4.5}$$

$$\bar{q} = \begin{bmatrix} q_1 & q_2 & ... & q_m \end{bmatrix}^T \tag{4.6}$$

where $\bar{q}$ and $\bar{r}$ are the column matrix representation of vectors containing joint variables and pose of the end-effector and $\bar{r}$ is a function of $\bar{q}$. The bar on the variables denotes that it is a column matrix. Subscripts n and m denote the nth and m^{th} variables of the respective vectors where $n \leq m$, $m \geq n$, and $n = m$ denote the deficient, sufficient, and redundant manipulator. In this Chapter, it is assumed that $n = m = 6$. Jacobian matrix contains 3 linear and 3 angular velocity influence coefficients for general case.

The Jacobian matrix $\hat{J}$ is computed by taking the partial derivative of $\bar{f}(\bar{q})$ with respect joint variables $\bar{q}$.

$$\hat{J} = \begin{bmatrix} \frac{\partial f_1}{\partial q_1} & \frac{\partial f_1}{\partial q_2} & \cdots & \frac{\partial f_1}{\partial q_m} \\ \frac{\partial f_2}{\partial q_1} & \frac{\partial f_2}{\partial q_2} & \cdots & \frac{\partial f_2}{\partial q_m} \\ \vdots & \vdots & \ddots & \vdots \\ \frac{\partial f_n}{\partial q_1} & \frac{\partial f_n}{\partial q_2} & \cdots & \frac{\partial f_n}{\partial q_m} \end{bmatrix} \tag{4.7}$$

The Jacobian matrix is a mapping matrix in between the joint space velocities and task space velocities. This relation is shown as follows;

$$\frac{d\bar{r}}{dt} = \frac{\partial \bar{f}(\bar{q})}{\partial \bar{q}} \frac{d\bar{q}}{dt} \tag{4.8}$$

$$\frac{d\bar{r}}{dt} = \dot{\bar{r}} \tag{4.9}$$

$$\frac{\bar{q}}{dt} = \dot{\bar{q}} \tag{4.10}$$

For n^{th} element of $\dot{\bar{r}}$: $\dot{r}_n = \frac{\partial f_n}{\partial q_1}\dot{q}_1 + \frac{\partial f_n}{\partial q_2}\dot{q}_2 + ... + \frac{\partial f_n}{\partial q_m}\dot{q}_m \tag{4.11}$

$$\text{Hence: } \frac{\partial \bar{f}(\bar{q})}{\partial \bar{q}} = \begin{bmatrix} \frac{\partial f_1}{\partial q_1} & \frac{\partial f_1}{\partial q_2} & \cdots & \frac{\partial f_1}{\partial q_m} \\ \frac{\partial f_2}{\partial q_1} & \frac{\partial f_2}{\partial q_2} & \cdots & \frac{\partial f_2}{\partial q_m} \\ \vdots & \vdots & \ddots & \vdots \\ \frac{\partial f_n}{\partial q_1} & \frac{\partial f_n}{\partial q_2} & \cdots & \frac{\partial f_n}{\partial q_m} \end{bmatrix} = \hat{J} \tag{4.12}$$

$$\dot{\bar{r}} = \hat{J}\dot{\bar{q}} \tag{4.13}$$

The force-torque relation between the joint space and the task space can also be established by using Jacobian matrix. Virtual work principle is employed for that and virtual displacements are mapped between the joint space and the task space as follows;

$$\delta\bar{r} = \hat{J}\delta\bar{q} \tag{4.14}$$

The virtual work principle;

$$\bar{F}_{ext}^T\delta\bar{r} + \bar{\tau}_e\delta\bar{q} = 0 \tag{4.15}$$

where $\bar{F}_{ext}$ and $\bar{\tau}_e$ denote the external wrench and reaction torques or forces of the external wrench on joints along their rotation or translation axis. δ denotes the change in virtual displacement. $\bar{F}_{ext}$ is a 6×1 vector and it is also called external force vector yet it contains both the forces and torques. The actuation torque/force on the joints is the negative of $\bar{\tau}_e$. Hence, the relation between the external wrench and actuation torques/forces $\bar{\tau}$ are denoted as;

$$\bar{F}_{ext}^T\delta\bar{r} = \bar{\tau}\delta\bar{q} \tag{4.16}$$

$$\text{Where: } \bar{\tau} = -\bar{\tau}_e \tag{4.17}$$

By substituting $\delta\bar{r}$ in Equation 4.14 into Equation 4.16, the following is obtained;

$$\bar{F}_{ext}^T\hat{J}\delta\bar{q} = \bar{\tau}^T\delta\bar{q} \tag{4.18}$$

The proposition must be true for all $\bar{q}$. Hence, the following statement can be made;

$$\bar{\tau} = \hat{J}^T\bar{F}_{ext} \tag{4.19}$$

In general approach of robotic applications, velocity mapping from the joint space to task space is considered for evaluation. Hence, this generates 2 possible mappings in total.

These 2 relations are listed as follows;

$$\dot{\bar{r}} = \hat{J}\dot{\bar{q}} \tag{4.20}$$

$$\bar{F}_{ext} = (\hat{J}^T)^{-1}\bar{\tau} \tag{4.21}$$

where Equations 4.20, and 4.21 denote the velocity mapping from the joint space to task space, and force mapping from joint space to task space, respectively.

The mapping quality of the Jacobian matrix is investigated by giving a unit input from the joint space. Such an input describes a 5 dimensional hyper-sphere for 6 dimensional space. The inputs of Equations 4.20 and 4.21 are $\dot{\bar{q}}$ and $\bar{\tau}$, respectively. The inputs are left alone by multipliying with the inverse of the Jacobian matrix multiplier.

$$\dot{\bar{q}} = \hat{J}^{-1}\dot{\bar{r}} \tag{4.22}$$

$$\bar{\tau} = \hat{J}^T \bar{F}_{ext} \tag{4.23}$$

The Equations are reduced to scalar values by multiplying the vectors by the transpose of them from the left side in order to study in a common work frame.

$$1 \geq \dot{\bar{q}}^T \dot{\bar{q}} = \dot{\bar{r}}^T (\hat{J}\hat{J}^T)^{-1}\dot{\bar{r}} \tag{4.24}$$

$$1 \geq \bar{\tau}^T \bar{\tau} = \bar{F}_{ext}^T (\hat{J}\hat{J}^T)\bar{F}_{ext} \tag{4.25}$$

The maximum value of the right hand side of the Equations 4.24 and 4.25 are bounded by the magnitude of the input vectors which are set to 1 at maximum. Hence, the dominant factor in inequalities are the Jacobian matrices which are used to denote the velocity and force ellipsoids. Above, Jacobian matrices are separately denoted by taking the inverse as follows;

$$\hat{J}_{VJT} = (\hat{J}\hat{J}^T) \tag{4.26}$$

$$\hat{J}_{FJT} = (\hat{J}\hat{J}^T)^{-1} \tag{4.27}$$

where $\hat{J}_{VJT}$ and $\hat{J}_{FJT}$ denote the multiplied Jacobian matrices for the velocity mapping from the joint space to task space and force mapping from joint space to task space, respectively.

The eigenvectors and square root of eigenvalues of $\hat{J}_{VJT}$ and $\hat{J}_{FJT}$ terms are used to illustrate ellipsoids. The radii of the ellipsoids are determined by the square root of eigenvalues while the orientation of the ellipsoids are designated by eigenvectors. The ellipsoid term in here is a general name for the illustration. The definition changes depending on the size of the multiplied Jacobian matrices. In general notation, $n-1$ dimensional curve, surface or hypersurface is generated for a $n \times n$ multiplied Jacobian matrix. The

1-dimensional ellipses (curves) are illustrated for 2×2 multiplied Jacobian matrices and 2-dimensional ellipsoids (surfaces) are generated for 3×3 multiplied Jacobian matrices. The illustration of $n-1$- ellipsoid for $n > 3$ is not easy to plot and comprehend. However, it is possible to divide the Jacobian matrices into smaller submatrices to make it easy to plot and understand where one maps the linear velocities and the other maps the angular velocities.

The physical interpretation of the radii and the orientations of the $n-1$-ellipsoid depends on which one of the Jacobian matrix multiplication is investigated. The ellipsoid of $\hat{J}_{VJT}$ shows a velocity ellipsoid to illustrate the directional velocity amplification ratio in task space for an input from the joints space. In other words, the velocity ellipsoid of $\hat{J}_{VJT}$ illustrates how fast and to which direction the end effector moves for an input from the actuators. Similarly, the ellipsoid of $\hat{J}_{FJT}$ shows a force ellipsoid to denote the directional force/torque output performance in task space for a torque/force input from the actuators. These two ellipsoids highlight the output performance of the manipulator. Hence, the ellipsoids are defined in task space and frequently used in robotic applications.

There is one important thing that should be pointed out. Notice that, the force ellipsoid and velocity ellipsoid are inverses of each other. Thus, we can conclude that if it is easy to move the end-effector for specified a direction, the force which can be generated for that direction is low. Conversely, if the manipulator can generate a high amount of force for a direction, the motion performance along that direction will be low. This inverse relationship between the force ellipsoid and velocity ellipsoid can be observed in Figure 4.1 for a 2R manipulator.

For a haptic manipulator, it is desired that the manipulator should move easily in any direction with low amount of forces which is the definition of back-drivability. In addition, the force ellipsoid and velocity ellipsoid should have same and equal amplifications to any direction in order to feel same haptic interaction at anywhere within the workspace. However, the only condition for the force ellipsoid and velocity ellipsoid to achieve same amplification ratio to any direction is when the ellipsoids become spheres.

4.1.3. Condition Number

The condition number is a scalar representation of motion resolution of the end effector. It is first utilized by Salisbury and Craig (1982). They have used the condition number as a performance metric of force amplification/transmission ratio between the actuator inputs and end effector output. Remember that, the force/torque relation between
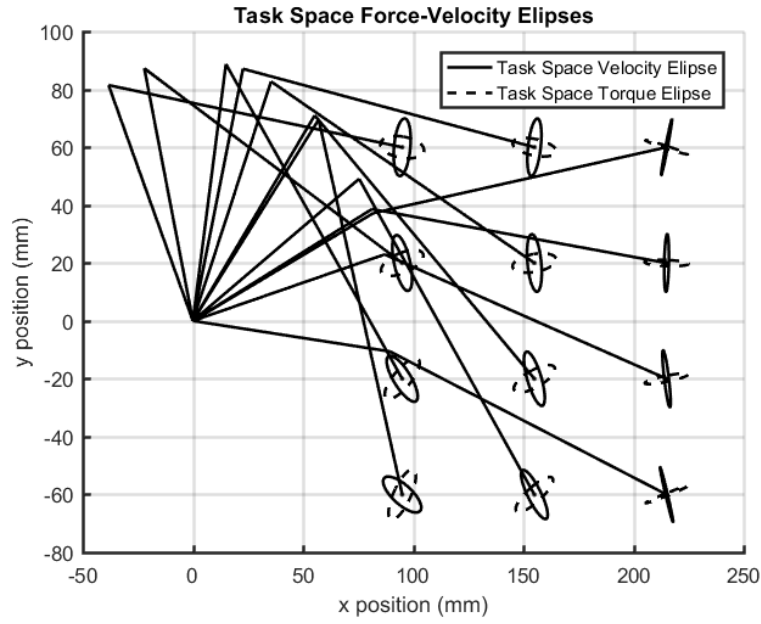
Figure 4.1. Task space velocity and force ellipse of a 2R Manipulator.

the joint and task spaces are established via the Jacobian matrix. Salisbury and Craig (1982) makes use of the relationship to procure the condition number by computing the ratio of the maximum to the minimum eigenvalues of the Jacobian matrix. In the same manner, condition number also represents the motion (also positioning) resolution of the end effector since the Jacobian matrix also maps the motion information between the spaces. The force/motion resolution performance of the manipulator is crucial to experience the small displacements and feel the small changes in force during haptic interaction.

To explain the condition number, first, the velocity and the force error relations between the spaces must be examined. Remember that, $\hat{J}$ is a mapping between the joint space and task space velocities. If the small increment in time is considered, the same Jacobian matrix is valid for the small amount of position and force change. Hence, the Equations 4.13 and 4.19 can be updated as follows;

$$\Delta \bar{r} = \hat{J} \Delta \bar{q} \tag{4.28}$$

$$\Delta \bar{\tau} = \hat{J}^T \Delta \bar{F}_{ext} \tag{4.29}$$

where Δ denote the small change in respective vector.

There are 2 possible ways to obtain the condition number either by using the Jacobian matrix or the transpose of the Jacobian matrix. First, the Jacobian matrix which maps the velocities between the spaces is used to obtain velocity condition number. Necessary,

steps to obtain condition number is described by Merlet (2006) by using the Euclidean norms ($\|.\|$) which defines the square root of the largest eigenvalue (or singular value) of a matrix. The norms of Equations 4.13 and 4.28;

$$\|\dot{\bar{r}}\| = \left\|\hat{J}\dot{\bar{q}}\right\| \leq \left\|\hat{J}\right\|\|\dot{\bar{q}}\| \text{ and } \left\|\hat{J}^{-1}\Delta\dot{\bar{r}}\right\| = \|\Delta\dot{\bar{q}}\| \leq \left\|\hat{J}^{-1}\right\|\|\Delta\dot{\bar{r}}\| \qquad (4.30)$$

$$\Rightarrow \|\Delta\dot{\bar{q}}\|\|\dot{\bar{r}}\| \leq \left\|\hat{J}\right\|\|\dot{\bar{q}}\|\left\|\hat{J}^{-1}\right\|\|\Delta\dot{\bar{r}}\| \qquad (4.31)$$

Divide both sides by $\|\dot{\bar{r}}\|$ and $\|\dot{\bar{q}}\|$;

$$\Rightarrow \frac{\|\Delta\dot{\bar{q}}\|}{\|\dot{\bar{q}}\|} \leq \left\|\hat{J}\right\|\left\|\hat{J}^{-1}\right\|\frac{\|\Delta\dot{\bar{r}}\|}{\|\dot{\bar{r}}\|} \qquad (4.32)$$

The norms of the Jacobian multiplications in Equation 4.32 indicates how much of the relative motion error in joint space is amplified to task space. This amplification relation is established with $\left\|\hat{J}\right\|\left\|\hat{J}^{-1}\right\|$, and is called the condition number. In more formal representation;

$$c_v(\hat{J}) = \left\|\hat{J}\right\|\left\|\hat{J}^{-1}\right\| \qquad (4.33)$$

where c_v denotes the condition number. Since one of the norms is $\left\|\hat{J}\right\|$ and the other is just the inverse $\left\|\hat{J}^{-1}\right\|$, the norm multiplication result as the ratio square root of maximum and minimum eigenvalues of $\hat{J}$.

The second approach to obtain the force condition number, which is originally described by Salisbury and Craig (1982), use the transpose of the Jacobian matrix. The same mathematical computations in Equations 4.30 and 4.31 is applied to Equations 4.19 and 4.29 to obtain the following Equation;

$$\frac{\|\Delta\bar{F}\|}{\|\bar{F}\|} \leq \left\|\hat{J}^T\right\|\left\|\hat{J}^{-T}\right\|\frac{\|\Delta\bar{\tau}\|}{\|\bar{\tau}\|} \qquad (4.34)$$

The norms of transpose of the Jacobian multiplications in Equation 4.34 indicates the ratio of the relative force amplification which is stated as force condition number given in Equation 4.35. Similar to velocity condition number, this relation is established by $\left\|\hat{J}^T\right\|\left\|\hat{J}^{-T}\right\|$. Note that $\left\|\hat{J}\right\| = \left\|\hat{J}^T\right\|$ and $\left\|\hat{J^{-1}}\right\| = \left\|\hat{J^{-T}}\right\|$. Thus, both condition number provides the same result. Therefore, the force condition number is equal to;

$$c_f(\hat{J}) = \left\|\hat{J}^T\right\|\left\|\hat{J}^{-T}\right\| \qquad (4.35)$$

Notice that condition number is a separate norm for each Jacobian matrix in force ellipsoid and velocity ellipsoid. The design objective is to convert the velocity and force ellipsoid into a sphere for any pose within the workspace. The spheres indicates that

equal force/motion performance can be exhibited by the manipulator along any direction. In this situation, the value of condition number becomes 1 which is the minimum possible and desired value for condition number since all eigenvalues are equal and force/velocity ellipsoids become coincident spheres. Hence, minimizing the condition number increases the kinematic performance of manipulator, and there is no need to separately check the force ellipsoid and velocity ellipsoid during design procedure since enhancing the performance of one of them enhances the other ones. If the condition number is equal to 1 for a pose of the manipulator, the pose is an isotropic pose. Similarly the condition number is computed to be 1 for all possible pose in the defined workspace, the workspace is an isotropic workspace.

4.1.4. Manipulability

Yoshikawa (1985b) proposed the manipulability measure to define the closeness to a singularity and easiness to move the end-effector. Most of the time manipulability is enough as the kinematic performance index as stated by Yoshikawa (1985b). However, if the designer desires both high performance in manipulability and condition number, these two indices should be considered in an objective function simultaneously because high performance in manipulability does not necessarily correspond to high performance in condition number. In fact, they are inversely related as indicated by Chiu (1988). Figure 4.2 show the inverse relation of a 2R manipulator in terms of condition number and manipulability.
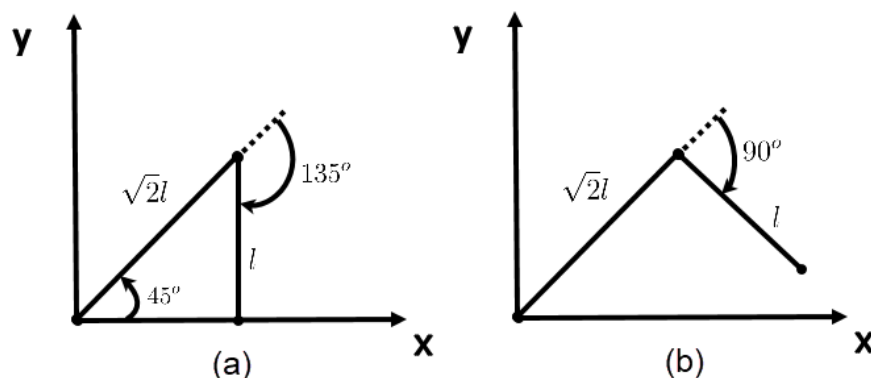
Figure 4.2. Isotropic pose (a) and highest manipulable pose (b) for a 2R manipulator.

Manipulability measure is related to the volume of the velocity ellipsoids as a scalar performance metric. The metric is given as follows;

$$\mu_v = \sqrt{\det\left(\hat{J}\hat{J}^T\right)} \tag{4.36}$$

where μ_v denotes the manipulability obtained via the velocity ellipsoid. The physical meaning of manipulability is the representation of the volume of velocity ellipsoid. For instance, the determinant of 3×3 translational Jacobian matrix will have a volume unit of m^3. However, for an $n \times n$ Jacobian matrix where both translational and rotational motion occurs, the unit of the manipulability loses its physical interpretation. This could be avoided via modifying the Jacobian matrix.

There are two problems of manipulability. One is its order dependency and the other is scale dependency as stated by Kim and Khosla (1991). The order dependency arises when a common performance measure is evaluated between the spatial or planar manipulator and depending on their degree of freedom. They propose;

$$\mu_{oi} = \sqrt[n]{\det\left(\hat{J}\hat{J}^T\right)} \tag{4.37}$$

where μ_{oi} denotes the order independent manipulability and n is the order of Jacobian matrix. This manipulability enables a fair comparison between different manipulators since with this measure they have the same unit. They solved the scale problem by dividing Equation 4.37 to the total link length of the manipulator. The problem may also be avoided by using characteristic length for normalization of the Jacobian matrix.

Another way to represent manipulability measure is by using its absolute value as proposed by Paul and Stevenson (1983). If the Jacobian matrices in Equation set 4.36 are square matrices, the resultant manipulability becomes the absolute values of Equation set 4.36 since $\hat{J}\hat{J}^T$ is the square of the Jacobian matrix. The formulation is given in Equation 4.38.

$$\mu_{av} = \left|\det\left(\hat{J}\right)\right| \tag{4.38}$$

Since the volume cannot get a negative value, the absolute value operation removes the sign change caused by the configuration of the manipulator.

If one of the ellipsoids' volume approaches 0, the ellipsoids take the form of 2-dimensional elliptic discs in 3-dimensional Cartesian space meaning that one of the eigenvalues approaches to 0. At the singularity, volume of the ellipsoid becomes 0 and condition number becomes infinite. According to manipulability measure, the manipulator cannot move anymore or the reason for the loss of manipulability cannot be determined.

Condition number, on the other hand, indicates that it cannot move along the eigenvector directions where the eigenvalue is equal to 0. However, it can still move to other directions. In the design process, manipulability can be used as performance metric but if the resolution quality is the desired objective, the condition number is still required since manipulability cannot distinguish the directional quality.

4.1.5. Effect of the Jacobian Matrix on Performance Metrics

Most of the performance metrics in Section 4.1 use the Jacobian matrix. Yet, it is hardly stated how a Jacobian matrix should be formed. In this section, first, the effects of the form of Jacobian matrix on the performance metrics are discussed and then, the requirements for the Jacobian matrix to be used it in performance metrics are explained.

4.1.5.1. Jacobian Matrix Effect on Condition Number and Manipulability Optimization

Optimization is achieved under the constraints to avoid the non-logical solutions. In manipulator design, generally, either the workspace is prescribed or the joint angles and link lengths are constrained. However, this is not enough to conclude that the optimization algorithm results in optimum solutions. Also, the objective function must have the proper form for optimization. In motion related performance metrics the Jacobian matrix should be normalized and dimensionally homogeneous.

The optimization problem changes depending on the consideration of the condition number or the manipulability. In terms of condition number optimization, the first method is to keep the link lengths constant and find the workspace where the condition number is at a minimum. This kind of optimization results with a workspace which contains only one discrete pose which has the same relative error amplification in any direction. Changing the position of this point or increasing the number of the discrete points (meaning increasing the size of the workspace) decreases the resolution of the manipulator. Second, if the workspace is predetermined and the link lengths are to be optimized, this time optimization algorithm will try to increase the link length to an infinite value so that the relative size of workspace with respect to the size of the manipulator becomes negligible. Since the desired workspace is an isotropic workspace, the variation in condition number is at the minimum when the workspace is at a single pose or very

small compared to the reachable workspace. The problems here are caused by the scaling problem of the Jacobian matrix.

In order to understand the problems for manipulability index, a 2R mechanism is used as a example. The determinant of Jacobian matrix in analytical form is defined as follows;

$$\mu_v = |l_1 l_2 \sin q_2| \tag{4.39}$$

where l_1 and l_2 are the respective link lengths and q_2 is the relative angle between the link.

Increasing manipulability is the desired objective. As it can be seen in Equation 4.39, there are two ways to do it. When the link lengths and the relative angles are designed, increasing the manipulability is achieved by either increasing the link lengths or operating near 90° for q_2. However, during link length synthesis, the amplification of link lengths on manipulability is the dominant factor compared to sine function is bounded between ± 1. Hence, manipulability enhancement results increasing in l_1 and l_2 which eventually both approach to infinite values.

The problem in optimization using both performance metrics is not the workspace or geometric constraints but the definition of the Jacobian matrix since the optimization algorithm cannot distinguish the scale of the manipulator.

Another common problem for both performance metrics is the dimensional consistency of the computed metric. The Jacobian matrix contains both the translational and rotational motion information. Mathematical operations for condition number and manipulability mixes these different units hence the performance metrics lose their physical meanings.

4.1.5.2. Normalized and Dimensionally Homogeneous Jacobian Matrix

For the problems described in Section 4.1.5.1, there is a simple method for a solution which is to use the normalized Jacobian matrix. Such a method was proposed by Stocco et al. (1998). They normalized and bounded elements of the Jacobian matrix between 0 and 1. The method they proposed uses pre and post-multiplication of the Jacobian matrix with diagonal scaling matrices.

Another method is introduced by Angeles (2002). He used the characteristic length to obtain normalized and unity Jacobian matrix. The characteristic length is defined

as follows;

$$L = \frac{R_d}{R_a} \quad (4.40)$$

R_d is the maximum desired reach and R_a is the maximum actual reach which can be achieved by synthesized link lengths. For a normalized Jacobian matrix the desired reach is $R_d = 1$. The normalized Jacobian matrix is obtained by multiplying Equation 4.40 with the Jacobian matrix as follows;

$$\hat{J}_n = L\hat{J} \text{ for } R_d = 1 \quad (4.41)$$

where $\hat{J}_n$ is the normalized Jacobian matrix. With this method, links are defined to be the ratios of each other. After finding link ratios, the desires workspace can be achieved just by multiplying the normalized Jacobian matrix with desired reach R_d.

The method can easily be applied to 2R mechanism as follows;

$$\hat{J}_n = \begin{bmatrix} -r_1 sin(\theta_1) - r_2 sin(\theta_{12}) & -r_2 sin(\theta_{12}) \\ r_1 cos(\theta_1) + r_2 cos(\theta_{12}) & r_2 cos(\theta_{12}) \end{bmatrix} \quad (4.42)$$

where $\hat{J}_n$ and r_1, r_2 denote the normalized Jacobian matrix and link ratios, respectively. $r_1 = l_1/(l_1 + l_2)$ and $r_2 = l_2/(l_1 + l_2)$ for 2R system. The relation between the normalized Jacobian matrix and the Jacobian matrix;

$$\hat{J} = R_d\hat{J}_n \quad (4.43)$$

$$R_d = l_1 + l_2 \quad (4.44)$$

Performance metrics in section 4.1 relies on the Jacobian matrix to extract a physical meaning from the manipulator to comprehend the manipulator's quality. If, however, Jacobian matrix does not have unit homogeneity, the outputs of the performance metric have unit inconsistency. For instance, from the aspect of manipulability, if the elements of Jacobian contain [Length] and [Angle] coefficients, the output is [Length]×[Angle]. Similarly, the condition number has the unit ratio of [Length]/[Angle] which should be only a unitless scalar amplification ratio.

The issue is avoided by using Plücker Coordinates to denote the Jacobian matrix as stated by Khan and Angeles (2006). Plücker Coordinates use dimensionally homogeneous space. Thus, the dimensionally homogeneous Jacobian matrix is obtained. Dimensionally, homogeneous and normalized Jacobian matrix removes the scaling and unit problem of the kinematic performance metrics.

4.2. Stiffness

Maximum impedance is the measure of maximum force output of the haptic device which is generally determined by actuators' maximum output. Higher the actuator torque, higher is the maximum impedance that can be felt unless the manipulator mechanically fails. From this aspect, maximum impedance is limited with the maximum force capacity of the manipulator. If the manipulator has high strength, it can endure high wrenches.

Although higher mechanical strength might ensure that the structure will not fail under larger loads, this may not be enough to conclude that manipulator has a high performance. Since the manipulator has a certain amount of compliance, the force interaction in terms of force fidelity will not have an accurate output. For instance, stiff interactions such as an impulse or touching a stiff wall in a haptic application will be reflected as softer interaction due to the compliance in manipulator structure. This will reduce the overall haptic quality and the accuracy of perception of haptic interaction. Therefore, compliant manipulators are not preferred for haptic systems and compliance is an index which should be minimized.

Most of the time, haptic interactions is coupled with other haptic feedbacks such as vision or sound. The inconsistency between the haptic feedbacks reduces the haptic perception quality. Maybe the most important relationship among these feedbacks is the relation of force and visual feedback or visuo-haptics. The visual consistency between the slave environment and the master system is determined by positioning coupling. For instance, while the user is touching a stiff object in a slave environment, if he still experiences position change in the master system the perception will not be a perfect one. Therefore, positioning accuracy is another important issue for haptic manipulators.

Another problem of compliant manipulators is the kinematic problems that may be caused. The bending in these kinds of manipulators may cause configuration change near the boundary of the workspace. The configuration changes cause failure in the model of the device by making it uncontrollable. In fact, most of the time, mechanism locks itself, enters a singularity condition or an unstable configuration.

The main measure that in the focus of the above problems is the stiffness property of the manipulator. Stiffness determines the angular and translational deflection robustness of the manipulator against the applied wrenches. In general, high stiffness corresponds to high structural strength and a stiff manipulator can carry high loads without bending. In other terms, stiffness specifies the maximum impedance and positioning ac-

curacy of the haptic manipulator. Therefore, stiffness is one of the main performance indices to determine the quality of the haptic manipulators and has to be included as a design objective which should be maximized.

The deflections from nominal (unbended) position can be compensated with a control strategy by using real-time position feedback from the end-effector. The position of the end-effector cannot be computed by using the feedback from the encoders at joints since they will not measure the elastic deflections on links. Hence, direct position measurement is required from the end-effector via laser or camera systems which are costly, not suitable to use in real-time and most of the time cannot be applicable due to the working environment. Using springs increases the non-linearity in the model, so it is difficult to handle. Consequently, designer prefers to estimate the end-effector position by means of stiffness (kinetostatic) model of the manipulator.

Perfectly rigid materials do not exist, thus, deflections of the links will always occur. Although the positioning errors caused by the deflections can be compensated via control, the maximum load capacity and stiffness of the manipulator are still mechanical properties. Hence, no matter how well the control is, haptic interaction is always limited by mechanical properties. For this reason, maximizing the mechanical stiffness is in the focal point of the high impedance performance rather than a control system design.

4.2.1. Factors Effecting the Stiffness

By increasing the stiffness performance, the deflections can be reduced. In order to achieve this, the reasons causing the deflections and factors affecting the stiffness should be exposed and understood. There are two main causes of deflection in parallel haptic manipulators. One is the wrenches either applied externally on the manipulator or composed internally in the manipulator. The other one is geometrical errors which cause internal stresses and result is deflections of the links. The factors affecting the stiffness for parallel manipulators are listed as material properties (elasticity modulus, density, yield strength, shear modulus) and geometry of the links (second moment of area, link lengths, volume).

Deflections can be reduce by removing the external wrenches, however, it is against the purpose of a haptic manipulator which is built to reflect forces to the user. The internal wrenches (internal stresses), on the other hand, can be reduced. There are two main causes of these stresses. First one is the geometrical (manufacturing) errors in construction. Since parallel manipulators comprise serial kinematic chains and these se-

rial chains have to have the same pose where they are connected to the platform, an error in the dimension of these serial chains will cause internal stresses which will also cause deflections in the links. The second one is the weight of the links and joints which will increase the load on the mechanism.

Geometrical errors are related with manufacturing or assembling problems. Precise manufacturing and flexible assembling techniques or assembling with fixtures can highly reduce this problem.

Internal wrenches, on the other hand, are difficult to deal with. For high stiffness, thick and short links are needed. However, thick links increase the weight of the manipulator which causes more bending and deflection. Short links may reduce weight but it causes lack of kinematic performance in manipulator so it is not the preferred option in design. Therefore, the problem of stiff design for a haptic manipulator is an optimization trade-off problem between the inertia and stiffness. Designers prefer to use high stiffness-to-weight ratio materials to minimize the compliance with least amount of added weight.

Another factor which defines the manipulator stiffness is the joint stiffness. In practice, joints have more effect on bending compared to links since the joints are the locations where the loads are visually accumulated. Another reason is that they are a combination of sub-parts with different stiffness properties. In addition, they have clearance and friction which makes them difficult to model. Therefore, the most suitable solution for joints is to use pre-loaded high-quality bearings and calibrate the manipulator after production. There are also other factors such as temperature which causes the change in material properties and the geometry. However, such subjects are beyond the interest of this thesis.

4.2.2. Stiffness Matrix and Modeling Methods

The stiffness model of a manipulator can be defined in matrix form. In literature, this matrix is known as stiffness matrix and represented as $\hat{K}$. The inverse of stiffness matrix is the compliance matrix and it is also used and represented as $\hat{k}$, $\hat{C}$ or $\hat{c}$ in the literature. The $\hat{K}$ stiffness matrix can be defined in both joint-space as $\hat{K_\theta}$ or as $\hat{K_C}$ in Cartesian (task) space. The relation between these stiffness matrices can be established via Jacobian matrices (Ciblak and Lipkin, 1999). This makes the Cartesian stiffness matrix pose and configuration dependent (Alici and Shirinzadeh, 2005). Huang et al. (2002) introduced the conservative congruence transformation method which relates the pose changes and stiffness matrix.

The size of the stiffness matrix of a single link is 6×6 and this matrix is symmetrical, semi-definite, non-negative in joint-space and always conservative. Simple models assume that the stiffness matrix of a link in joint-space is a diagonal matrix. More accurate models, however, to use a non-diagonal stiffness matrix (Connor, 1976). Stiffness matrix has same matrix properties in Cartesian Space unless there is a pre-load on the manipulator. If there is pre-load on the manipulator, asymmetry can be observed. Kövecses and Angeles (2007) pointed out the conditions when an asymmetric stiffness matrix occurs and how a symmetric stiffness matrix can be obtained. Griffis and Duffy (1993) have investigated the non-diagonal, non-symmetric Cartesian stiffness matrix under applied wrenches and derived a simple model of stiffness matrix. Howard et al. (1998) showed that the Cartesian stiffness matrix is non-symmetrical for non-zero wrenches by using Lie groups and they introduced a method which uses appropriate moving reference frames to obtain a symmetric stiffness matrix.

In literature, the general approach to construct stiffness matrix is to assume that there is no load on the system other than the forces applied on the end-effector. In this approach, it is assumed that the manipulator is in unloaded mode. The derived stiffness matrix depending on this assumption is simple and may be linearized thus, it is easy to be calculated. In the loaded mode, computations become more complex and the system becomes highly nonlinear since, in this mode, internal stresses and weights of links are included. The computation in this mode requires an iterative solution to calculate the end-effector deflection. Yet, it is more accurate compared to the results actually unloaded mode. The computational complexity of this mode can be reduced via elimination of some of the DoF in compliant links if there is no force or the force is relatively small compared to other forces in those DoFs.

The stiffness modeling methods using the loaded mode and unloaded mode approaches can be divided into three groups as Finite Element Method (FEM), Matrix Structural Method (MSM), and Virtual Joint Method(VJM) which are shown in Figure 4.3 by indicating the modeling technique.

Among them, FEM produces the most accurate results. In FEM, the components of a manipulator are decomposed into small discrete elements and each element is connected to each other with nodes. By calculating the deflections in these nodes with respect to applied forces, stiffness model of the manipulator can be obtained by using kinematic and material properties. This method is computationally intensive. Thus, it cannot be used in real-time applications. However, this method can handle the links and joints which have complex shapes. Consequently, this method is preferred at the final stage of
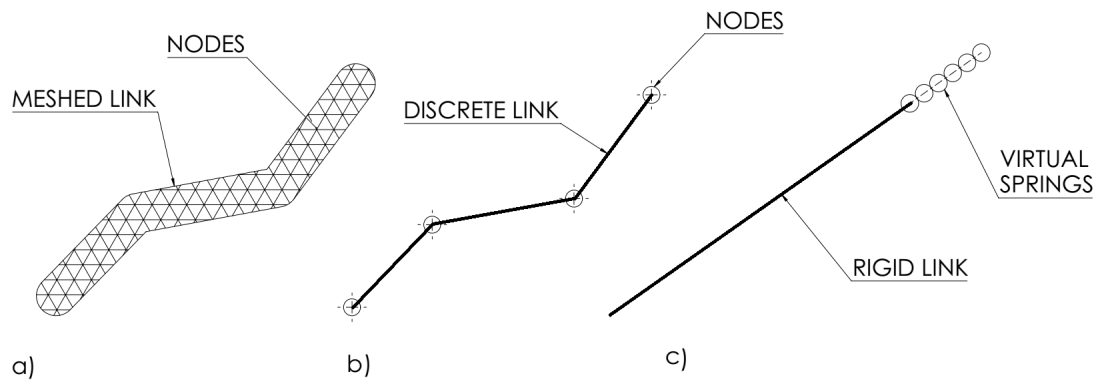
Figure 4.3. Stiffness Modeling Methods. a) Finite Element Method, b) Matrix Structural Method, c) Virtual Joint Method

the design to analyze the global stiffness of the manipulator.

The second method, MSM is a similar method to FEM. Yet, it is more simple and computationally less intensive. Both methods use discrete elements and nodes. In MSM, however, the discretization step is larger and the elements are modeled as simple structural elements like beams (Martin, 1966). The stiffness information of discrete parts are lumped on both side of the part. By this means, it is less complex than FEM. However, it still requires a considerable amount of computation power.

The final method is VJM. In VJM, the links are assumed to be rigid, and the stiffness information of the link is accumulated in a virtual spring with three rotational and three translational DoF. The spring is attached at the end of the rigid link as a 6 DoF joint. The advantages of this method compared to above ones are that it needs less computation power, it is easier to analytically represent, and it has a good accuracy with respect to required computation power. Also, this model can easily be updated for complex shapes via using the results of FEM. Therefore, the adopted model in this thesis is VJM.

4.2.3. Stiffness Matrix Calculation with Virtual Joint Method

The technique is first used by Salisbury (1980) for control system design to represent the actuation stiffness. Later, it has been extended for structural stiffness of serial manipulators. The stiffness of a joint and its coupled link is lumped on the virtual joint (Gosselin, 1990). First time, the stiffness matrix is formulated by VJM for parallel mechanism by Gosselin (2002) and Majou et al. (2007). In the works of Pashkevich et al.

(2009) and Pashkevich et al. (2011), this application is further developed and simplified.

Currently, most of the stiffness studies are devoted to serial manipulators. Obtaining the stiffness matrix defined in Cartesian space of these manipulators are easy compared to parallel ones since the parallel manipulators are more complex in terms of kinematics. For parallel manipulators, all kinematic chains are computed simultaneously for stiffness modeling because the stiffness model must be in equilibrium for both statics and kinematics (Gosselin, 1990). In the study of Klimchik (2011), the serial chains of parallel manipulators are first computed separately and then aggregated. This method makes the analytical representation simpler and the Cartesian stiffness matrix turns out to be a simple summations of stiffness matrices of each serial chain.

Stiffness matrix is calculated based on forward kinematics, static equilibrium and Hooke's Law (Gosselin, 1990; Duffy, 2007). These equations can be stated as follows;

$$\Delta \bar{\kappa} = \hat{J}_K \Delta \bar{Q} \tag{4.45}$$

$$\hat{J}_K = \begin{bmatrix} \hat{J}_\theta & \hat{J}_p \end{bmatrix} \tag{4.46}$$

$$\Delta \bar{Q} = \begin{bmatrix} \Delta \bar{\theta}^T & \Delta \bar{q}_p^T \end{bmatrix}^T \tag{4.47}$$

$$\Delta \bar{\kappa} = \hat{J}_\theta \Delta \bar{\theta} + \hat{J}_p \Delta \bar{q}_p \tag{4.48}$$

$$\bar{F}_K = \hat{J}_K^T \bar{F}_{ext} \tag{4.49}$$

$$\bar{F}_K = \hat{K}_\theta \Delta \bar{\theta} \tag{4.50}$$

where $\Delta \bar{\kappa}$ denotes the platform deflection in Cartesian space including both deflections in the translation and rotation, $\hat{J}_\theta$ is the Jacobian matrix including the virtual joints, $\hat{J}_p$ is the Jacobian matrix including the passive joints, $\hat{J}_K$ is the combined Jacobian matrix including virtual and passive joints, $\Delta \bar{\theta}$ is the deflection in virtual joint space (both deflections in rotational and translational calculated for virtual joints), $\Delta \bar{q}_p$ is the change in the position of passive joints, $\Delta \bar{Q}$ is the combined deflections including the virtual and passive joints, $\bar{F}_K$ is the reaction force and moment matrix in joint-space due to $\bar{F}_{ext}$ which is the applied wrenches to platform in task-space, and finally, $\hat{K}_\theta$ is the joint space stiffness matrix which relates the joint space deflections and the applied external wrenches. The size of the $\hat{K}_\theta$ matrix depends on the number of the virtual joints. Diagonal $\hat{K}_\theta$ is defined as follows for an n number of 6-DoF virtual joints.

$$\hat{K}_\theta = diag\big(\begin{bmatrix} \hat{K}_{\theta_1} & \hat{K}_{\theta_2} & \cdots & \hat{K}_{\theta_n} \end{bmatrix}_{6n \times 6n} \big) \tag{4.51}$$

In order to obtain the Cartesian stiffness matrix, Equations 4.48, 4.49, and 4.50 are manipulated and the following relations are established;

$$\hat{J}_p^T \bar{F}_{ext} = \bar{0} \tag{4.52}$$

$$\hat{J}_\theta^T \bar{F}_{ext} = \hat{K}_\theta \Delta \bar{\theta} \qquad (4.53)$$

$$\bar{F}_{ext} = (\hat{J}_\theta \hat{K}_\theta^{-1} \hat{J}_\theta^T)^{-1} \Delta \bar{\kappa} \qquad (4.54)$$

$$\hat{K}_{Ci} = (\hat{J}_\theta \hat{K}_\theta^{-1} \hat{J}_\theta^T)^{-1} \qquad (4.55)$$

where $\hat{K}_{Ci}$ is Cartesian stiffness matrix. The right-hand side of the equation is the mapping of Joint stiffness matrix to Cartesian which is Conservative Congruency Transformation (Huang et al., 2002).

Auxiliary wrenches, the weights of the links, and the dynamic wrenches acting on the intermediate virtual joints can also be modeled via VJM. These wrenches can be expressed in Cartesian space and mapped to Joint space.

$$\hat{J}_{\theta a}^T \bar{F}_{aux} + \hat{J}_{\theta d}^T \bar{\tau}_\theta + \hat{J}_{\theta g}^T \bar{G} + \hat{J}_\theta^T \bar{F}_{ext} = \hat{K}_\theta \Delta \bar{\theta} \qquad (4.56)$$

where $\hat{J}_{\theta a}$, $\hat{J}_{\theta d}$ and $\hat{J}_{\theta g}$ denote the extended Jacobian matrices for auxiliary wrenches, dynamic wrenches and the weights of the links. $\bar{F}_{aux}$, $\bar{\tau}_\theta$, and $\bar{G}$ are the vectors containing auxiliary wrenches, dynamic wrenches and the weights of the links, respectively.

The Cartesian space stiffness matrix, $\hat{K}_C$ of the manipulator is computed by summing the stiffness matrix of each serial chain of the manipulator as shown in Equation 4.57. $\hat{K}_{Ci}$ is the Cartesian stiffness matrix which belongs the ith serial chain.

$$\hat{K}_C = \sum_{i=1}^{3} \hat{K}_{Ci} \qquad (4.57)$$

$\hat{K}_C$ is later used for stiffness performance evaluation of the manipulator.

4.2.4. Stiffness Matrix for Composite Link Design

$\hat{K}_\theta$ is diagonal if the forces and torques are decoupled. This simplifies the calculations. However, in reality, non-diagonal stiffness matrix represents a more realistic case. Hence, $\hat{K}_\theta$, for the links made from isotropic materials, is defined by Connor (1976) as;

$$\hat{K}_{\theta_k} = \begin{bmatrix} \frac{E_k A_k}{L_k} & 0 & 0 & 0 & 0 & 0 \\ 0 & \frac{12 E_k I_{zk}}{L_k^3} & 0 & 0 & 0 & \frac{-6 E_k I_{zk}}{L_k^2} \\ 0 & 0 & \frac{12 E_k I_{yk}}{L_k^3} & 0 & \frac{6 E_k I_{yk}}{L_k^2} & 0 \\ 0 & 0 & 0 & \frac{G_{xyk} J_k}{L_k} & 0 & 0 \\ 0 & 0 & \frac{6 E_k I_{yk}}{L_k^2} & 0 & \frac{4 E_k I_{yk}}{L_k} & 0 \\ 0 & \frac{-6 E_k I_{zk}}{L_k^2} & 0 & 0 & 0 & \frac{4 E_k I_{zk}}{L_k} \end{bmatrix} \qquad (4.58)$$

where A_k, I_{zk}, I_{yk} are the area and the second moments of the link cross-section, E_k and G_{xyk} are the Young and Coulomb modules of material, J_k is the polar moment. Sub-script k denotes k^{th} link. A generic link and its axes alignment of the stiffness matrix $\hat{K}_{\theta_k}$ is shown in Figure 4.4
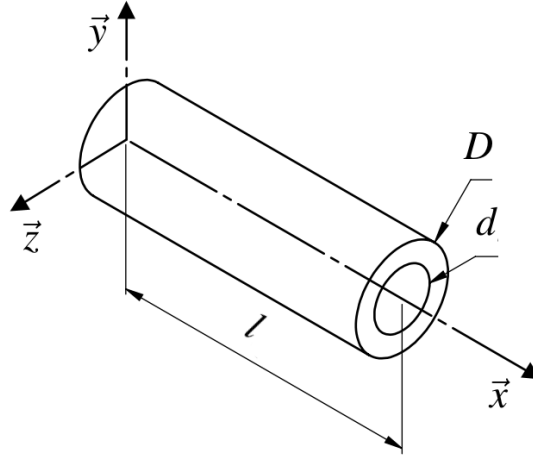
Figure 4.4. Dimension parameters and the axes alignment of a single link. D, d, and l denote the outer and inner diameters and the link length.

Standard stiffness matrix of the materials includes the internal stress-deformation. In VJM, internal stress and deformations are omitted. Only the macro scale deformations with respect to applied wrenches are considered. Nevertheless, $\hat{K}_{\theta_k}$ still contains the material parameters E_k and G_{xyk}. Note that, $\hat{K}_{\theta_k}$ defined above, is formulated with the assumption that the material is isotropic. Orthotropic (composite) materials, on the other hand, has different stiffness matrix in micro-scale (Jones, 1975). This difference also affects the macro-scale deflections. Thus, a little manipulation on $\hat{K}_\theta$ is required to make it compatible with the application. This modification can be achieved as follows;

$$\hat{K}_{\theta_k} = \begin{bmatrix} \frac{E_{xk}A_k}{L_k} & 0 & 0 & 0 & 0 & 0 \\ 0 & \frac{12E_{yk}I_{zk}}{L_k^3} & 0 & 0 & 0 & \frac{-6E_{zk}I_{zk}}{L_k^2} \\ 0 & 0 & \frac{12E_{zk}I_{yk}}{L_k^3} & 0 & \frac{6E_{yk}I_{yk}}{L_k^2} & 0 \\ 0 & 0 & 0 & \frac{G_{xyk}J_k}{L_k} & 0 & 0 \\ 0 & 0 & \frac{6E_{yk}I_{yk}}{L_k^2} & 0 & \frac{4E_{yk}I_{yk}}{L_k} & 0 \\ 0 & \frac{-6E_{zk}I_{zk}}{L_k^2} & 0 & 0 & 0 & \frac{4E_{zk}I_{zk}}{L_k} \end{bmatrix} \tag{4.59}$$

where, E_{xk}, E_{yk}, E_{zk} and G_{xyk} are the Young and Coulomb modules of kth composite linkage for corresponding axes and $E_{yk} = E_{zk}$.

Determination of E_{xk}, E_{yk}, E_{zk} and G_{xyk} requires more attention on composite materials. Composite materials are combinations of at least two materials, usually one being fiber and the other being the matrix (the glue). They form lamina together (only one layer composite sheet). Then, laminae are used to form the laminate by placing them in different orientations (see Figure 4.5).
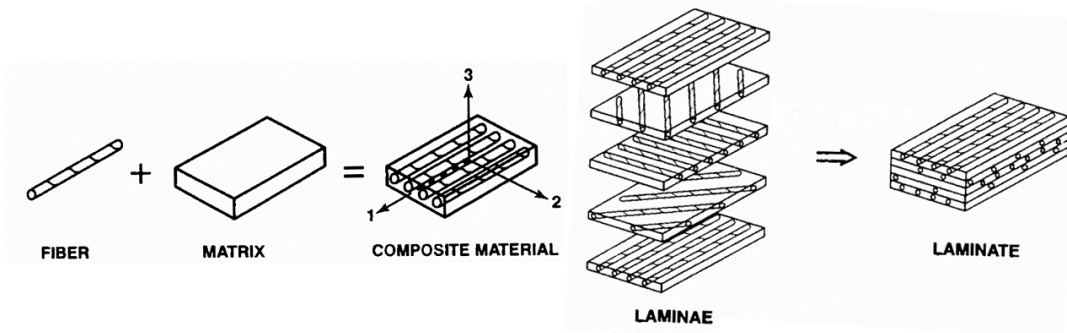
Figure 4.5. Composite material structure.
(Source: Jones 1975)
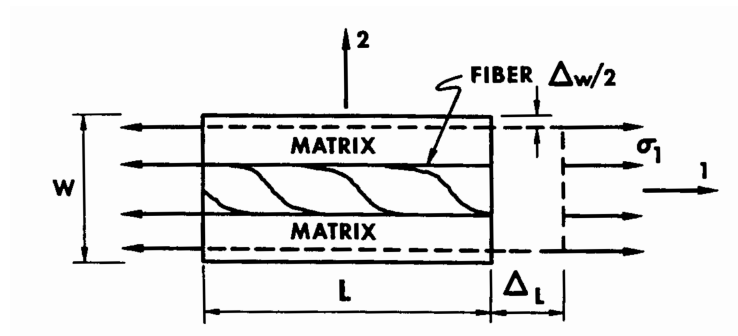
Figure 4.6. Representative Volume Element Loaded in 1-Direction.
(Source: Jones 1975)

Laminate is the final product to be used as linkage. The calculation of Young and Coulomb modulus of laminate must start from the fiber and matrix. The formulation by referring Figure 4.6 is as follows;

$$E_1 = E_f V_f + E_m V_m \tag{4.60}$$

$$E_2 = \frac{E_f E_m}{V_m E_f + V_f E_m} \tag{4.61}$$

$$v_{12} = -\frac{\varepsilon_2}{\varepsilon_1} \tag{4.62}$$

$$v_{21} = -\frac{E_2}{E_1}v_{12} \tag{4.63}$$

$$\varepsilon_1 = \frac{\Delta L}{L} \tag{4.64}$$

$$\varepsilon_2 = \frac{\Delta w}{W} \tag{4.65}$$

$$G_{12} = \frac{G_m}{V_m + V_f(G_m/G_f)} \tag{4.66}$$

where E_1, E_2, and G_{12} are the Young and Coulomb modulus of composite material along 1 and 2 axes. E_f, and E_m are the Young modulus of fiber and matrix. V_f and V_m are the volume fractions of fiber and matrix in composite material. G_f and G_m are the Coulomb modulus of fiber and matrix. v_{12} and v_{21} are Poisson ratios.
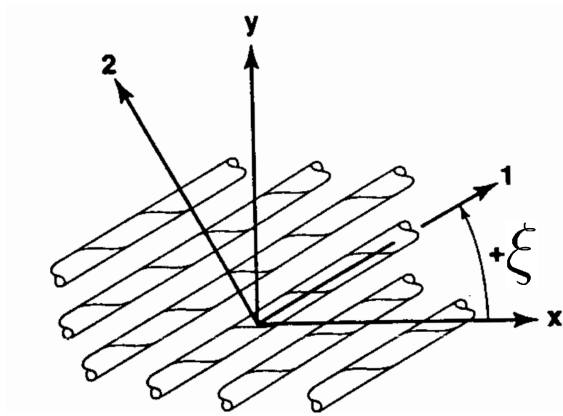
Figure 4.7. Positive rotation of composite material frame axes from x-y axes.
(Source: Jones 1975)

The final step is to calculate the mechanical properties of Laminate in global axes, see Figure 4.7.

$$\frac{1}{E_x} = \frac{1}{E_1}\cos^4(\xi) + \left(\frac{1}{G_{12}} - \frac{2v_{12}}{E_1}\right)\sin^2(\xi)\cos^2(\xi) + \frac{1}{E_2}\sin^4(\xi) \tag{4.67}$$

$$\frac{1}{E_y} = \frac{1}{E_1}\sin^4(\xi) + \left(\frac{1}{G_{12}} - \frac{2v_{12}}{E_1}\right)\sin^2(\xi)\cos^2(\xi) + \frac{1}{E_2}\cos^4(\xi) \tag{4.68}$$

$$\frac{1}{G_{xy}} = 2\left(\frac{2}{E_1} + \frac{2}{E_2} + \frac{4v_{12}}{E_1} - \frac{1}{G_{12}}\right)\sin^2(\xi)\cos^2(\xi) + \frac{1}{G_{12}}(\sin^4(\xi) + \cos^4(\xi)) \tag{4.69}$$

One thing to be noticed is that the angle ξ is a parameter that the designer specifies. That is one of the main reasons why a composite material would be chosen for link material. Since an isotropic stiffness matrix $\hat{K}_\theta = \hat{K}_\theta(E, A, L, G, J, I_z, I_y)$, by making use of composite materials, the designer recieve have an extra parameter to be designed $\hat{K}_\theta = \hat{K}_\theta(E_x, E_y, A, L, G_{xy}, J, I_z, I_y)$, which gives extra flexibility in design. By adjust-

55

ing ξ and lay up of composite sheets, it is possible to obtain desired link strength in certain directions with minimum amount of material.

4.2.5. Stiffness Performance Metrics

The evaluation of the stiffness of the manipulator directly is conducted using $\hat{K}_\theta$ or $\hat{K}_C$. Evaluation of $\hat{K}_\theta$ only reveals the stiffness of the links. Yet, inspecting the $\hat{K}_C$ gives the stiffness performance of the manipulator in which the kinematics is included.

Since $\hat{K}_C$ is a matrix, standard matrix operations such as singular value decomposition (SVD), determinant, and norm operations can be applied as shown by Carbone and Ceccarelli (2010). Each operation exhibits specific performance criteria of the stiffness of the manipulator.

First, application of SVD operation on $\hat{K}_C$ discloses the stiffness property of each rotation and translation axis. SVD operation for $\hat{K}_C$ for an n DoF manipulator is shown as follows;

$$SVD(\hat{K}_C) = \hat{L}\hat{E}\hat{R} \tag{4.70}$$

$$\hat{E} = diag([e_1, e_2, ..., e_6]) \tag{4.71}$$

where $\hat{L}$, $\hat{R}$, and $\hat{E}$ denote the left, right singular matrices containing the singular vectors and singular values, respectively. e_i for $i = 1, 2, ..., 6$ are the singular values of the matrix $\hat{K}_C$. A direct evaluation of the magnitude of e_n values exhibits the stiffness performance of the manipulator along the nth axis of Cartesian space. By using singular vectors and singular values, the stiffness performance can be graphically illustrated. The illustration, however, results in similar stiffness ellipsoids with the force ellipsoids. The reason is that the variables of $\hat{K}_C$ are the kinematic variables.

In terms of a haptic manipulator, an even stiffness distribution in the workspace is desired for even force distribution. The scalar performance metric which evaluates the stiffness uniformity or stiffness condition number is obtained by making use of the Euclidean norms of $\hat{K}_C$ and $\hat{K}_C^{-1}$. The stiffness uniformity index S_e is shown in the following equation.

$$S_e = \|\hat{K}_C\|\|(\hat{K}_C)^{-1}\| \tag{4.72}$$

Obviously, $S_e = 1$ when the uniformity is achieved. The manipulator which contains revolute joints has an isotropic pose, path or surface in terms of stiffness due to the non-linear effects of revolute joints.

Not only the uniformity but also the magnitude of the stiffness is vital to determine the design with better stiffness performance. An average evaluation of stiffness matrix is conducted via Frobenius norm of $\hat{K}_C$. The index S_f gives the average stiffness value of the manipulator for a given pose.

$$S_f = \sqrt{tr(\hat{K}_C \hat{K}_C^T)} \tag{4.73}$$

Another method of evaluation of $\hat{K}_C$ is to apply the determinant operation. Similar to force and velocity ellipsoids, the determinant is related to the volume of stiffness ellipsoids. High volumes are the indication of a stiff manipulator. The index S_d is defined as the determinant of $\hat{K}_C$.

$$S_d = \det\left(\hat{K}_C\right) = \det\left(\hat{J}_\theta \hat{K}_\theta^{-1} \hat{J}_\theta^T\right)^{-1} \tag{4.74}$$

4.3. Dynamics

Dynamic property of the manipulator is the main protagonist which designates the minimum impedance. The minimum impedance is where no force is desired to be reflected to the user while the end-effector is moved by the user. Even if the weight of the manipulator and frictions are compensated, there is still dynamic wrenches felt by the user. The dynamic wrenches can partially be compensated via a proper control method, but cannot be fully diminished. In addition, the control strategy is limited by the mechanical properties of the manipulator and actuators. In high-frequency operations, for instance, the manipulator can be controlled if and only if the natural frequency of the manipulator is large enough. Therefore, the total inertia of the manipulator must be as low as possible so that the control exhibits its best performance. To indicate the effect of dynamics, a generic transfer function for a parallel connected mass-spring-damper system is written in the s domain, in the following equations.

$$F = m\ddot{x} + b\dot{x} + kx \tag{4.75}$$

$$F(s) = msV(s) + bV(s) + \frac{k}{s}V(s) \tag{4.76}$$

$$Z(s) = \frac{F(s)}{V(s)} = ms + b + \frac{k}{s} \tag{4.77}$$

where m, b, and k are the mass, damper, and spring constants of the mechanical system, respectively. x is the position of the system with respect to inertial frame and $V(s)$ denotes

the speed in the s domain. Assuming that for an ideal system, $b = 0$ then, $Z(s)$ is updated as follows.

$$Z(s) = ms + \frac{k}{s} \tag{4.78}$$

Notice that, while the system is in motion only factor affecting the impedance is the mass of the system since k is position dependent. If the mass is small, the impedance during free motion will be low. When the natural frequency of the system in Equation 4.79 is inspected, it can be seen that reducing the mass increases the frequency range.

$$\omega_n = \sqrt{\frac{k}{m}} \tag{4.79}$$

4.3.1. Dynamic Model of the Manipulator

In order to implement the dynamic objectives into the design procedure, the dynamic model of the system must be obtained. There are two main methods to procure the model, Newton-Euler method, and Energy-based methods. Newton-Euler method is mostly used when the design is in the focal point of the study since by Newton-Euler method the dynamic wrenches on the intermediate passive joints are also computed. Among the energy based methods, since the Lagrange's method only relates to the actuated joints and the mobile platform, it is mostly considered as a black box approach. Yet, with proper modification in forwarding kinematics, Lagrange's method can also be used in the calculation of reaction wrenches at the passive joints. Using virtual joints, Lagrange's method can be used in a systematic way, and auxiliary wrenches can also be included in the calculation of the stiffness.

Dynamics is the last stage of the design. In literature, almost no dynamics oriented design exist. The main reason for this is because desired kinematic and stiffness properties already define the manipulator dynamics. Dynamics oriented designs, on the other hand, is achieved via iterative calculations which requires designing the whole manipulator again and again. In order to carry out this iterative procedure, some dynamic evaluation metrics are used. All these metrics are readjusted versions of each other highlighting different properties of dynamics of the manipulator. The main equation used in dynamic evaluations is the following;

$$\bar{\tau} = \hat{M}(\bar{q})\ddot{\bar{q}} + \hat{V}(\bar{q}, \dot{\bar{q}})\dot{\bar{q}} + \hat{K}(\bar{q})\bar{q}_d + \bar{G}(\bar{q}) + \bar{f}(\bar{q}) + \hat{J}^T(\bar{q})\bar{F}_{desired} \tag{4.80}$$

where $\hat{J}(\bar{q})$ is the Jacobian matrix of the manipulator, $\bar{q}$ are the actuated joint variables, $\bar{q}_d$ is the deflections in joint space, $\bar{\tau}$ contains the actuation force and torques, $\hat{M}(\bar{q})$ is the generalized inertia matrix, $\hat{V}(\bar{q}, \dot{q})$ contains the Coriolis and centripetal coefficients, $\hat{K}(\bar{q})$ is the stiffness matrix, $\bar{G}(\bar{q})$ is the gravitational forces, $\bar{f}(\bar{q})$ denotes the friction forces and torques, and finally $\bar{F}_{desired}$ is the desired force output to be displayed at the mobile platform. $\bar{\tau}$ can be simplified as $\bar{\tau}^*$ in order to reveal dynamic properties of the manipulator. Also, $\ddot{\bar{r}}$ acceleration of the mobile platform is introduced and simplified to $\ddot{\bar{r}}^*$, in the following equation set. Simplifications are achieved by removing the terms which are related to the motion.

$$\bar{\tau} = \hat{M}(\bar{q})\ddot{\bar{q}} + \hat{V}(\bar{q}, \dot{q})\dot{\bar{q}} \tag{4.81}$$

$$\bar{\tau}^* = \bar{\tau} - \hat{V}(\bar{q}, \dot{q})\dot{\bar{q}} \tag{4.82}$$

$$\dot{\bar{r}} = \hat{J}(\bar{q})\dot{\bar{q}} \tag{4.83}$$

$$\ddot{\bar{r}} = \hat{J}(\bar{q})\ddot{\bar{q}} + \dot{\hat{J}}(\bar{q})\dot{\bar{q}} \tag{4.84}$$

$$\ddot{\bar{r}}^* = \ddot{\bar{r}} - \dot{\hat{J}}(\bar{q})\dot{\bar{q}} \tag{4.85}$$

Note that, all the equations are defined in the joint space. A transformation to task space is desired because the user who will interact with the manipulator also works in task space. By doing so, the effects of all parameters can easily be observed by physical intuition. The followings represent the required manipulation in equations. First, the joint space and task space relation is given by;

$$\hat{J}^T \bar{F}_{ext} = \bar{\tau} \tag{4.86}$$

By multiplying Equation 4.86 with $\hat{J}^{-T}$ from left;

$$\hat{J}^{-T}\bar{\tau} = \hat{J}^{-T}\hat{M}\ddot{\bar{q}} + \hat{J}^{-T}\hat{V}\dot{\bar{q}} \tag{4.87}$$

Also acceleration of joint variables is

$$\ddot{\bar{q}} = \hat{J}^{-1}\ddot{\bar{r}}^* \tag{4.88}$$

By substituting $\ddot{\bar{q}}$, $\dot{\bar{q}}$, and $\bar{\tau}$ in Equation 4.88

$$\hat{J}^{-T}\bar{\tau}^* + \hat{J}^{-T}\hat{V}\hat{J}^{-1}\dot{\bar{r}} = \hat{J}^{-T}\hat{M}\hat{J}^{-1}\ddot{\bar{r}}^* + \hat{J}^{-T}\hat{V}\hat{J}^{-1}\dot{\bar{r}} \tag{4.89}$$

$$\Rightarrow \hat{J}^{-T}\bar{\tau}^* = \hat{M}_C\ddot{\bar{r}}^* \tag{4.90}$$

where $\hat{M}_C = \hat{J}^{-T}\hat{M}\hat{J}^{-1}$ is the generalized inertia matrix defined in Cartesian space. The force felt by the user $\bar{F}_{ext}^*$ is defined as follows;

$$\bar{F}_{ext}^* = \hat{M}_C\ddot{\bar{r}}^* \tag{4.91}$$

4.3.2. Dynamic Performance Metrics

$\hat{M}_C$ matrix indicates the inertia of the manipulator in Cartesian space. Therefore, the performance metric evaluates the $\hat{M}_C$. Asada (1983) used this matrix to investigate the inertial performance of the manipulator. He used the geometrical representation in order to reveal its intuitional meaning. He plotted the ellipsoids using the eigenvalues and eigenvectors of $\hat{M}_C$ and named them as generalized inertia ellipsoids (GIE). Regarding haptics, the meaning of GIE is the graphical illustration of the relationship between the user input motion to manipulator ($\ddot{\bar{r}}$) and the force felt by the user $\bar{F}_{ext}^*$. The mapping is achieved via $\hat{M}_C$.

The purpose is to minimize the volume of these ellipsoids which means minimizing the determinant of inertia matrix and/or maximizing the determinant of the Jacobian matrix. That way, the force felt by the user would be minimized as well. I_m indicates the volume of the ellipsoid for a given pose.

$$I_m = \det\left(\hat{M}_C\right) = \det\left(\hat{J}^{-T}\hat{M}\hat{J}^{-1}\right) \tag{4.92}$$

$$I_m = \frac{\det\left(\hat{M}\right)}{\det\left(\hat{J}^T\hat{J}\right)} \tag{4.93}$$

A similar index is introduced by Yoshikawa (1985a) as dynamic manipulability. He investigated the torque input and acceleration output relation of the end-effectors. The index proposed by Yoshikawa can be derived by making use of Equations 4.91 and 4.86.

$$\bar{F}_{ext}^* = \hat{M}_C\ddot{\bar{r}}^* \tag{4.94}$$

$$\hat{M}_C^{-1}\bar{F}_{ext}^* = \ddot{\bar{r}}^* \tag{4.95}$$

by substituting $\hat{M}_C$ and $\bar{F}_{ext}^*$;

$$\ddot{\bar{r}}^* = \hat{J}\hat{M}^{-1}\bar{\tau}^* \tag{4.96}$$

Yoshikawa (1985a) defines the dynamic manipulability as the determinant of $\hat{J}\hat{M}^{-1}$ which should be maximized. This index denotes the amplification rate between the torque input and acceleration output at the end platform. While I_m evaluates the inertial value of the manipulator, dynamic manipulability I_d evaluates the load on the actuators to give motion to the manipulator.

$$I_d = \det\left(\hat{J}\hat{M}^{-1}\right)$$
$$I_d = \frac{\det\left(\hat{J}\right)}{\det\left(\hat{M}\right)} \tag{4.97}$$

Similar to the determinant of generalized inertia matrix I_m, dynamic manipulability I_d is also dominated by the inertia matrix. In order to increase the dynamic manipulability, total mass in the system should be reduced.

Another approach to the evaluation of dynamic capability of a mechanism is investigated by Graettinger and Krogh (1988). They have introduced the acceleration radius of the end-effector using the term $\hat{J}\hat{M}^{-1}$ in Equation 4.96 through the computation of eigenvalues and eigenvectors. Acceleration radius measures the maximum acceleration capability of the end platform for any arbitrary direction. They have extracted the largest spheres which represent the maximum isotropic acceleration capability within the ellipsoids of $\hat{J}\hat{M}^{-1}$. A similar evaluation is proposed by Khatib and Burdick (1987). They have investigated the maximum acceleration capability of the mobile platform when the capabilities of the actuators are included in the dynamic model.

Similar to stiffness performance metrics, Frobenius norm I_f and Euclidean norm I_e can be computed for the GIM. Naturally, I_e denotes the maximum and minimum ratio of the Cartesian space axes. Frobenius norm I_f, on the other hand, results in an average value of the inertia matrix for a given pose. While I_e is important to ensure the even mass distribution over the workspace, it should be compatible with I_f since the objective is not only to obtain the dynamic uniformity but also to minimize the inertia.

$$I_f = \sqrt{tr(\hat{M}_C \hat{M}_C^T)} \tag{4.98}$$

$$I_e = \|\hat{M}_C\|\|(\hat{M}_C)^{-1}\| \tag{4.99}$$

4.3.3. Natural Frequency Performance on Frequency Range and Impedance Performance

Until now, the relations between dynamics-kinematics and stiffness-kinematics are investigated through the inertia matrix $\hat{M}_C$ and the stiffness matrix $\hat{K}_C$. The final evaluation is conducted on dynamics-stiffness relation to reveal the frequency range of the manipulator. Frequency range depends on the value of the natural frequency. Higher natural frequency enables higher frequency range and enhanced performance in terms of haptic interaction variety. In order to denote the natural frequency by making use of the inertia and the stiffness matrices, the model of the system is obtained by omitting the damping factor as follows.

$$\bar{\tau} = \hat{M}\ddot{\bar{q}} + \hat{K}\bar{q}_d \tag{4.100}$$

$$\Delta\bar{\tau} = \hat{M}\Delta\ddot{q} + \hat{K}\Delta\bar{q}_d \tag{4.101}$$

Assuming that the system's initial conditions are set to zero

$$\bar{\tau} = \bar{0} \tag{4.102}$$

$$\hat{M}\Delta\ddot{q} = -\hat{K}\Delta\bar{q}_d \tag{4.103}$$

$$\Delta\ddot{q} = -\hat{M}^{-1}\hat{K}\Delta\bar{q}_d \tag{4.104}$$

$$\hat{D} = -\hat{M}^{-1}\hat{K} \tag{4.105}$$

where $\hat{D}$ is the dynamic matrix. This matrix can also be represented in task space.

$$\hat{D}_C = \hat{J}\hat{D}\hat{J}^{-1}$$
$$\hat{M}_C = \hat{J}^{-T}\hat{M}\hat{J}^{-1} \tag{4.106}$$
$$\hat{K}_C = \hat{J}^{-T}\hat{K}\hat{J}^{-1}$$

where $\hat{D}_C$ is the generalized dynamic matrix. The dynamic matrix is useful to understand the mechanical properties of the mechanism. Eigenvalues of D are the natural frequencies and eigenvectors are the modal vectors. It is known that increasing the natural frequency decreases the response time, enhances the frequency range, maximizes the maximum impedance and minimizes the minimum impedance of a second order system. Evaluation of the dynamic matrix is the most logical way for this optimization of a haptic device. Maximizing the eigenvalues or the Frobenius norm of D is the objective in the dynamic sense.

$$\omega_n = \|D\|_f \tag{4.107}$$

where ω_n is the weighted natural frequency.

4.4. Globalization of Performance Metrics

Performance metrics for kinematics, stiffness, and dynamics are all pose-dependent. Thus, they have different values at each specific discrete position in the workspace. Optimizing the performance matrix for a specific pose enhances the overall performance of the manipulator for that pose. However, a manipulator cannot be designed for a single pose. The desired performance should be obtained for the whole workspace. In order to design a high-performance manipulator, performance metrics should be evaluated for all possible poses in the workspace.

Design an optimal manipulator which satisfies the design objectives for all poses is achieved via using global performance index proposed by Gosselin and Angeles (1991). The proposed method requires the integration of the performance metrics with respect to workspace poses. Most of the time, an analytical model is difficult to obtain and not suitable to be use in computer-aided optimization. Therefore, the general approach is to divide the workspace into discrete points and reduce the integration into simple summations. The method sums the performance indices at each discrete pose and divides by the total number of the discrete poses to compute an average value of the performance metrics. The reason to obtain an average value is that a manipulator cannot achieve the design objectives at each discrete pose however an average value would provide an average performance information of the manipulator. This formulation can be established as follows;

$$k = \frac{\sum_{i=1}^{W_n} k_i}{W_n} \tag{4.108}$$

where W_n is the number of discrete poses, k_i is the value of the any of the performance metric at the ith discrete pose, k is the average value of the inspected performance metric.

The quality of the globalized performance metric depends on the number of the discrete points and their location in the workspace. The determination of the discrete points may vary depending on the manipulator type. They can be equally distributed in the workspace or the density of the discrete points in more critical regions can be increased. This also increases the weighting factor of the inspected performance metric. In general, however, the discrete points should be located at least on the boundaries of the workspace and the nominal poses when the active joints are set to their initial positions. If the manipulator has a symmetric workspace, the number of discrete points can further be reduced. In such workspaces, 2 discrete points are generally sufficient which are located on the most and the least critical points.

4.5. Conclusion

In this Chapter, the performance metrics and their physical intuitions are investigated which are used in literature by stating the importance of each of them in design. It has been shown that the kinematic performance metrics, manipulability, and condition number, are the scalar representation of the volume of the velocity ellipsoids and motion resolution. Then, stiffness performance metrics are investigated by using stiffness model procured via VJM. Finally, dynamic performance metrics are shown.

CHAPTER 5

CASE STUDY: MODELING OF THE R-CUBE MANIPULATOR

The R-CUBE manipulator is introduced by Li et al. (2005). The transnational manipulator comprises only revolute joints with a decoupled motion structure. There are 3 serial chains each manipulating one of the DoF in Cartesian space. Each serial chain contains 1 DoF actuated parallelogram and 2R passive serial chain on top of the parallelograms. Parallelograms are located on the base structure and mobile platform is connected to the 2R passive chains.

In the modified version of R-CUBE, the parallelogram is replaced with a single link. This link is connected to the 2R passive mechanism with a universal joint. The modification does not change the forward or inverse kinematics of the mobile platform. By removing the parallelogram, each serial chain has 3 less revolute joints and 2 fewer links. The benefits of this modification are listed as follows;

1. Less number of joints reduces the total friction force/torque.
2. Less number of joints reduces internal stress caused by the manufacturing.
3. The total cost is reduced.
4. Amount of moving mass is reduced.
5. Stiffness model is easier to formulate and faster to compute.
6. Dynamic model is easier to formulate and faster to compute.

However, there are also a few drawbacks;

1. Stiffness of actuated portion of the mechanism is reduced in by replacing the parallelogram with a single link.
2. A complex joint structure to be manufactured (universal joint).

Since the advantages are more than the disadvantages, the modified version of R-CUBE is considered in this thesis.

5.1. Kinematics Model

The performance metrics are mainly oriented around the Jacobian matrix. Derivation of the Jacobian matrix requires the kinematic analysis of the manipulator. In addition, dynamic and stiffness models of a manipulator are formulated by using the results of kinematic analysis. Thus, the very first step for performance evaluation and determination of design parameters must start with the kinematic analysis. Kinematic analysis consists of forward and inverse kinematics relation between the moving platform and base frame. Both kinematic analyses must be carried out in order to be used in developing performance metrics.

$$\vec{u}_1^{(0)} \parallel \vec{u}_1^{(p)} = \vec{u}_3^{(14)}, \vec{u}_3^{(15)}, \vec{u}_1^{(35)}$$

$$\vec{u}_2^{(0)} \parallel \vec{u}_2^{(p)} = \vec{u}_3^{(24)}, \vec{u}_3^{(25)}, \vec{u}_1^{(15)}$$

$$\vec{u}_3^{(0)} \parallel \vec{u}_3^{(p)} = \vec{u}_3^{(34)}, \vec{u}_3^{(35)}, \vec{u}_1^{(25)}$$
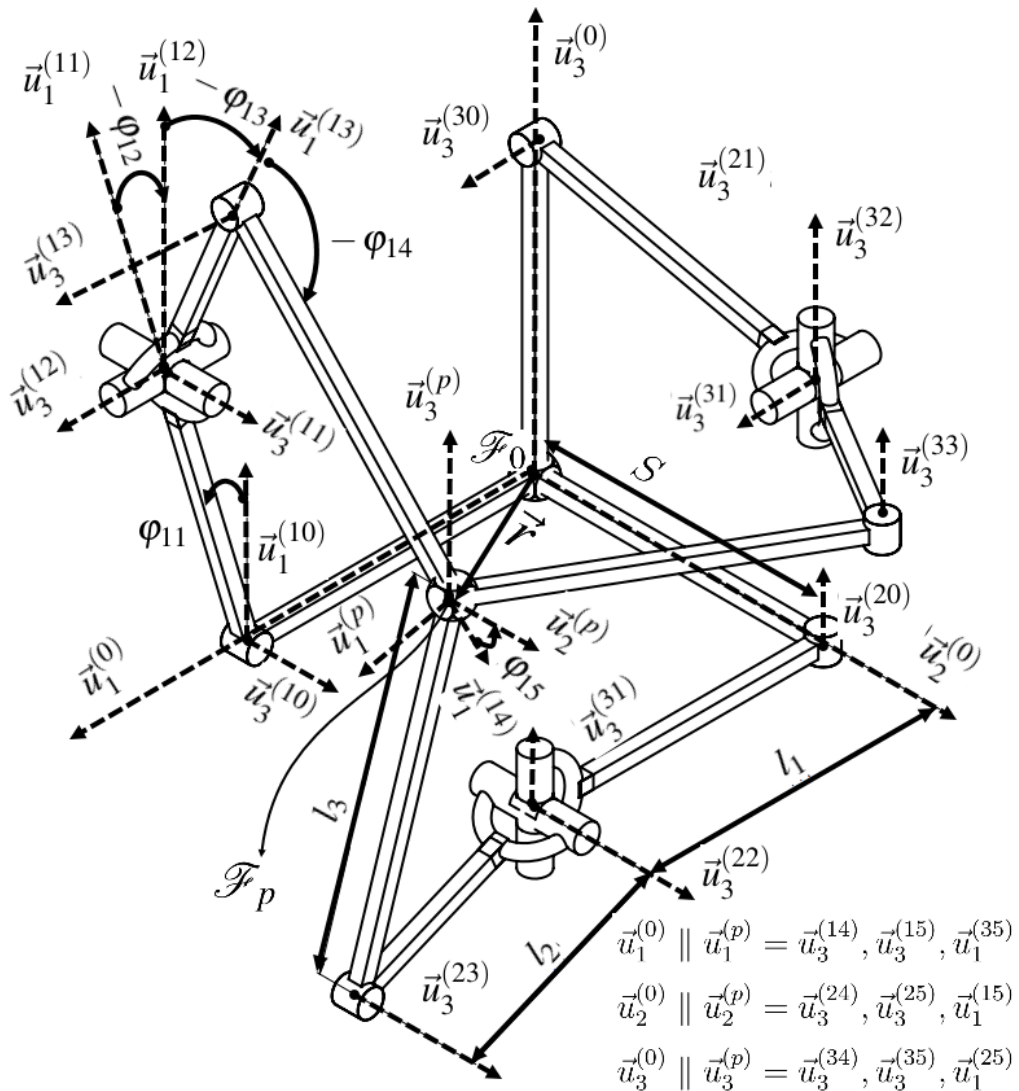
Figure 5.1. Modified R-CUBE Mechanism

A simple sketch of the modified R-CUBE manipulator was shown in Figure 5.1 denoting the necessary parameters and link frames to represent the kinematic architecture of the mechanism. One benefit of R-CUBE is the simplicity in the derivation of kinematic equations compared to other parallel mechanisms. Another benefit is the symmetry in the topology. Due to this property, most of the time it is enough to evaluate only one of the serial chains.

5.1.1. Forward Kinematics

The mechanism is a combination of three separate serial chains. Therefore, forward kinematic equations of each serial chain must be in equilibrium at the tip point located on the mobile platform. Given in Figure 5.1, initial frames of these serial chains are located on $\vec{u}_1^{(0)}$, $\vec{u}_2^{(0)}$, and $\vec{u}_3^{(0)}$ axes of the manipulator and numbered as the 1st, 2nd, and 3rd serial chains, respectively. In this representation, superscript in the parenthesis indicates the frame that the unit vector belongs to. Column matrix representation of these unit vectors are denoted as in their own frames in Equation 5.1.

$$\bar{u}_1^{(0/0)} = \bar{u}_1 = \begin{bmatrix} 1 \\ 0 \\ 0 \end{bmatrix}, \bar{u}_2^{(0/0)} = \bar{u}_2 = \begin{bmatrix} 0 \\ 1 \\ 0 \end{bmatrix}, \bar{u}_3^{(0/0)} = \bar{u}_3 = \begin{bmatrix} 0 \\ 0 \\ 1 \end{bmatrix} \tag{5.1}$$

Using the notation in Figure 5.1, the forward kinematics of the mechanism can be written by combining the kinematic formulation, from base frame origin each serial chain's initial frame and then, from the initial frames of each serial chain to mobile platform frame. Pose of each serial chain's initial frame with respect to the base frame is represented as follows;

$$\hat{H}^{(0,10)} = \hat{T}_{u1}(S)\hat{R}_{u1}(\pi/2)\hat{R}_{u3}(-\pi/2)$$
$$\hat{H}^{(0,20)} = \hat{T}_{u2}(S) \tag{5.2}$$
$$\hat{H}^{(0,30)} = \hat{T}_{u3}(S)\hat{R}_{u3}(\pi/2)\hat{R}_{u1}(\pi/2)$$

where $\hat{H}^{(0,ij)}$ denotes the 4×4 homogeneous transformation matrix, the superscript $(0, ij)$ denotes the homogeneous transformation from 0th frame (base frame) to ij^{th} frame. S is the distance from 0th frame to ij^{th} frame. i index stands for the inspected serial chain for $i = 1, 2, 3$ and j is the body fixed frame defined at the joints of the ith serial chain. Matrices $\hat{T}_{uk}$ and $\hat{R}_{uk}$ are 4×4 matrix representation of pure translation and pure rotation homogeneous transformation matrices as shown in Equations 5.3 and 5.4. Subscript uk denotes the translation along or rotation about the $\vec{u}_k$ axis for $k = 1, 2, 3$.

$$\hat{T}_{u1}(\psi) = \begin{bmatrix} 1 & 0 & 0 & \psi \\ 0 & 1 & 0 & 0 \\ 0 & 0 & 1 & 0 \\ 0 & 0 & 0 & 1 \end{bmatrix} \quad \hat{T}_{u2}(\psi) = \begin{bmatrix} 1 & 0 & 0 & 0 \\ 0 & 1 & 0 & \psi \\ 0 & 0 & 1 & 0 \\ 0 & 0 & 0 & 1 \end{bmatrix} \quad \hat{T}_{u3}(\psi) = \begin{bmatrix} 1 & 0 & 0 & 0 \\ 0 & 1 & 0 & 0 \\ 0 & 0 & 1 & \psi \\ 0 & 0 & 0 & 1 \end{bmatrix} \tag{5.3}$$

$$\hat{R}_{u1}(\varphi) = \begin{bmatrix} 1 & 0 & 0 & 0 \\ 0 & \cos\varphi & -\sin\varphi & 0 \\ 0 & \sin\varphi & \cos\varphi & 0 \\ 0 & 0 & 0 & 1 \end{bmatrix}$$

$$\hat{R}_{u2}(\varphi) = \begin{bmatrix} \cos\varphi & 0 & \sin\varphi & 0 \\ 0 & 1 & 0 & 0 \\ -\sin\varphi & 0 & \cos\varphi & 0 \\ 0 & 0 & 0 & 1 \end{bmatrix} \tag{5.4}$$

$$\hat{R}_{u3}(\varphi) = \begin{bmatrix} \cos\varphi & -\sin\varphi & 0 & 0 \\ \sin\varphi & \cos\varphi & 0 & 0 \\ 0 & 0 & 1 & 0 \\ 0 & 0 & 0 & 1 \end{bmatrix}$$

where ψ is the variable for translations in meters and φ is the variable for rotations in radians.

From initial frame where the active joints are located to last frame of the ith serial chain $i5$, homogeneous transformation $\hat{H}^{(i0,i5)}$, is identical for all serial chains with their own joint variables, φ_{ik} for $k = 1, 2, ...5$.

$$\hat{H}^{(i0,i1)} = \hat{R}_{u3}(\varphi_{i1})\hat{T}_{u1}(l_1) \tag{5.5}$$

$$\hat{H}^{(i1,i2)} = \hat{R}_{u3}(\varphi_{i2})\hat{R}_{u1}(-\pi/2) \tag{5.6}$$

$$\hat{H}^{(i2,i3)} = \hat{R}_{u3}(\varphi_{i3})\hat{T}_{u1}(l_2) \tag{5.7}$$

$$\hat{H}^{(i3,i4)} = \hat{R}_{u3}(\varphi_{i4})\hat{T}_{u1}(l_3) \tag{5.8}$$

$$\hat{H}^{(i4,i5)} = \hat{R}_{u3}(\varphi_{i5}) \tag{5.9}$$

When each serial chain is connected to each other on the mobile platform, variables from φ_{i2} to φ_{i5} become dependent variables. φ_{i3} and φ_{i4} are determined via the

inverse kinematics solution. However, φ_{i2} and φ_{i5} depend on φ_{i1}, φ_{i3} and φ_{i4}. Therefore, the variables for a single serial chain can be reduced to 3. In order to preserve the general notation, the joint variables are updated as follows;

$$q_{i1} = \varphi_{i1} \tag{5.10}$$

$$q_{i2} = \varphi_{i3} \tag{5.11}$$

$$q_{i3} = \varphi_{i4} \tag{5.12}$$

$$\varphi_{i2} = -\varphi_{i1} \tag{5.13}$$

$$\varphi_{i5} = -(\varphi_{i3} + \varphi_{i4}) \tag{5.14}$$

For each serial chain, the transformation from their last frame $i5$ to the mobile platform, a constant rotation is defined in order to align the axes of the base frame and mobile platform frame.

$$\hat{H}^{(15,p)} = \hat{R}_{u2}(-\pi/2)\hat{R}_{u1}(-\pi/2) \tag{5.15}$$

$$\hat{H}^{(25,p)} = \hat{R}_{u2}(\pi/2)\hat{R}_{u3}(\pi/2) \tag{5.16}$$

$$\hat{H}^{(35,p)} = \hat{I}_{4\times4} \tag{5.17}$$

where p denotes the mobile platform frame and $\hat{I}$ is the identity matrix. Note that, there is no translation defined for mobile platform frame. Since the size of the mobile platform reduced into a single point where axes of action of the last joint of each serial chain is intersected. Therefore, the distance parameter in these equations is not considered. As a result of this, the last frames of each serial chain are coincident.

The homogeneous transformation matrix from the origin of the manipulator to the mobile platform ($\hat{H}_i$) for i^{th} serial chain is;

$$\hat{H}_i = \hat{H}^{(0,i0)}\hat{H}^{(i0,i1)}\hat{H}^{(i1,i2)}\hat{H}^{(i2,i3)}\hat{H}^{(i3,i4)}\hat{H}^{(i4,i5)}\hat{H}^{(i5,p)} \tag{5.18}$$

$$\hat{H}_i = \begin{bmatrix} \hat{R}_i & \bar{r}_i \\ \bar{0}^T & 1 \end{bmatrix} \tag{5.19}$$

where $\hat{R}_i$ denotes the 3×3 rotation matrix for i^{th} serial chain and $\bar{r}_i$ is the 3×1 position column matrix. Due to kinematic constraints, the pose of the mobile platform must be equal when calculated from each serial chain.

$$\hat{H}_1 = \hat{H}_2 = \hat{H}_3 \tag{5.20}$$

For R-Cube mechanism, orientation of the mobile platform is always constant and equal to identity matrix $\hat{R}_1 = \hat{R}_2 = \hat{R}_3 = \hat{I}_{3\times3}$. Only the position of mobile

platform changes with respect to origin. The position of end-platform can be written as in Equations. 5.21, 5.22, and 5.23 in open form calculated by using each serial chain's kinematics.

$$\bar{r}_1 = \begin{bmatrix} r_{11} \\ r_{12} \\ r_{13} \end{bmatrix} = \begin{bmatrix} S + l_1 \sin q_{11} \\ -l_2 \sin q_{12} - l_3 \sin (q_{12} + q_{13}) \\ l_1 \cos q_{11} + l_2 \cos q_{12} + l_3 \cos (q_{12} + q_{13}) \end{bmatrix} \tag{5.21}$$

$$\bar{r}_2 = \begin{bmatrix} r_{21} \\ r_{22} \\ r_{23} \end{bmatrix} = \begin{bmatrix} l_1 \cos q_{21} + l_2 \cos q_{22} + l_3 \cos (q_{22} + q_{23}) \\ S + l_1 \sin q_{21} \\ -l_2 \sin q_{22} - l_3 \sin (q_{22} + q_{23}) \end{bmatrix} \tag{5.22}$$

$$\bar{r}_3 = \begin{bmatrix} r_{31} \\ r_{32} \\ r_{33} \end{bmatrix} = \begin{bmatrix} -l_2 \sin q_{32} - l_3 \sin (q_{32} + q_{33}) \\ l_1 \cos q_{31} + l_2 \cos q_{32} + l_3 \cos (q_{32} + q_{33}) \\ S + l_1 \sin q_{31} \end{bmatrix} \tag{5.23}$$

$$\bar{r}_i = \bar{r} \text{ for } i = 1, 2, 3 \tag{5.24}$$

where $\bar{r}$ is the column matrix representation of position vector of mobile platform with respect to base frame. In Equation 5.24, the r_1, r_2, and r_3 components of $\bar{r}$ can determined by using anyone of the $\bar{r}_i$ vectors. Therefore, any of theses equations in a set can be used to define the position of the mobile platform;

$$r_1 = (S + l_1 \sin q_{11})$$
$$r_1 = (l_1 \cos q_{21} + l_2 \cos q_{22} + l_3 \cos (q_{22} + q_{23})) \tag{5.25}$$
$$r_1 = (-l_2 \sin q_{32} - l_3 \sin (q_{32} + q_{33}))$$

$$r_2 = (S + l_1 \sin q_{21})$$
$$r_2 = (l_1 \cos q_{31} + l_2 \cos q_{32} + l_3 \cos (q_{32} + q_{33})) \tag{5.26}$$
$$r_2 = (-l_2 \sin q_{12} - l_3 \sin (q_{12} + q_{13}))$$

$$r_3 = (S + l_1 \sin q_{31})$$
$$r_3 = (l_1 \cos q_{11} + l_2 \cos q_{12} + l_3 \cos (q_{12} + q_{13})) \tag{5.27}$$
$$r_3 = (-l_2 \sin q_{22} - l_3 \sin (q_{22} + q_{23}))$$

In each set, the obvious choice is the $S + l_1 \sin q_{i1}$ since it only contains one variable q_{i1} and it is the actuated joint. Therefore, the forward kinematics of the mechanism

can be written as;

$$\begin{bmatrix} S + l_1 \sin q_{11} \\ S + l_1 \sin q_{21} \\ S + l_1 \sin q_{31} \end{bmatrix} = \begin{bmatrix} r_1 \\ r_2 \\ r_3 \end{bmatrix} = \bar{r} \tag{5.28}$$

or in more compact form;

$$S + l_1 \sin q_{i1} = r_i \text{ for } i = 1, 2, 3 \tag{5.29}$$

It can be seen that in Equations 5.21, 5.22, and 5.23 forward kinematics formulation of each serial chain is identical with the other ones in a different order. Therefore, there exists a symmetry in the mechanism. By making use of the symmetry, it can be stated if one of the serial chains is designed in terms of kinematics, since the other serial chains are identical, the whole manipulator is designed simultaneously.

5.1.2. Inverse Kinematics

q_{i1} variable for $i = 1, 2, 3$ in Equation 5.29 is the required input to specify the end-platform position. Equation 5.29 shows that each actuator controls the related axis of motion. Therefore, the inverse kinematic solution is conveniently formulated as;

$$q_{i1} = \text{asin} \left(\frac{r_i - S}{l_1} \right) \text{ for } i = 1, 2, 3 \tag{5.30}$$

After solving the Equation 5.30 for q_{i1}, q_{i2} and q_{i3} which are the variables of passive joints can be calculated. By making use of Equations 5.25, 5.26, and 5.27 following equalities are obtained;

$$l_2 \cos q_{12} + l_3 \cos (q_{12} + q_{13}) = r_3 - l_1 \cos q_{11}$$
$$-l_2 \sin q_{12} - l_3 \sin (q_{12} + q_{13}) = r_2 \tag{5.31}$$

$$l_2 \cos q_{22} + l_3 \cos (q_{22} + q_{23}) = r_1 - l_1 \cos q_{21}$$
$$-l_2 \sin q_{22} - l_3 \sin (q_{22} + q_{23}) = r_3 \tag{5.32}$$

$$l_2 \cos q_{32} + l_3 \cos (q_{32} + q_{33}) = r_2 - l_1 \cos q_{31}$$
$$-l_2 \sin q_{32} - l_3 \sin (q_{32} + q_{33}) = r_1 \tag{5.33}$$

The above-mentioned equations are generalized as follows;

$$l_2 \cos q_{a2} + l_3 \cos (q_{a2} + q_{a3}) = r_c - l_1 \cos q_{a1}$$
$$l_2 \sin q_{a2} + l_3 \sin (q_{a2} + q_{a3}) = -r_b \tag{5.34}$$

70

The selection of a, b, and c is done in following order for each serial chain's solution set.

$$\text{Solution set } 1 \rightarrow [a = 1, b = 2, c = 3] \tag{5.35}$$

$$\text{Solution set } 2 \rightarrow [a = 2, b = 3, c = 1] \tag{5.36}$$

$$\text{Solution set } 3 \rightarrow [a = 3, b = 1, c = 2] \tag{5.37}$$

The solution for q_{a3};

$$(r_c - l_1 \cos q_{a1})^2 = (l_2 \cos q_{a2} + l_3 \cos (q_{a2} + q_{a3}))^2$$

$$(-r_b)^2 = (l_2 \sin q_{a2} + l_3 \sin (q_{a2} + q_{a3}))^2$$

$$(r_c - l_1 \cos q_{a1})^2 + (-r_b)^2 = l_2^2 \cos^2(q_{a2}) + l_3^2 \cos^2(q_{a2} + q_{a3})$$

$$+ 2l_2 l_3 \cos(q_{a2}) \cos(q_{a2} + q_{a3})$$

$$+ l_2^2 \sin^2(q_{a2}) + l_3^2 \sin^2(q_{a2} + q_{a3})$$

$$+ 2l_2 l_3 \sin(q_{a2}) \sin(q_{a2} + q_{a3})$$

$$\begin{aligned} (r_c - l_1 \cos q_{a1})^2 + (-r_b)^2 - l_2^2 - l_3^2 = {} & 2l_2 l_3 [\cos(q_{a2}) \cos(q_{a2} + q_{a3}) \\ & + \sin(q_{a2}) \sin(q_{a2} + q_{a3})] \end{aligned} \tag{5.38}$$

Now, by making use of sum and difference formulas it can be concluded that;

$$\cos q_{a3} = \frac{(r_c - l_1 \cos q_{a1})^2 + (-r_b)^2 - l_2^2 - l_3^2}{2l_2 l_3} \tag{5.39}$$

In final form;

$$\cos^2(q_{a3}) + \sin^2(q_{a3}) = 1$$

$$\sin(q_{a3}) = \sigma \sqrt{1 - \cos^2(q_{a3})} \tag{5.40}$$

$$q_{a3} = \text{atan}_2(\sin(q_{a3}), \cos(q_{a3})) \tag{5.41}$$

$$\sigma = \pm 1 \tag{5.42}$$

where the σ sign denotes the configuration of the manipulator which is to be set by the designer for desired passive joint configuration. It is chosen as "$-$" configuration and the configuration change is constrained by the mechanical limits at the joints.

The solution for q_{a2} by applying sum and difference formulas;

$$\Rightarrow \begin{bmatrix} l_2 + l_3 \cos q_{a3} & -l_3 \sin q_{a3} \\ l_3 \sin q_{a3} & l_2 + l_3 \cos q_{a3} \end{bmatrix} \begin{bmatrix} \cos q_{a2} \\ \sin q_{a2} \end{bmatrix} = \begin{bmatrix} r_c - l_1 \cos q_{a1} \\ -r_b \end{bmatrix} \tag{5.43}$$

by applying Cramer's Rule for $\cos q_{a2}$ and $\sin q_{a2}$, the following is obtained.

$$
\begin{aligned}
\cos q_{a2} &= \frac{l_2(r_c - l_1 \cos q_{a1}) + l_3(r_c - l_1 \cos q_{a1}) \cos q_{a3} - l_3 r_b \sin q_{a3}}{l_2^2 + l_3^2 + 2l_2 l_3 \cos q_{a3}} \\
\sin q_{a2} &= \frac{-l_2 r_b - l_3 r_b \cos q_{a3} - l_3(r_c - l_1 \cos q_{a1}) \sin q_{a3}}{l_2^2 + l_3^2 + 2l_2 l_3 \cos q_{a3}}
\end{aligned}
\tag{5.44}
$$

Finally q_{a2} is;

$$
q_{a2} = \operatorname{atan} 2(\sin q_{a2}, \cos q_{a2}) \tag{5.45}
$$

5.1.3. Jacobian Matrix for the Manipulator Considered in This Thesis

The equation set in Equation 5.29 can be represented as a function of joint variables.

$$
\bar{r} = \bar{f}(\bar{q}_m) = \bar{g}(\bar{q}_i) \tag{5.46}
$$

where $\bar{q}_m$ denote the vector of active joints. $\bar{q}_i$ is the vector of joints variables in a serial chain. The definition of the vectors are given in Equation 5.47.

$$
\bar{q}_m = \begin{bmatrix} q_{11} \\ q_{21} \\ q_{31} \end{bmatrix}, \bar{q}_i = \begin{bmatrix} q_{i1} \\ q_{i2} \\ q_{i3} \end{bmatrix} \text{ for } i = 1, 2, 3 \tag{5.47}
$$

By taking the derivative of the forward kinematics Equation 5.46 with respect to time, Jacobian matrix for active joints is derived. The formulation of the derivative is shown in Equation 5.48.

$$
\frac{\mathrm{d}\bar{r}}{\mathrm{d}t} = \frac{\partial \bar{f}(\bar{q}_m)}{\partial \bar{q}_m} \frac{\mathrm{d}\bar{q}_m}{\mathrm{d}t} \tag{5.48}
$$

Hence, the Jacobian matrix of the manipulator is;

$$
\frac{\partial \bar{f}(\bar{q}_m)}{\partial \bar{q}_m} = \hat{J}_m = \begin{bmatrix} l_1 \cos q_{11} & 0 & 0 \\ 0 & l_1 \cos q_{21} & 0 \\ 0 & 0 & l_1 \cos q_{31} \end{bmatrix} \text{ and } \dot{\bar{q}}_m = \begin{bmatrix} \dot{q}_{11} \\ \dot{q}_{21} \\ \dot{q}_{31} \end{bmatrix} \tag{5.49}
$$

where $\hat{J}_m$ and $\dot{\bar{q}}_m$ are the Jacobian matrix and joint speed column matrix of the manipulator, respectively.

Although $\hat{J}_m$ gives the relation between the actuator motion and the mobile platform motion, using Equation 5.46 to obtain Jacobian matrix omits the design parameters for passive links and joints. Therefore, Jacobian matrix for each serial chain is needed especially for stiffness and dynamic model derivations.

The forward kinematic equation including the passive joints are derived as follows for each serial chain;

$$\frac{\mathrm{d}\bar{r}_i}{\mathrm{d}t} = \frac{\partial \bar{g}(\bar{q}_i)}{\partial \bar{q}_i} \frac{\mathrm{d}\bar{q}_i}{\mathrm{d}t} \tag{5.50}$$

$$\dot{\bar{r}}_i = \hat{J}_i \dot{\bar{q}}_i \tag{5.51}$$

$$\hat{J}_i = \begin{bmatrix} \dfrac{\partial r_{i1}}{\partial q_{i1}} & \dfrac{\partial r_{i1}}{\partial q_{i2}} & \dfrac{\partial r_{i1}}{\partial q_{i3}} \\[2mm] \dfrac{\partial r_{i2}}{\partial q_{i1}} & \dfrac{\partial r_{i2}}{\partial q_{i2}} & \dfrac{\partial r_{i2}}{\partial q_{i3}} \\[2mm] \dfrac{\partial r_{i3}}{\partial q_{i1}} & \dfrac{\partial r_{i3}}{\partial q_{i2}} & \dfrac{\partial r_{i3}}{\partial q_{i3}} \end{bmatrix} \text{ and } \dot{\bar{q}}_i = \begin{bmatrix} \dfrac{\mathrm{d}q_{i1}}{\mathrm{d}t} \\[2mm] \dfrac{\mathrm{d}q_{i2}}{\mathrm{d}t} \\[2mm] \dfrac{\mathrm{d}q_{i3}}{\mathrm{d}t} \end{bmatrix} = \begin{bmatrix} \dot{q}_{i1} \\[2mm] \dot{q}_{i2} \\[2mm] \dot{q}_{i3} \end{bmatrix} \tag{5.52}$$

where $\hat{J}_i$, $\dot{\bar{q}}_i$ and t denotes the Jacobian matrix, joint speed column matrix and time, respectively. The final form of Jacobian matrices, for each serial chain is presented as follows;

$$\hat{J}_1 = \begin{bmatrix} l_1 \cos q_{11} & 0 & 0 \\[2mm] 0 & -l_2 \cos q_{12} - l_3 \cos(q_{12} + q_{13}) & -l_3 \cos(q_{12} + q_{13}) \\[2mm] -l_1 \sin q_{11} & -l_2 \sin q_{12} - l_3 \sin(q_{12} + q_{13}) & -l_3 \sin(q_{12} + q_{13}) \end{bmatrix} \tag{5.53}$$

$$\hat{J}_2 = \begin{bmatrix} -l_1 \sin q_{21} & -l_2 \sin q_{22} - l_3 \sin(q_{22} + q_{23}) & -l_3 \sin(q_{22} + q_{23}) \\[2mm] l_1 \cos q_{21} & 0 & 0 \\[2mm] 0 & -l_2 \cos q_{22} - l_3 \cos(q_{22} + q_{23}) & -l_3 \cos(q_{22} + q_{23}) \end{bmatrix} \tag{5.54}$$

$$\hat{J}_3 = \begin{bmatrix} 0 & -l_2 \cos q_{32} - l_3 \cos(q_{32} + q_{33}) & -l_3 \cos(q_{32} + q_{33}) \\[2mm] -l_1 \sin q_{31} & -l_2 \sin q_{32} - l_3 \sin(q_{32} + q_{33}) & -l_3 \sin(q_{32} + q_{33}) \\[2mm] l_1 \cos q_{31} & 0 & 0 \end{bmatrix} \tag{5.55}$$

Due to the kinematic constraints, mobile platform velocity must be equal for all serial chains. Using this relation following equality can be established.

$$\hat{J}_i \dot{\bar{q}}_i = \hat{J}_m \dot{\bar{q}}_m \tag{5.56}$$

$$\Rightarrow \dot{\bar{q}}_i = \hat{J}_i^{-1} \hat{J}_m \dot{\bar{q}}_m \tag{5.57}$$

73

From here, two important results are obtained. First, $\ddot{\bar{q}}_i$ is a function of $\bar{q}_m$ so an inverse kinematic solution in velocity level is required. The second one is that above equality is valid if and only if $\hat{J}_i$ is invertible. If $\hat{J}_i$ is non-invertible then the corresponding pose is a singular pose.

Acceleration with respect to generalized coordinates can be derived by taking the time derivative of Equation 5.50 or 5.48.

$$\frac{\mathrm{d}\dot{\bar{r}}}{\mathrm{d}t} = \frac{\mathrm{d}(\hat{J}_m \dot{\bar{q}}_m)}{\mathrm{d}t} = \frac{\mathrm{d}(\hat{J}_i \dot{\bar{q}}_i)}{\mathrm{d}t} \tag{5.58}$$

Equation 5.57 is more suitable to derive constraint equation between the acceleration of active and passive joints can be obtained. The following acceleration relation will be used in the dynamic model of the manipulator;

$$\frac{\mathrm{d}\dot{\bar{q}}_i}{\mathrm{d}t} = \frac{\mathrm{d}(\hat{J}_i^{-1} \hat{J}_m \dot{\bar{q}}_m)}{\mathrm{d}t} \tag{5.59}$$

$$\ddot{\bar{q}}_i = \hat{J}_i^{-1} \dot{\hat{J}}_m \dot{\bar{q}}_m + \hat{J}_i^{-1} \hat{J}_m \ddot{\bar{q}}_m + \dot{\hat{J}}_i^{-1} \hat{J}_m \dot{\bar{q}}_m \tag{5.60}$$

5.1.4. Extended Jacobian Matrix

The extended Jacobian matrix is useful when translation and rotation motion accrue simultaneously. For the R-cube mechanism, there is no rotation at the mobile platform. However, obtaining extended Jacobian matrix is required for stiffness modeling since the technique includes extra DoF to the manipulator. In addition, dynamic modeling includes motion of the intermediate links which have both translational and rotational motion. Therefore, the extended Jacobian matrix is derived in order to keep the generality.

Derivation of the extended Jacobian Matrix requires the homogeneous transformation matrix differentiation with respect to joint variables. $\hat{H}_i$ matrix is differentiated with respect to q_{ij}^{th} variable in order to obtain angular and linear velocity coefficients.

$$\frac{\partial \hat{H}_i}{\partial q_{ij}} = \begin{bmatrix} \frac{\partial \hat{R}_i}{\partial q_{ij}} & \frac{\partial \bar{r}_i}{\partial q_{ij}} \\ \bar{0}^T & 1 \end{bmatrix} \quad \text{for } j = 1, 2, 3 \tag{5.61}$$

Angular velocity coefficients are be obtained by using the derivative of the rotation matrix.

$$\tilde{J}_{\omega ij} = \frac{\partial \hat{R}_i}{\partial q_{ij}} \hat{R}_i^T \tag{5.62}$$

where $\tilde{J}_{\omega ij}$ is a skew symmetric matrix which contains the angular velocity coefficients.

$$\tilde{J}_{\omega ij} = \begin{bmatrix} 0 & -\beta ij3 & \beta ij2 \\ \beta ij3 & 0 & -\beta ij1 \\ -\beta ij2 & \beta ij1 & 0 \end{bmatrix} \tag{5.63}$$

By using the column (col) operator, the angular velocity coefficients can be obtained in column matrix form.

$$\bar{J}_{\omega ij} = col(\tilde{J}_{\omega ij}) = \begin{bmatrix} \beta ij1 \\ \beta ij2 \\ \beta ij3 \end{bmatrix} \tag{5.64}$$

Linear velocity coefficients in column matrix form $\bar{J}_{rij}$ are obtained by differentiating $\bar{r}_i$ with respect to q_{ij}^{th} variable.

$$\bar{J}_{rij} = \frac{\partial \bar{r}_i}{\partial q_{ij}} \tag{5.65}$$

The extended 6×1 Jacobian column matrix $\bar{J}_{H_{ij}}$ for q_{ij}^{th} variable is formed as follows;

$$\bar{J}_{H_{ij}} = \begin{bmatrix} \bar{J}_{rij} \\ \bar{J}_{\omega ij} \end{bmatrix}_{6 \times 1} \tag{5.66}$$

The extended Jacobian matrix $\hat{J}_{H_i}$ for i^{th} serial chain is written by using Jacobian column matrices.

$$\hat{J}_{H_i} = \begin{bmatrix} \bar{J}_{H_{i1}} & \bar{J}_{H_{i2}} & \bar{J}_{H_{i3}} \end{bmatrix}_{6 \times 3} \tag{5.67}$$

Note that, there is no rotation at the mobile platform. By using this information, further manipulation can easily be achieved for $\hat{J}_m$ in order to acquire the extended Jacobian matrix of the manipulator $\hat{J}_{Hm}$.

$$\hat{J}_{Hm} = \begin{bmatrix} \hat{J}_m \\ \hat{0}_{3 \times 3} \end{bmatrix}_{6 \times 3} \tag{5.68}$$

$$\hat{J}_{Hm}\dot{\bar{q}}_m = \hat{J}_{H_i}\dot{\bar{q}}_i \tag{5.69}$$

5.1.5. Singularity Analysis

The singular poses are where the manipulator loses one DoF, momentarily. These poses can be computed by making use of Jacobian matrices. Since the manipulator also contains passive joints, Jacobian matrix including the passive joints should be investigated. At singular poses, Jacobian matrix cannot be inverted. Meaning that the poses which make the determinant of Jacobian matrix zero are the singular poses.

$$\det\left(\hat{J}_i\right) = 0 \text{ at singularity} \tag{5.70}$$

The solution for the determinant gives the singular poses of the manipulator. The determinant of $\hat{J}_i$ is computed as follows.

$$\det\left(\hat{J}_i\right) = l_1 l_2 l_3 \cos q_{i1} \sin q_{i3} = 0 \tag{5.71}$$

Since the link lengths are desired to be larger than zero, the solutions for Equation 5.71 are obtained for q_{i1} and q_{i3}.

$$\cos q_{i1} = 0 \text{ and } \sin q_{i3} = 0 \tag{5.72}$$

$$\Rightarrow q_{i1} = \pm\pi/2 \text{ and } q_{i3} = 0, \pm\pi \tag{5.73}$$

Focusing on q_{i1}, there are three other poses which are used to define some critical poses of the manipulator. These poses are used in simplification of performance metrics. The home pose of the manipulator is defined to be where $q_{i1} = 0$ for $i = 1, 2, 3$. Other two poses are the fully folded where the $q_{i1} = q_{min}$ and fully extended where the $q_{i1} = q_{max}$ poses. $q_{min} < 0$ and $0 < q_{max}$ are the minimum and maximum limits of the active joints. Since the symmetry is desired for uniformity, $|q_{min}| = |q_{max}|$. The poses are shown in Figure 5.2

5.1.6. Verification of Kinematics

The forward and inverse kinematics analyses are verified by using a CAD software (Solidworks). For the verification of velocity and acceleration level kinematic, Sim-mechanics blocks in MATLAB Simulink are used to generate the model. The errors between results of kinematic analysis and obtained results from simulation programs are the numerical errors which are in the range of 10^{-18} m, 10^{-18} m/s, and 10^{-18} m/s^2, respectively for position, velocity, and acceleration.
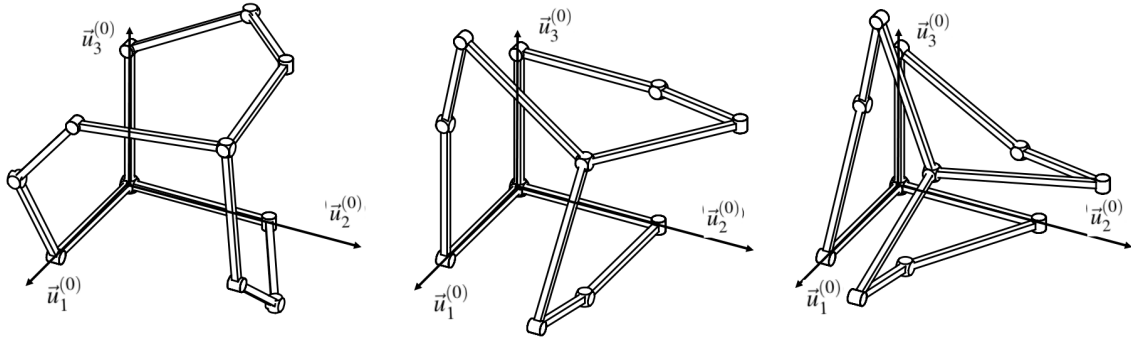
Figure 5.2. The predefined poses of the manipulator. From left to right, fully extended, home, and fully folded poses, respectively.

5.2. Stiffness Model

The stiffness of the manipulator is procured by lumping the stiffness of each elastic body on virtual joints by using the results of kinematic analysis. This makes the stiffness model pose-dependent. The pose can be determined by using forward kinematics. Forward kinematics is also used to map the external wrenches to joint space to compute the load on each elastic body. However, even if the joints are locked, the wrenches cause compliant displacement on each elastic body. This compliant displacement modifies the forward kinematics and due to this, the force/torque distribution of the external wrenches on joint space changes again. Thus, an iterative solution is required to find the equilibrium pose and to compute compliant displacements using the stiffness model. In order to reduce the computational power and solution time, the linear stiffness model assumption can be made. If the deflections are small enough, this assumption will generate a highly accurate solution with lower computational effort.

Another use of forward kinematics appears if the change in the pose is relatively; the relationship between the joints and mobile platform pose can be established the Jacobian matrix as follows;

$$\Delta \bar{r} \approx \hat{J}_m \Delta \bar{q}_m \approx \hat{J}_i \Delta \bar{q}_i \qquad (5.74)$$

In stiffness modeling, extra degree of freedom are needed to illustrate the deflection caused by the elasticity of the manipulator. For that, forward kinematics must be modified such that it includes virtual joints. In addition, Jacobian matrices must be designated in homogeneous coordinates.

Even though, an actual joint should constraint at leas one DoF, a virtual joint is

defined as a 6 DoF joint which includes 3 translations and 3 rotations. In a general format, a virtual joint can be defined as follows;

$$\hat{H}_v(\bar{\theta}_{ij}) = \hat{T}_{u1}(\theta_{ij}^1)\hat{T}_{u2}(\theta_{ij}^2)\hat{T}_{u3}(\theta_{ij}^3)\hat{R}_{u1}(\theta_{ij}^4)\hat{R}_{u2}(\theta_{ij}^5)\hat{R}_{u3}(\theta_{ij}^6) \tag{5.75}$$

$$\bar{\theta}_{ij} = \begin{bmatrix} \psi_{ij1} & \psi_{ij2} & \psi_{ij3} & \varphi_{ij1} & \varphi_{ij2} & \varphi_{ij3} \end{bmatrix}^T \tag{5.76}$$

where $\hat{H}_v$ denotes the homogeneous transformation matrix for virtual joints and $\bar{\theta}_{ij}$ is the column matrix containing virtual joint variables of jth body in i^{th} serial chain. ψ_{ijk} and φ_{ijk} denote the translational and rotational virtual joint variables and sub-script k denotes the respective translation or rotation axis for $k = 1, 2, 3$. Superscripts of θ_{ij} denote element number in the column matrix.

5.2.1. Unloaded Mode

In unloaded mode weights of intermediate links are neglected. The solution of stiffness model with that assumption is easier and faster. If the manipulator is a parallel manipulator and the weight of the links are much smaller than the external wrenches, the assumption causes small errors.
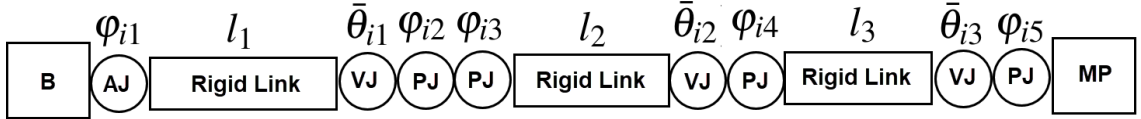
Figure 5.3. Serial kinematic of a single chain and its virtual joint model. AJ (Active Joint), PJ (Passive Joint), VJ (Virtual Joint), MP (Mobile Platform), B (Base)

The forward kinematics model for stiffness modeling is shown in Figure 5.3 for a single serial chain and the mathematical subsequent model is constructed by using Equation 5.75, which is represented by Equations 5.77 to 5.83.

$$\hat{H}^{(i0, K_{i1})} = \hat{R}_{u3}(\varphi_{i1})\hat{T}_{1u}(l_1)\hat{H}_v(\bar{\theta}_{i1}) \tag{5.77}$$

$$\hat{H}^{(K_{i1}, K_{i2})} = \hat{R}_{u3}(\varphi_{i2})\hat{R}_{u1}(-\pi/2)\hat{R}_{u3}(\varphi_{i3})\hat{T}_{u1}(l_2)\hat{H}_v(\bar{\theta}_{i2}) \tag{5.78}$$

$$\hat{H}^{(K_{i2}, K_{i3})} = \hat{R}_{3u}(\varphi_{i4})\hat{T}_{u1}(l_3)\hat{H}_v(\bar{\theta}_{i3}) \tag{5.79}$$

$$\hat{H}^{(K_{i3}, i5)} = \hat{R}_{u3}(\varphi_{i5}) \tag{5.80}$$

$$\hat{H}_{Ki} = \hat{H}^{(0,i0)} \hat{H}^{(i0,K_{i1})} \hat{H}^{(K_{i1},K_{i2})} \hat{H}^{(K_{i2},K_{i3})} \hat{H}^{(K_{i3},i5)} \hat{H}^{(i5,p)} \tag{5.81}$$

$$\hat{H}_{Ki} = \begin{bmatrix} \hat{R}_{Ki} & \bar{r}_{Ki} \\ \bar{0}^T & 1 \end{bmatrix} \tag{5.82}$$

$$\hat{H}_{K1} = \hat{H}_{K2} = \hat{H}_{K3} \tag{5.83}$$

where $\hat{H}_{Ki}$ is the homogeneous transformation matrix containing the active, passive and virtual joints. $\hat{H}_{K1} = \hat{H}_{K2} = \hat{H}_{K3}$ are assumed to be equal to each other since the stiffness of the mobile platform is relatively higher than the links. Hence, it is assumed to be rigid. These constraints are also valid when the manipulator is deflected under external wrenches. Thus, $\Delta\hat{H}_{K1} = \Delta\hat{H}_{K2} = \Delta\hat{H}_{K3}$.

The joint variables are constructed in column matrix form for proper representation.

$$\bar{q}_{pi} = \begin{bmatrix} \varphi_{i2} & \varphi_{i3} & \varphi_{i4} & \varphi_{i5} \end{bmatrix}^T_{4\times 1} \tag{5.84}$$

$$\bar{\theta}_i = \begin{bmatrix} \bar{\theta}_{i1}^T & \bar{\theta}_{i2}^T & \bar{\theta}_{i3}^T \end{bmatrix}^T_{18\times 1} \tag{5.85}$$

$$\bar{Q}_i = \begin{bmatrix} \bar{\theta}_i^T & \bar{q}_{pi}^T & q_{i1} \end{bmatrix}^T_{23\times 1} \tag{5.86}$$

where $\bar{Q}_i$ contains all joint variables for i^{th} serial chain. By making use of general notation of $\bar{Q}_i$, homogeneous Jacobian matrix can be procured for all joint variables, active, passive and virtual ones.

$$\frac{\partial\hat{H}_{Ki}}{\partial Q_{ik}} = \begin{bmatrix} \frac{\partial\hat{R}_{Ki}}{\partial Q_{ik}} & \frac{\partial\bar{r}_{Ki}}{\partial Q_{ik}} \\ \bar{0}^T & 1 \end{bmatrix} \text{ for } k = 1, 2, ..., 23 \tag{5.87}$$

where $\hat{R}_{K_i}$ and $\bar{r}_{Ki}$ denote the rotation and position matrices of the mobile platform including the virtual joints. Subscript k is used to denote the kth variable of Q_i.

Homogeneous Jacobian column matrices can be obtained in the same manner as it was done in the kinematic modeling section. Angular velocity coefficients are obtained by using the derivative of the rotation matrix.

$$\tilde{\Omega}_{ik} = \frac{\partial\hat{R}_{Ki}}{\partial Q_{ik}} \hat{R}_{Ki}^T \tag{5.88}$$

where $\tilde{\Omega}_{ik}$ is a skew symmetric matrix which contains the angular velocity coefficients.

$$\tilde{\Omega}_{ik} = \begin{bmatrix} 0 & -\Omega ik_3 & \Omega ik_2 \\ \Omega ik_3 & 0 & -\Omega ik_1 \\ -\Omega ik_2 & \Omega ik_1 & 0 \end{bmatrix} \tag{5.89}$$

By using the *col* operator the angular velocity coefficients are obtained in column matrix form.

$$\bar{\Omega}_{ik} = col(\tilde{\Omega}_{ik}) = \begin{bmatrix} \Omega ik_1 \\ \Omega ik_2 \\ \Omega ik_3 \end{bmatrix} \tag{5.90}$$

Linear velocity coefficients in column matrix form $\bar{\chi}_{ik}$ are obtained by differentiating the $\bar{r}_{Ki}$ with respect to Q_{ik}^{th} variable.

$$\bar{\chi}_{ik} = \frac{\partial \bar{r}_{Ki}}{\partial Q_{ik}} \tag{5.91}$$

Homogeneous 6×1 Jacobian column matrix $\bar{J}_{K_{ik}}$ for Q_{ik}^{th} variable is formed as follows;

$$\bar{J}_{K_{ik}} = \begin{bmatrix} \bar{\chi}_{ik} \\ \bar{\Omega}_{ik} \end{bmatrix}_{6 \times 1} \tag{5.92}$$

The homogeneous Jacobian matrix $\hat{J}_{K_i}$ containing active, passive and virtual joints for i^{th} serial chain can be written by using homogeneous Jacobian column matrices.

$$\hat{J}_{Ki} = \begin{bmatrix} \bar{J}_{K_{i1}} & \bar{J}_{K_{i2}} & ... & \bar{J}_{K_{i23}} \end{bmatrix}_{6 \times 23} \tag{5.93}$$

Here, $\hat{J}_{K_i}$ can be divided into sub-matrices using the properties of each joint. $\hat{J}_{\theta_i}$, $\hat{J}_{p_i}$, and $\bar{J}_{a_i}$ denote homogeneous Jacobian matrices obtained by differentiating with respect to the virtual joints, passive joints and active joint, respectively, for the ith serial chain.

$$\hat{J}_{\theta_i} = \begin{bmatrix} \bar{J}_{K_{i1}} & \bar{J}_{K_{i2}} & ... & \bar{J}_{K_{i18}} \end{bmatrix}_{6 \times 18} \tag{5.94}$$

$$\hat{J}_{p_i} = \begin{bmatrix} \bar{J}_{K_{i19}} & \bar{J}_{K_{i20}} & \bar{J}_{K_{i21}} & \bar{J}_{K_{i22}} \end{bmatrix}_{6 \times 4} \tag{5.95}$$

$$\bar{J}_{a_i} = \begin{bmatrix} \bar{J}_{K_{i23}} \end{bmatrix}_{6 \times 1} \tag{5.96}$$

$$\hat{J}_{Ki} = \begin{bmatrix} \hat{J}_{\theta_i} & \hat{J}_{p_i} & \bar{J}_{a_i} \end{bmatrix}_{6 \times 23} \tag{5.97}$$

Now, the obtained Jacobian matrices are organized in accordance with Equation 5.74 in order to denote the deflection at the mobile platform with respect to the base frame by making use of homogeneous Jacobian matrices.

$$\bar{\kappa}_i = \bar{f}(\bar{Q}_i) \tag{5.98}$$

$$\Delta \bar{\kappa}_i = \hat{J}_{K_i} \Delta \bar{Q}_i \tag{5.99}$$

$$\Delta \bar{\kappa}_i = \hat{J}_{\theta_i} \Delta \bar{\theta}_i + \hat{J}_{p_i} \Delta \bar{q}_{pi} + \bar{J}_{a_i} \Delta q_{i1} \tag{5.100}$$

where $\Delta \bar{\kappa}_i$ is 6×1 column matrix containing translational and rotational compliant deflections of the mobile platform frame calculated form the ith serial chain with respect to the base frame. The Δ operator denotes the difference between the initial and final states of deflection. In the initial state, there is no external wrench on the mobile platform. When the external wrenches are applied, the final state slightly changes due to the elasticity of the manipulator.

The relation between the external force/torque and joint space force/torque is provided via the Jacobian matrices as shown in Equation 4.19. By making use of $\hat{J}_{K_i}$ in Equation 5.99, the mapping mapping of the external wrenches from the Cartesian space to joint space is shown as in the following Equation;

$$\bar{F}_{K_i} = \hat{J}_{K_i}^T \bar{F}_{ext} \tag{5.101}$$

where $[\bar{F}_{K_i}]_{23 \times 1}$ is the joint space force/torque vector for virtual, passive, and active joints respectively. $[\bar{F}_{ext}]_{6 \times 1}$ is the external wrench including force and torque. However, since modified R-CUBE mechanism has 3-DoF translational motion in Cartesian space, only forces are considered in this thesis. $\bar{F}_{K_i}$ can be divided into sub-components and the force/torque vector of each type of joint are found as follows.

$$\bar{F}_{K_i} = \begin{bmatrix} \bar{F}_{\theta i} \\ \bar{F}_{pi} \\ \bar{F}_{ai} \end{bmatrix} \tag{5.102}$$

$$\begin{bmatrix} \bar{F}_{\theta i} \\ \bar{F}_{pi} \\ F_{ai} \end{bmatrix} = \begin{bmatrix} \hat{J}_{\theta_i}^T \\ \hat{0} \\ \hat{0} \end{bmatrix} \bar{F}_{ext} + \begin{bmatrix} \hat{0} \\ \hat{J}_{p_i}^T \\ \hat{0} \end{bmatrix} \bar{F}_{ext} + \begin{bmatrix} \hat{0} \\ \hat{0} \\ \bar{J}_{a_i}^T \end{bmatrix} \bar{F}_{ext} \tag{5.103}$$

where $[\bar{F}_{\theta_i}]_{18 \times 1}$, $[\bar{F}_{pi}]_{4 \times 1}$, and F_{ai} are the joint space force/torque for virtual, passive, and active joints respectively.

$\bar{F}_{K_i}$ also represents the structural reaction forces and torques. Therefore, $\bar{F}_{K_i}$ can be defined in terms of the function of stiffness matrix defined in joints space and deflections in joint space.

$$\bar{F}_{K_i} = \begin{bmatrix} \hat{K}_{\theta_i} & \hat{0} & \hat{0} \\ \hat{0} & \hat{K}_{p_i} & \hat{0} \\ \hat{0} & \hat{0} & K_{a_i} \end{bmatrix} \Delta \bar{Q}_i \qquad (5.104)$$

$$\hat{K}_{\theta_i} = \begin{bmatrix} \hat{K}_{\theta_i 1} & \hat{0} & \hat{0} \\ \hat{0} & \hat{K}_{\theta_i 2} & \hat{0} \\ \hat{0} & \hat{0} & \hat{K}_{\theta_i 3} \end{bmatrix}_{18 \times 18} \qquad (5.105)$$

where $\hat{K}_{\theta_i}$ denotes the structural stiffness matrix of a single serial chain in joint space. $\hat{K}_{\theta_i j}$ for $j = 1, 2, 3$ denotes each respective links' stiffness matrix with the size of 6×6 matrix which is defined in Equation 4.59. Therefore, the size of $\hat{K}_{\theta_i}$ is 18×18. $\hat{K}_{p_i}$ and $\hat{K}_{a_i}$ denote the 4×4 stiffness matrix and stiffness coefficient for passive and active joints.

Equation 5.104 is expressed in Cartesian space by making use of Equation 5.101 and Equation 5.99.

$$\hat{J}_{K_i}^T \bar{F}_{ext} = \begin{bmatrix} \hat{K}_{\theta_i} & \hat{0} & \hat{0} \\ \hat{0} & \hat{K}_{p_i} & \hat{0} \\ \hat{0} & \hat{0} & K_{a_i} \end{bmatrix} \Delta \bar{Q}_i \text{ and } \hat{J}_{K_i}^{-1} \Delta \bar{\kappa}_i = \Delta \bar{Q}_i \qquad (5.106)$$

$$\Rightarrow \bar{F}_{ext} = \hat{J}_{K_i}^{-T} \begin{bmatrix} \hat{K}_{\theta_i} & \hat{0} & \hat{0} \\ \hat{0} & \hat{K}_{p_i} & \hat{0} \\ \hat{0} & \hat{0} & K_{a_i} \end{bmatrix} \hat{J}_{K_i}^{-1} \Delta \bar{\kappa}_i \qquad (5.107)$$

when $\hat{J}_{K_i}$ is substituted to the above equation:

$$\bar{F}_{ext} = \begin{bmatrix} \hat{J}_{\theta_i}^{-T} & \hat{J}_{p_i}^{-T} & \bar{J}_{a_i}^{-T} \end{bmatrix} \begin{bmatrix} \hat{K}_{\theta_i} & \hat{0} & \hat{0} \\ \hat{0} & \hat{K}_{p_i} & \hat{0} \\ \hat{0} & \hat{0} & K_{a_i} \end{bmatrix} \begin{bmatrix} \hat{J}_{\theta_i}^{-1} \\ \hat{J}_{p_i}^{-1} \\ \bar{J}_{a_i}^{-1} \end{bmatrix} \Delta \bar{\kappa}_i \qquad (5.108)$$

$$\bar{F}_{ext} = (\hat{J}_{\theta_i}^{-T} \hat{K}_{\theta_i} \hat{J}_{\theta_i}^{-1} + \hat{J}_{p_i}^{-T} \hat{K}_{p_i} \hat{J}_{p_i}^{-1} + \bar{J}_{a_i}^{-T} K_{a_i} \bar{J}_{a_i}^{-1}) \Delta \bar{\kappa}_i \qquad (5.109)$$

Equation 5.109 can be further simplified. To do that, first $\Delta \bar{\kappa}_i$ should be investigated. Note that, operator Δ achieves the following computations:

$$\Delta \bar{\kappa}_i = \bar{\kappa}_i^{final} - \bar{\kappa}_i^{initial} \qquad (5.110)$$

$$\Delta\bar{\theta}_i = \bar{\theta}_i^{final} - \bar{\theta}_i^{initial} \tag{5.111}$$

$$\Delta\bar{q}_{pi} = \bar{q}_{pi}^{final} - \bar{q}_{pi}^{initial} \tag{5.112}$$

$$\Delta q_{i1} = q_{i1}^{final} - q_{i1}^{initial} \tag{5.113}$$

$\bar{\kappa}_i^{initial}$ is the computed position of the mobile platform by making use of kinematics in the initial condition. $\bar{q}_{pi}^{initial}$ is the computed passive joint variables in the initial condition. $\bar{\theta}_i^{initial} = \bar{0}$ since there is no external wrench in the initial state. In final state, $\bar{\kappa}_i^{final}$ and $\bar{q}_{pi}^{final}$ are computed in the deflected pose of the manipulator. Therefore, $\bar{\theta}_i^{final} \neq \bar{0}$ and $\bar{\theta}_i^{final} = \bar{\theta}_i$, $\bar{\kappa}_i^{final}$, and $\bar{q}_{pi}^{final}$ must be computed. $\Delta q_{i1} = 0$, since only the structural stiffness is investigated actuator stiffness neglected. As a result, $\Delta\bar{\kappa}_i$ in Equation 5.100 is updated as following.

$$\Delta\bar{\theta}_i = \bar{\theta}_i, \Delta\bar{q}_{pi} \neq \bar{0}, \Delta q_{i1} = 0$$
$$\Rightarrow \Delta\bar{\kappa}_i = \hat{J}_{\theta_i}\bar{\theta}_i + \hat{J}_{p_i}\Delta\bar{q}_{pi} \tag{5.114}$$

When the above equation is implemented in Equation 5.109, a simplified version this equation can be written as follows.

$$\bar{F}_{ext} = (\hat{J}_{\theta_i}^{-T}\hat{K}_{\theta_i}\hat{J}_{\theta_i}^{-1} + \hat{J}_{p_i}^{-T}\hat{K}_{p_i}\hat{J}_{p_i}^{-1})\Delta\bar{\kappa}_i \tag{5.115}$$

The passive joints do not generate reaction torques in their rotation axes assuming that there is no friction. So, $\hat{K}_{p_i} = \hat{0}$. Thus, $\bar{F}_{K_i}$ only contains reaction forces and torques of virtual joints. Therefore, Equation 5.115 is further simplified in Equation 5.116 and the Equation 5.118 is obtained. $\bar{\theta}_i$ is solved from Equation 5.117 to compute the $\hat{K}_{C_i}$.

$$\bar{F}_{ext} = (\hat{J}_{\theta_i}^{-T}\hat{K}_{\theta_i}\hat{J}_{\theta_i}^{-1})\Delta\bar{\kappa}_i \tag{5.116}$$

$$\bar{F}_{ext} = \hat{J}_{\theta_i}^{-T}\hat{K}_{\theta_i}\bar{\theta}_i \tag{5.117}$$

$$\hat{J}_{p_i}^{T}\bar{F}_{ext} = \bar{0} \tag{5.118}$$

The structural stiffness matrix $\hat{K}_{C_i}$ of ith serial chain, hence, is the coefficient matrix of $\Delta\bar{\kappa}_i$.

$$\hat{K}_{C_i} = (\hat{J}_{\theta_i}^{-T}\hat{K}_{\theta_i}\hat{J}_{\theta_i}^{-1})_{6\times6} \tag{5.119}$$

$$rank(\hat{K}_{Ci}) = 6 \tag{5.120}$$

Direct multiplication of $\hat{J}_{\theta_i}^{-T}\hat{K}_{\theta_i}\hat{J}_{\theta_i}^{-1}$, however, omits the effects of passive joints and has the full rank of 6. Passive joints are normally constrained by the connection of several serial chains. However, in VJM each serial chain is assumed as independent serial manipulators and later they are summed in order to procure the Cartesian stiffness matrix.

Therefore, the effect of passive joints should be included in stiffness matrix $\hat{K}_{C_i}$. The effect is induced by constructing the following homogeneous relation matrix structure.

$$
\begin{bmatrix} (\hat{J}_{\theta_i} \hat{K}_{\theta_i}^{-1} \hat{J}_{\theta_i}^T) & \hat{J}_{p_i} \\ \hat{J}_{p_i}^T & \hat{0} \end{bmatrix} \begin{bmatrix} \bar{F}_{ext} \\ \Delta \bar{q}_{pi} \end{bmatrix} = \begin{bmatrix} \Delta \bar{\kappa}_i \\ \bar{0} \end{bmatrix}
\tag{5.121}
$$

The matrix at the left-hand side of Equation 5.121, contains the compliance information. Taking its inverse produces rank deficient $\hat{K}_{Ci}$ matrix.

$$
\begin{bmatrix} (\hat{J}_{\theta_i} \hat{K}_{\theta_i}^{-1} \hat{J}_{\theta_i}^T) & \hat{J}_{p_i} \\ \hat{J}_{p_i}^T & \hat{0} \end{bmatrix}^{-1} = \begin{bmatrix} \hat{K}_{Ci} & * \\ * & * \end{bmatrix}
\tag{5.122}
$$

Since the passive joints generate an extra degree of freedom in Cartesian space, modified $\hat{K}_{Ci}$ is rank deficient. The rank of $\hat{K}_{Ci}$ depends on the pose of the manipulator. When the position of the last frame in a serial chain aligns with the rotation axis of second joint φ_{i2}, the rank of $\hat{K}_{Ci} = 2$ is shown in Figure 5.4. This means that the torsional load along the φ_{i2} from the last frame does not generate any reaction force/torque on the links and it freely rotates under torsional load. This pose corresponds to the home position of the designed manipulator. The rank of $\hat{K}_{Ci} = 3$ for an arbitrary pose other than the singular and home position. There are multiple conditions for singularity. At each singular pose, the rank increases by 1.
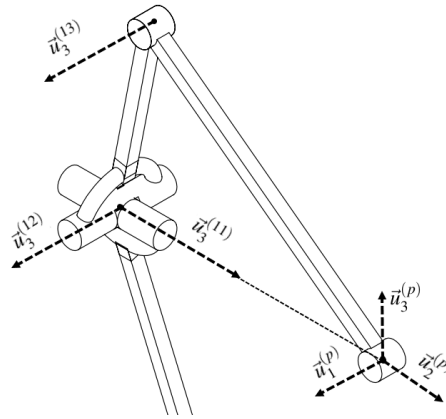
Figure 5.4. $\vec{u}_3$ axis of (11) frame of 1st serial chain is aligned with the mobile platform frame.

VJM stiffness modeling technique firstly computes each serial chain, independently. Then sums them up in order to obtain the Cartesian stiffness matrix as if they are

parallel connected springs as shown in Equation 5.123.

$$\hat{K}_C = \sum_{i=1}^{3} \hat{K}_{Ci} \qquad (5.123)$$

If there is no external wrench on the mobile platform $\bar{F}_{ext} = \bar{0}$, $\hat{K}_{Ci}$ takes the following form assuming that the manipulator is not in singular or home pose.

$$\hat{K}_{C1} = \begin{bmatrix} K_{C1}11 & 0 & 0 & 0 & K_{C1}15 & K_{C1}16 \\ 0 & 0 & 0 & 0 & 0 & 0 \\ 0 & 0 & 0 & 0 & 0 & 0 \\ 0 & 0 & 0 & 0 & 0 & 0 \\ K_{C1}15 & 0 & 0 & 0 & K_{C1}55 & K_{C1}56 \\ K_{C1}16 & 0 & 0 & 0 & K_{C1}56 & K_{C1}66 \end{bmatrix} \qquad (5.124)$$

$$\hat{K}_{C2} = \begin{bmatrix} 0 & 0 & 0 & 0 & 0 & 0 \\ 0 & K_{C2}22 & 0 & K_{C2}24 & 0 & K_{C2}26 \\ 0 & 0 & 0 & 0 & 0 & 0 \\ 0 & K_{C2}24 & 0 & K_{C2}44 & 0 & K_{C2}46 \\ 0 & 0 & 0 & 0 & 0 & 0 \\ 0 & K_{C2}26 & 0 & K_{C2}46 & 0 & K_{C2}66 \end{bmatrix} \qquad (5.125)$$

$$\hat{K}_{C3} = \begin{bmatrix} 0 & 0 & 0 & 0 & 0 & 0 \\ 0 & 0 & 0 & 0 & 0 & 0 \\ 0 & 0 & K_{C3}33 & K_{C3}34 & K_{C3}35 & 0 \\ 0 & 0 & K_{C3}34 & K_{C3}44 & K_{C3}45 & 0 \\ 0 & 0 & K_{C3}35 & K_{C3}45 & K_{C3}55 & 0 \\ 0 & 0 & 0 & 0 & 0 & 0 \end{bmatrix} \qquad (5.126)$$

After obtaining the modified $\hat{K}_{Ci}$, the stiffness matrix of the manipulator in Cartesian space is calculated by summing the $\hat{K}_{Ci}$ matrices for $i = 1, 2, 3$ and its rank is found to be 6.

$$
\hat{K}_C = \begin{bmatrix}
K_{C1}11 & 0 & 0 & 0 & K_{C1}15 & K_{C1}16 \\
0 & K_{C2}22 & 0 & K_{C2}24 & 0 & K_{C2}26 \\
0 & 0 & K_{C3}33 & K_{C3}34 & K_{C3}35 & 0 \\
0 & K_{C2}24 & K_{C3}34 & K_{C2}44 + K_{C3}44 & K_{C3}45 & K_{C2}46 \\
K_{C1}15 & 0 & K_{C3}35 & K_{C3}45 & K_{C1}55 + K_{C3}55 & K_{C1}56 \\
K_{C1}16 & K_{C2}26 & 0 & K_{C2}46 & K_{C1}56 & K_{C1}66 + K_{C2}66
\end{bmatrix}
$$

$$(5.127)$$

If the serial chains are identical in terms of link geometry, the stiffness matrix in joint space is the same for all of them. This effect can be seen in stiffness matrix in Cartesian space as well such that;

$$K_{C1}11 = K_{C2}22 = K_{C3}33,$$

$$K_{C1}15 = K_{C2}26 = K_{C3}34,$$

$$K_{C1}16 = K_{C2}24 = K_{C3}35,$$

$$K_{C1}56 = K_{C2}46 = K_{C3}45,$$

$$K_{C1}55 = K_{C2}66 = K_{C3}44,$$

$$K_{C1}66 = K_{C2}44 = K_{C3}55.$$

A special case occurs when the manipulator is at home position. The rank of $\hat{K}_{Ci} = 2$. Yet, the rank $\hat{K}_C = 6$. The stiffness matrix is given below for the home position considering that;

$$K_{C1}15 = K_{C2}26 = K_{C3}34 = 0,$$

$$K_{C1}56 = K_{C2}46 = K_{C3}45 = 0,$$

$$K_{C1}55 = K_{C2}66 = K_{C3}44 = 0.$$

$$
\hat{K}_C = \begin{bmatrix}
K_{C1}11 & 0 & 0 & 0 & 0 & K_{C1}16 \\
0 & K_{C2}22 & 0 & K_{C2}24 & 0 & 0 \\
0 & 0 & K_{C3}33 & 0 & K_{C3}35 & 0 \\
0 & K_{C2}24 & 0 & K_{C2}44 & 0 & 0 \\
0 & 0 & K_{C3}35 & 0 & K_{C3}55 & 0 \\
K_{C1}16 & 0 & 0 & 0 & 0 & K_{C1}66
\end{bmatrix}
$$

$$(5.128)$$

If the active joint does not generate resistance torque to the user, the rank of $\hat{K}_C$ is reduced to 3. This loss occurs at the upper and lower left and upper right 3×3 part of $\hat{K}_C$ which indicates that there is no resistance to translational motion. However, torque inputs from the mobile platform will cause structural deflection even if the actuators are not powered. Yet, there will be no translatory motion on the mobile platform.

In the case of the existence of external wrench, extra elements appear on non-diagonal parts of $\hat{K}_{Ci}$. The construction is updated according to the following equations.

$$\bar{F}_{ext} = \begin{bmatrix} 1 & 1 & 1 & 1 & 1 & 1 \end{bmatrix}^T \tag{5.129}$$

$$\hat{K}_{Ci} = \begin{bmatrix} K_{Ci}11 & K_{Ci}12 & K_{Ci}13 & K_{Ci}14 & K_{Ci}15 & K_{Ci}16 \\ K_{Ci}12 & K_{Ci}22 & K_{Ci}23 & K_{Ci}24 & K_{Ci}25 & K_{Ci}26 \\ K_{Ci}13 & K_{Ci}23 & K_{Ci}33 & K_{Ci}34 & K_{Ci}35 & K_{Ci}36 \\ K_{Ci}14 & K_{Ci}24 & K_{Ci}34 & K_{Ci}44 & K_{Ci}45 & K_{Ci}46 \\ K_{Ci}15 & K_{Ci}25 & K_{Ci}35 & K_{Ci}45 & K_{Ci}55 & K_{Ci}56 \\ K_{Ci}16 & K_{Ci}26 & K_{Ci}36 & K_{Ci}46 & K_{Ci}56 & K_{Ci}66 \end{bmatrix} \tag{5.130}$$

$$rank(\hat{K}_{Ci}) = 6 \tag{5.131}$$

When the force/torque in all directions is applied to the mobile platform, deflections accrue in joint space. The forward kinematic parameters change in accordance with the deflections. As a result of this, resistance to motion is generated and the manipulator becomes more stiff compared to no load case. Although the effect of passive joints still exists, $\hat{K}_{Ci}$ in no longer rank deficient. Yet, thanks to passive joints, some terms can be neglected due to their incomparable magnitude among the dominant ones. This elimination only valid if the external wrenches are small enough or the manipulator is rigid compared to applied wrenches. The following stiffness matrices are obtained for $l_1 = 0.12$m, $l_2 = 0.1$m, $l_3 = 0.18$m. The links are assumed to be hollow tubes with $D_{ij} = 10$mm and $d_{ij} = 4$mm for outer and inner diameters, respectively. The link material is chosen as structural steel.

$$\hat{K}_{C1} = \begin{bmatrix} 16584 & -446 & -1486 & 257 & -2370 & 2737 \\ -446 & 13 & 38 & -6 & 64 & -56 \\ -1486 & 38 & 136 & -24 & 213 & -271 \\ 257 & -6 & -24 & 5 & -37 & 54 \\ -2370 & 64 & 213 & -37 & 339 & -394 \\ 2737 & -56 & -271 & 54 & -394 & 663 \end{bmatrix} \tag{5.132}$$

$$\hat{K}_{C2} = \begin{bmatrix} 136 & -1486 & 38 & -271 & -24 & 213 \\ -1486 & 16584 & -446 & 2737 & 257 & -2370 \\ 38 & -446 & 13 & -56 & -6 & 64 \\ -271 & 2737 & -56 & 663 & 54 & -394 \\ -24 & 257 & -6 & 54 & 5 & -37 \\ 213 & -2370 & 64 & -394 & -37 & 339 \end{bmatrix} \tag{5.133}$$

$$\hat{K}_{C3} = \begin{bmatrix} 13 & 38 & -446 & 64 & -56 & -6 \\ 38 & 136 & -1486 & 213 & -271 & -24 \\ -446 & -1486 & 16584 & -2370 & 2737 & 257 \\ 64 & 213 & -2370 & 339 & -394 & -37 \\ -56 & -271 & 2737 & -394 & 663 & 54 \\ -6 & -24 & 257 & -37 & 54 & 5 \end{bmatrix} \tag{5.134}$$

Neglecting the relatively smaller values;

$$\hat{K}_{C1} = \begin{bmatrix} K_{C1}11 & K_{C1}12 & K_{C1}13 & K_{C1}14 & K_{C1}15 & K_{C1}16 \\ K_{C1}12 & 0 & 0 & 0 & 0 & 0 \\ K_{C1}13 & 0 & 0 & 0 & K_{C1}35 & K_{C1}36 \\ K_{C1}14 & 0 & 0 & 0 & 0 & 0 \\ K_{C1}15 & 0 & K_{C1}35 & 0 & K_{C1}55 & K_{C1}56 \\ K_{C1}16 & 0 & K_{C1}36 & 0 & K_{C1}56 & K_{C1}66 \end{bmatrix} \tag{5.135}$$

$$\hat{K}_{C2} = \begin{bmatrix} 0 & K_{C2}12 & 0 & K_{C2}14 & 0 & K_{C2}16 \\ K_{C2}12 & K_{C2}22 & K_{C2}23 & K_{C2}24 & K_{C2}25 & K_{C2}26 \\ 0 & K_{C2}23 & 0 & 0 & 0 & 0 \\ K_{C2}14 & K_{C2}24 & 0 & K_{C2}44 & 0 & K_{C2}46 \\ 0 & K_{C2}25 & 0 & 0 & 0 & 0 \\ K_{C2}16 & K_{C2}26 & 0 & K_{C2}46 & 0 & K_{C2}66 \end{bmatrix} \tag{5.136}$$

$$\hat{K}_{C3} = \begin{bmatrix} 0 & 0 & K_{C3}13 & 0 & 0 & 0 \\ 0 & 0 & K_{C3}23 & K_{C3}24 & K_{C3}25 & 0 \\ K_{C3}13 & K_{C3}23 & K_{C3}33 & K_{C3}34 & K_{C3}35 & K_{C3}36 \\ 0 & K_{C3}24 & K_{C3}34 & K_{C3}44 & K_{C3}45 & 0 \\ 0 & K_{C3}25 & K_{C3}35 & K_{C3}45 & K_{C3}55 & 0 \\ 0 & 0 & K_{C3}36 & 0 & 0 & 0 \end{bmatrix} \tag{5.137}$$

After neglecting the small values, the ranks are calculated as;

$$rank(\hat{K}_{C1}) = rank(\hat{K}_{C2}) = rank(\hat{K}_{C3}) = 5$$

By summing them, stiffness matrix in Cartesian space is obtained.

$$\hat{K}_C = \begin{bmatrix} K_{C1}11 & K_{C1}12 + K_{C2}12 & K_{C1}13 + K_{C3}13 & K_{C1}14 + K_{C2}14 & K_{C1}15 & K_{C1}16 + K_{C2}16 \\ & K_{C2}22 & K_{C2}23 + K_{C3}23 & K_{C2}24 + K_{C3}24 & K_{C2}25 + K_{C3}25 & K_{C2}26 \\ & & K_{C3}33 & K_{C3}34 & K_{C1}35 + K_{C3}35 & K_{C1}36 + K_{C3}36 \\ & & & K_{C2}44 + K_{C3}44 & +K_{C3}45 & K_{C2}46 \\ & & & & K_{C1}55 + K_{C3}55 & K_{C1}56 \\ & & & & & K_{C1}66 + K_{C2}66 \end{bmatrix}$$
$$\tag{5.138}$$

where $\hat{K}_C$ is a symmetric stiffness matrix in Cartesian space with a rank of 6.

5.2.2. Loaded Mode

In the loaded mode, the weights of the links are included in the computation of Cartesian stiffness matrix. An additional forward kinematic analysis is needed to illustrate the mass center location of the links so that the weights of the links can be included in stiffness model. Figure 5.5 shows kinematic model for loaded mode where l_{gj} for
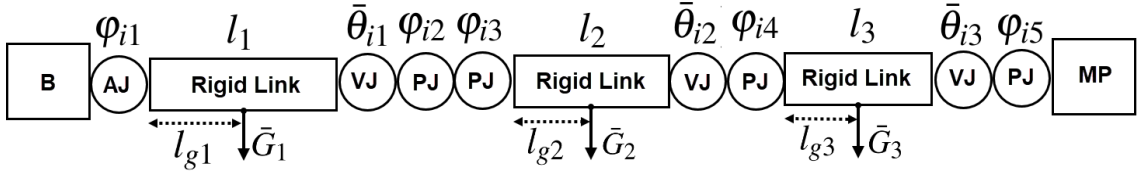
Figure 5.5. Serial kinematic of a single chain and its virtual joint model with the weights. AJ (Active Joint), PJ (Passive Joint), VJ (Virtual Joint), MP (Mobile Platform), B (Base)

$j = 1, 2, 3$ is the distance of mass center with respect to body fixed frame of jth link. $\bar{G}_j$ for $j = 1, 2, 3$ is the weight vector of jth link defined in Cartesian space.

$$\hat{H}^{(i0, K_{gi1})} = \hat{R}_{u3}(\varphi_{i1})\hat{T}_{u1}(l_{g1}) \tag{5.139}$$

$$\hat{H}^{(i0, K_{gi2})} = \hat{H}^{(i0, K_{i1})}\hat{R}_{u3}(\varphi_{i2})\hat{R}_{u1}(-\pi/2)\hat{R}_{u3}(\varphi_{i3})\hat{T}_{u1}(l_{g2}) \tag{5.140}$$

$$\hat{H}^{(i0, K_{gi3})} = \hat{H}^{(i0, K_{i1})}\hat{H}^{(K_{i1}, K_{i2})}\hat{R}_{u3}(\varphi_{i4})\hat{T}_{u1}(l_{g3}) \tag{5.141}$$

$$\hat{H}^{(i0, K_{gi4})} = \hat{H}^{(i0, K_{i1})}\hat{H}^{(K_{i1}, K_{i2})}\hat{H}^{(K_{i2}, K_{i3})}\hat{R}_{u3}(\varphi_{i5}) \tag{5.142}$$

$$\hat{H}_{K_{gij}} = \hat{H}^{(0, i0)}\hat{H}^{(i0, K_{gij})} \tag{5.143}$$

$$\hat{H}_{K_{gij}} = \begin{bmatrix} \hat{R}_{Kgij} & \bar{r}_{Kgij} \\ \bar{0}^T & 1 \end{bmatrix} \tag{5.144}$$

where $\hat{H}_{Kgij}$ denotes homogeneous transformation matrix from base frame to mass center frame of jth body. $j = 4$ stands for the mobile platform. $\hat{H}_{Kgij}$ includes the virtual joints as well. Thus, the pose of the mass center can be computed for the deflected manipulator pose. Notice that, for the first link's center of mass, there is no virtual joint defined. The reason for this is because the virtual joint method presumes the deflections occurs at the end of the link. Since the mass center is defined before the first virtual joint, the weight of the link cannot be computed in stiffness calculation. To solve this problem, finite element method or structural matrix method can be used. Another method might be moving the virtual joints to the tip of the links which require modification in stiffness matrices. However, both methods are beyond the scope of the study.

The homogeneous Jacobian matrices are obtained in the same manner as the unloaded mode. In order to denote each weight, separate Jacobian matrices are derived for each body. Derivatives are only taken with respect to virtual joint variables because Jacobian matrix for passive joints is already obtained.

$$\frac{\partial \hat{H}_{Kgi1}}{\partial \theta_{ik}} = \begin{bmatrix} \frac{\partial \hat{R}_{Kgi1}}{\partial \theta_{ik}} & \frac{\partial \bar{r}_{Kgi1}}{\partial \theta_{ik}} \\ \bar{0}^T & 1 \end{bmatrix} \tag{5.145}$$

$$\frac{\partial \hat{H}_{Kgi2}}{\partial \theta_{ik}} = \begin{bmatrix} \frac{\partial \hat{R}_{Kgi2}}{\partial \theta_{ik}} & \frac{\partial \bar{r}_{Kgi2}}{\partial \theta_{ik}} \\ \bar{0}^T & 1 \end{bmatrix} \tag{5.146}$$

$$\frac{\partial \hat{H}_{Kgi3}}{\partial \theta_{ik}} = \begin{bmatrix} \frac{\partial \hat{R}_{Kgi3}}{\partial \theta_{ik}} & \frac{\partial \bar{r}_{Kgi3}}{\partial \theta_{ik}} \\ \bar{0}^T & 1 \end{bmatrix} \tag{5.147}$$

$$\frac{\partial \hat{H}_{Kgi4}}{\partial \theta_{ik}} = \begin{bmatrix} \frac{\partial \hat{R}_{Kgi4}}{\partial \theta_{ik}} & \frac{\partial \bar{r}_{Kgi4}}{\partial \theta_{ik}} \\ \bar{0}^T & 1 \end{bmatrix} \tag{5.148}$$

Procured Jacobian matrices;

$$\hat{J}_{\theta g i1} = \begin{bmatrix} \bar{0} & \bar{0} & ... & \bar{0} \end{bmatrix}_{6 \times 18} \tag{5.149}$$

$$\hat{J}_{\theta g i2} = \begin{bmatrix} \bar{J}_{\theta g i21} & \bar{J}_{\theta g i22} & ... & \bar{J}_{\theta g i26} & ... & \bar{0} \end{bmatrix}_{6 \times 18} \tag{5.150}$$

$$\hat{J}_{\theta g i3} = \begin{bmatrix} \bar{J}_{\theta g i31} & \bar{J}_{\theta g i32} & ... & \bar{J}_{\theta g i312} & ... & \bar{0} \end{bmatrix}_{6 \times 18} \tag{5.151}$$

$$\hat{J}_{\theta g i4} = \begin{bmatrix} \bar{J}_{\theta g i41} & \bar{J}_{\theta g i42} & ... & \bar{J}_{\theta g i418} \end{bmatrix}_{6 \times 18} \tag{5.152}$$

$$\hat{J}_{\theta g i} = \begin{bmatrix} \hat{J}_{\theta g i1}^T & \hat{J}_{\theta g i2}^T & \hat{J}_{\theta g i3}^T & \hat{J}_{\theta g i4}^T \end{bmatrix}_{24 \times 18}^T \tag{5.153}$$

The weights of the links are calculated as external forces in Cartesian space because the nature of them is same as the external wrenches applied on the mobile platform. They do not vary with respect to pose of the manipulator.

$$\bar{G}_{ij} = \left(\begin{bmatrix} m_{ij}\bar{g}^T & \bar{0}_{1\times3}^T \end{bmatrix}^T \right)_{6\times1} \text{ for } j = 1, 2, 3, 4 \tag{5.154}$$

$$\bar{g} = \begin{bmatrix} 0 & 0 & -9.81 \end{bmatrix}^T \text{ m/s}^2 \tag{5.155}$$

$$\bar{G}_i = \begin{bmatrix} \bar{G}_{i1}^T & \bar{G}_{i2}^T & \bar{G}_{i3}^T & \bar{G}_{i4}^T \end{bmatrix}^T \tag{5.156}$$

m_{ij} is the mass of jth body in i^{th} serial chain, $\bar{G}_{ij}$ denotes the weight column matrix, $\bar{g}$ is the gravitational acceleration in Cartesian space, $\bar{G}_i$ is the lumped weight column matrix.

By making use of the Jacobian matrices for mass centers and weights of the links, deflection and force/torque equilibrium is constructed as follows;

$$\hat{J}_{\theta g i}^T \bar{G}_i + \hat{J}_{\theta i}^T \bar{F}_{ext} = \hat{K}_{\theta i} \bar{\theta}_i \tag{5.157}$$

Equation 5.157 is solved in order to obtain $\bar{\theta}_i$. Then, $\bar{\theta}_i$ is substituted in $\hat{J}_{\theta_i}$. $\hat{J}_{\theta_i}$ is used to obtain the stiffness matrix of the manipulator $\hat{K}_{Cgf}$ in loaded mode.

$$\begin{bmatrix} (\hat{J}_{\theta_i} \hat{K}_{\theta_i} \hat{J}_{\theta_i}^T) & \hat{J}_{p_i} \\ \hat{J}_{p_i}^T & \hat{0} \end{bmatrix}^{-1} = \begin{bmatrix} \hat{K}_{Cgfi} & * \\ * & * \end{bmatrix} \tag{5.158}$$

$$rank(\hat{K}_{Cgfi}) = 3 \tag{5.159}$$

$$\hat{K}_{Cg} = \sum_{i=1}^{3} \hat{K}_{Cgfi} \tag{5.160}$$

$$rank(\hat{K}_{Cgf}) = 6 \tag{5.161}$$

Note that, $\bar{F}_{ext}$ may change direction and magnitude depending on the haptic interaction type. $\bar{G}_i$, on the other hand, does not change since it is generated by constant mass of the link and constant gravitational acceleration. This property can be used to generate stiffness matrix $\hat{K}_{Cg}$ which is obtained by excluding the external wrenches. Computed stiffness matrix $\hat{K}_C$ for external wrenches can be summed with the stiffness matrix $\hat{K}_{Cg}$ in order to obtain $\hat{K}_{Cgf}$.

5.2.3. Solution Algorithm

The objective for both modes is to obtain the deflected joint space variables $\bar{\theta}_i$ in order to accrue the Cartesian stiffness matrix. The solution can be computed via direct solution method or iterative solution methods. It is obvious that the iterative solution will result in more accurate solutions in exchange for computation time. Although the computation time may not be crucial in design process, it is vital if the stiffness model is used in the control algorithm to operate in real-time. Hence, direct solution of stiffness model should be preferred if it is used in control. The iterative solution should be preferred in design stage due to its accuracy since there is no need for computation in real time.

The direct solution algorithm is shown in Figure 5.6. It is assumed that the external wrench is known. The solution of 5.117 in unloaded mode and 5.157 in loaded mode for $\bar{\theta}_i$ is obtained by constructing the $\hat{J}_{\theta_i} = \hat{J}_{\theta_i}^{initial} = \hat{J}_{\theta_i}(\bar{\theta}_i^{initial}, \bar{q}_{pi}^{initial}, q_{i1}^{initial})$. Thus, $\hat{J}_{\theta_i}$ is never updated and assumed to be constant where for $\bar{\theta}_i^{initial} = \bar{0}$.

In iterative solution, $\hat{J}_{\theta_i}$ is updated in each iteration with respect to obtained solution of $\bar{\theta}_i^n$ where superscript n denotes the nth iteration. $\hat{J}_{\theta_i} = \hat{J}_{\theta_i}^n$ computed in for n iterations until the force equilibrium is ensured in Equation 5.117 in unloaded mode and

in Equation 5.157 in loaded mode. Again it is assumed that the external wrench is known. The solution algorithm is shown in Figure 5.7.

For the above solution, methods are focused on a single serial chain each time. In reality, if one of the serial chains is deflected, other ones also must be deflected. This effect should be considered during the solution. This requires an extension in iterative solution for the whole manipulator.

The multiplication of external wrench and the weights with the respective Jacobian matrices gives the reaction force/torque distribution in virtual joints. As the serial chain bends, the force distribution also copes with the deflection. In the above calculations, the change in force distribution is considered in terms of a single serial chain but the magnitude of the force on a single serial chain is kept constant. When the whole manipulator is investigated, it can be concluded that as the deflections accrue, the force acting on a single serial is distributed on the other serial chains. Therefore, the solution must be in equilibrium at the last frames of serial chains in terms of force and position. In order to get the most accurate solution, equilibrium of the whole manipulator should be checked. Figure 5.8 illustrates the required algorithm to accommodate this solution.

5.2.4. Stiffness Matrix of a Single Composite Link

In this section, the stiffness matrix of a composite link is derived. $\hat{J}_{\theta_i}$ has already been procured and $\hat{K}_{\theta_i}$ is known in general format but link shapes are not discussed yet. Hence, it is necessary to derive the mathematical model of the links to obtain the properties such as the second moment of area and cross-section area. This model is useful when discussing the implementation of the performance metrics in the objective function. Figure 5.9 shows the axes with respect to a link and the dimensional notations are given.

$\hat{K}_C$ is a function of $E_x, E_y, A, L, G_{xy}, J, I_y, I_z$. The geometric properties are the cross section area A, link length L, polar moment J, second moment of area I_y and I_z. For a tube, computation of the geometric values are straightforward and given as

$$I_y = \frac{\pi}{4}((\frac{D_{ij}}{2})^4 - (\frac{d_{ij}}{2})^4) \tag{5.162}$$

$$I_z = I_y \tag{5.163}$$

$$J = \frac{\pi}{2}((\frac{D_{ij}}{2})^4 - (\frac{d_{ij}}{2})^4) \tag{5.164}$$

$$A = \pi((\frac{D_{ij}}{2})^2 - (\frac{d_{ij}}{2})^2) \tag{5.165}$$

$$L = l_{ij} \tag{5.166}$$
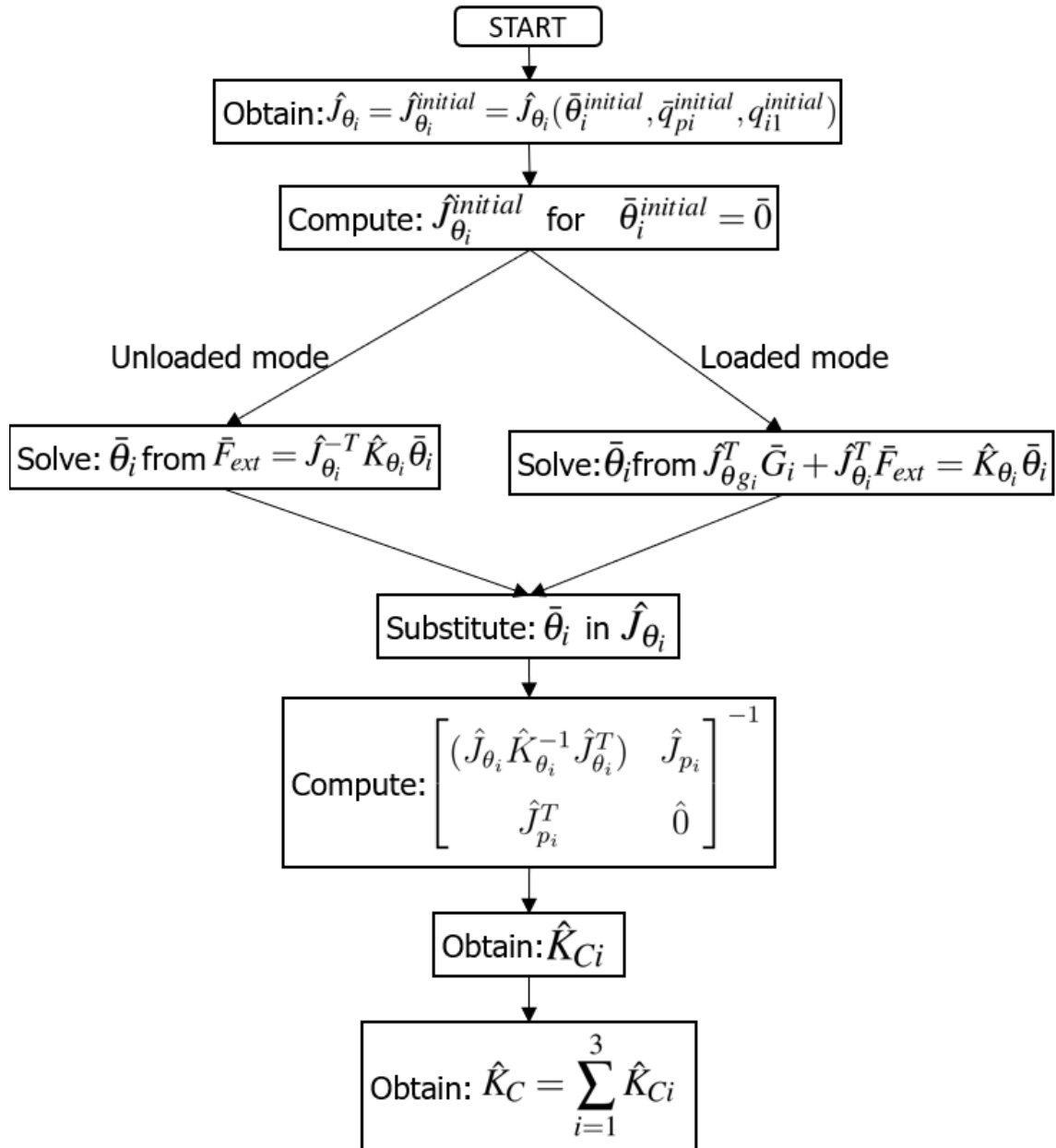
Figure 5.6. Direct solution flow chart.
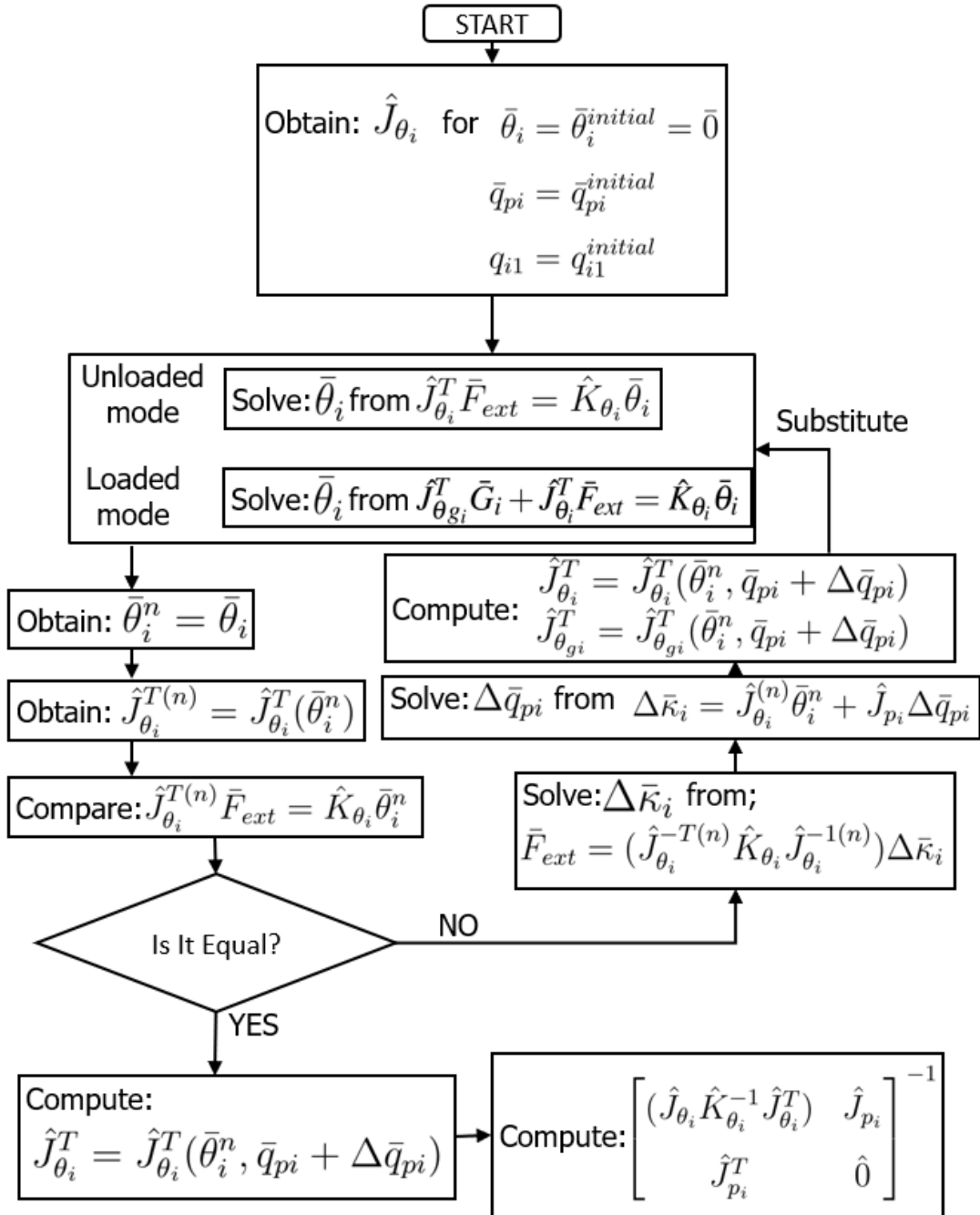
Figure 5.7. Iterative solution flow chart for force equilibrium.
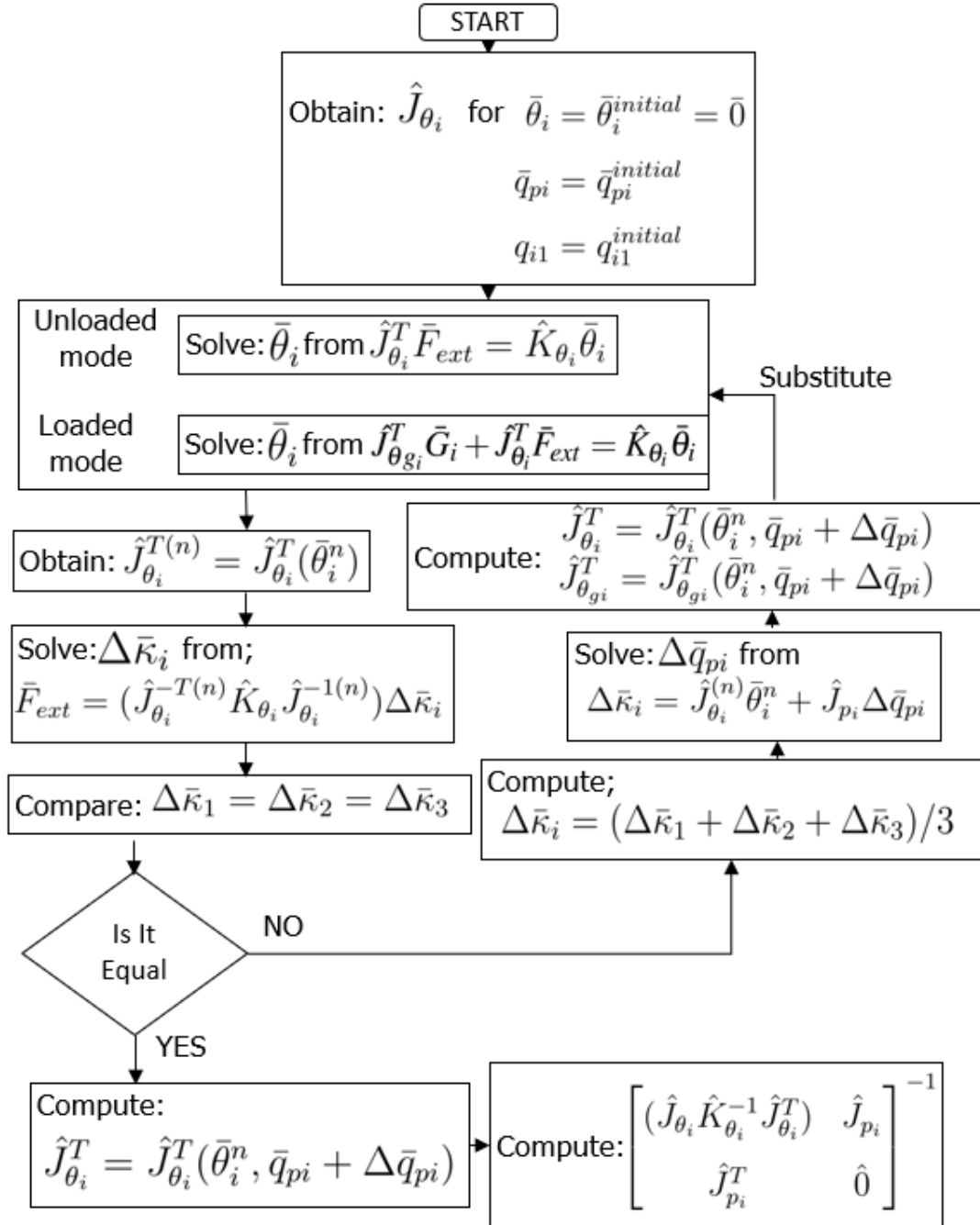
Figure 5.8. Iterative solution flow chart for pose equilibrium.
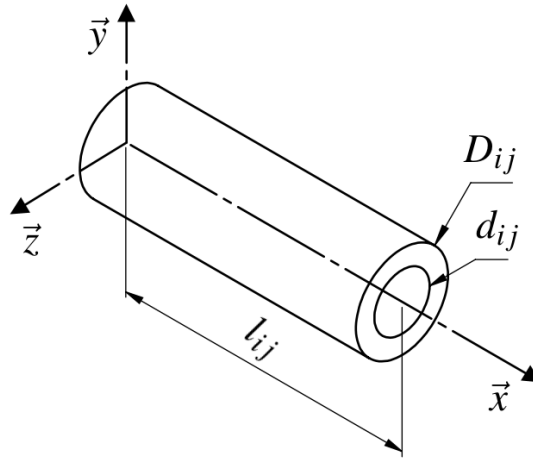
Figure 5.9. Dimensional parameters and the axes alignment of a single link. D_{ij}, d_{ij}, and l_{ij} denote the outer and inner diameters and the link length of jth link belonging the ith axis.

E_x, E_y, and G_{xy} depend on in which angle the plies are laid up. Commercially available composite links are generally have the angle of $0°$, $90°$, $-45°$ and $45°$. Custom orientation is also possible yet it is not desired due to the costs. While $0°$ and $90°$ lay up enhances the strength of the link against the bending and crushing forces, $-45°$ and $45°$ guarantee that the link is durable under the torsional loads. When the manipulator is assumed to be rigid, there is no torsion acting on the 3rd link which is connected with the mobile platform. In reality, however, the links are compliant and all of them experience torsion under load. Therefore, the composite tube plies should be laid up in all orientations.

The mechanical properties of carbon composite are adopted from the '6K M55J' model composite material (see Appendix A). Given properties are listed as;

$$E_1 = 300 GPa$$
$$E_2 = 12 GPa$$
$$G_{12} = 5 GPa$$
$$\nu_{12} = 0.3$$

Assuming that all layers have the same thickness, E_x, E_y, and G_{xy} are computed for $0°$, $90°$, $-45°$ and $45°$ orientation as follows;

$$@0°: \frac{1}{E_x^{0°}} = \frac{1}{E_1} \tag{5.167}$$

97

$$\frac{1}{E_y^{0°}} = \frac{1}{E_2} \tag{5.168}$$

$$\frac{1}{G_{xy}^{0°}} = \frac{1}{G_{12}} \tag{5.169}$$

$$@90°: \frac{1}{E_x^{90°}} = \frac{1}{E_2} \tag{5.170}$$

$$\frac{1}{E_y^{90°}} = \frac{1}{E_1} \tag{5.171}$$

$$\frac{1}{G_{xy}^{90°}} = \frac{1}{G_{12}} \tag{5.172}$$

$$@-45°: \frac{1}{E_x^{-45°}} = \frac{1}{4E_1} + \left(\frac{1}{4G_{12}} - \frac{2v_{12}}{4E_1}\right) + \frac{1}{4E_2} \tag{5.173}$$

$$\frac{1}{E_y^{-45°}} = \frac{1}{4E_1} + \left(\frac{1}{4G_{12}} - \frac{2v_{12}}{4E_1}\right) + \frac{1}{4E_2} \tag{5.174}$$

$$\frac{1}{G_{xy}^{-45°}} = 2\left(\frac{2}{4E_1} + \frac{2}{4E_2} + \frac{4v_{12}}{4E_1} - \frac{1}{4G_{12}}\right) + \frac{1}{4G_{12}} \tag{5.175}$$

$$@45°: \frac{1}{E_x^{45°}} = \frac{1}{4E_1} + \left(\frac{1}{4G_{12}} - \frac{2v_{12}}{4E_1}\right) + \frac{1}{4E_2} \tag{5.176}$$

$$\frac{1}{E_y^{45°}} = \frac{1}{4E_1} + \left(\frac{1}{4G_{12}} - \frac{2v_{12}}{4E_1}\right) + \frac{1}{4E_2} \tag{5.177}$$

$$\frac{1}{G_{xy}^{45°}} = 2\left(\frac{2}{4E_1} + \frac{2}{4E_2} + \frac{4v_{12}}{4E_1} - \frac{1}{4G_{12}}\right) + \frac{1}{4G_{12}} \tag{5.178}$$

The overall stiffness of laminate is computed by the arithmetic average of Young's and shear moduli.

$$E_x = (aE_x^{0°} + bE_x^{90°} + cE_x^{-45°} + dE_x^{45°})/(a + b + c + d) \tag{5.179}$$

$$E_y = (aE_y^{0°} + bE_y^{90°} + cE_y^{-45°} + dE_y^{45°})/(a + b + c + d) \tag{5.180}$$

$$G_{xy} = (aG_{xy}^{0°} + bG_{xy}^{90°} + cG_{xy}^{-45°} + dG_{xy}^{45°})/(a + b + c + d) \tag{5.181}$$

where a, b, c, and d are the numbers of respective plies that are used in the laminate.

5.2.5. Verification of the Stiffness Model

In order to approve the formulation approach of the VJM, first, a hollow cylinder link is modeled with 50 mm length, 4 mm inner diameter, and 6 mm outer diameter. Structural steel is chosen as the link material. The model of the hollow tube is obtained

in MATLAB with VJM. Then, the tube is modeled in ADAMS and ANSYS Workbench. Unit force and torques are induced to all models. The direct solution method is adopted for all models. It is observed that the compliant displacement errors between the models are less than 1% for both translational and rotational compliant displacements.
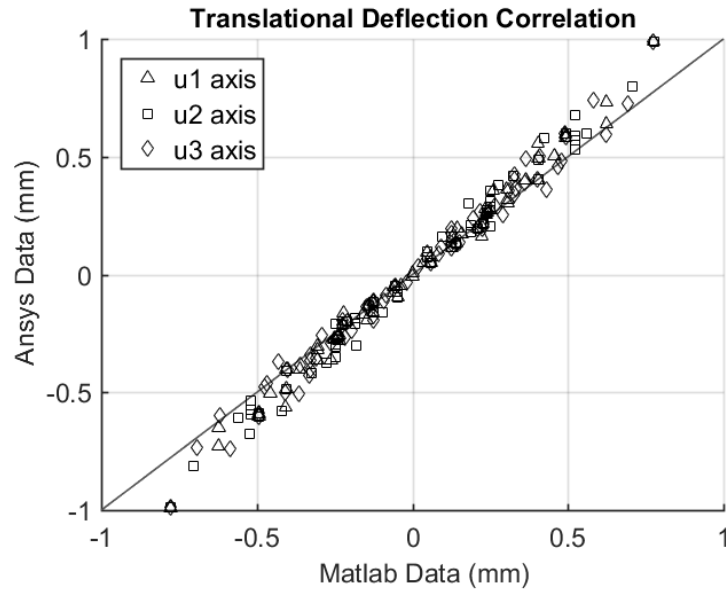
Figure 5.10. Correlation of the results for the manipulator.

After validating the formulation approach for a single link, the VJM is adapted for the whole manipulator. The link dimensions are designated as 6 mm inner diameter and 10 mm outer diameter for all links. The link lengths are $l_1 = 111.7$ mm, $l_2 = 74.1$ mm, and $l_3 = 121.8$ mm. The results obtained from ANSYS Workbench and VJM model programmed in MATLAB are compared under ± 5 N directional wrenches applied on the mobile platform. The combination of applied forces are given in Table 5.1.

Table 5.1. Load points for simulation. LC: Load Combination

	LC1	LC2	LC3	LC4	LC5	LC6	LC7	LC8
Direction $\vec{u}_1$	+5 N	+5 N	+5 N	+5 N	-5 N	-5 N	-5 N	-5 N
Direction $\vec{u}_2$	+5 N	+5 N	-5 N	-5 N	+5 N	+5 N	+5 N	-5 N
Direction $\vec{u}_3$	+5 N	-5 N	+5 N	-5 N	+5 N	-5 N	+5 N	-5 N

The comparison is conducted for 10 different test points of the manipulator and the corresponding active joint angles for the test points are given in Table 5.2. With

Table 5.2. TP: Test Points of chosen configurations, $-30 \Rightarrow -30°$, $+30 \Rightarrow +30°$, $0 \Rightarrow 0°$

	TP1	TP2	TP3	TP4	TP5	TP6	TP7	TP8	TP9	TP10
$\vec{u}_1 \; \varphi_{11}$	+30	0	+30	0	0	0	0	-30	0	+30
$\vec{u}_2 \; \varphi_{21}$	-30	-30	-30	-30	0	+30	0	-30	0	+30
$\vec{u}_3 \; \varphi_{31}$	+30	+30	-30	-30	+30	+30	-30	-30	0	+30

the combination of ± 5 N applied forces in all orthogonal axes, 80 tests are conducted. Correlation between the ANSYS and MATLAB results are shown in Figure 5.10. It can be seen that for small amount of deflections the ANSYS and MATLAB results are close to each other. Small deffelctions occurs where manipulator is close to fully folded pose. As the manipulator approaches to fully extended pose which is the most compliant pose, the correlation between the obtained results decreases due to the high displacements. This difference is caused by the solution approach of both simulation. In ANSYS Workbench, iterative solution method is adopted whereas in MATLAB, direct solution approach is used. The reason of the direct approach selection is to reduce the computation time for optimization. The main objective in stiffness optimization for design purposes is to reduce the maximum displacement under external wrenches but not to compute its precise value.

5.3. Dynamic Model

The dynamic model of a system is acquired by representing the inertial effects with respect to an inertial frame. These inertial effects are caused by the mass and the inertia of the inspected body. In order to derive the dynamic model formulation, the position of the mass center should be denoted with respect to the base frame. Then, linear and angular acceleration and velocities of the mass center can be determined. Later, this information can be combined with the inertial properties of the manipulator to procure the dynamic model.

The forward kinematics for mass center frames g_{ij} of jth body in i^{th} serial chain are written in homogeneous transformation matrix form as follows;

$$\hat{H}^{(i0,g_{i1})} = \hat{R}_{u3}(q_{i1})\hat{T}_{u1}(l_{g1}) \tag{5.182}$$

$$\hat{H}^{(i0,g_{i2})} = \hat{H}^{(i0,i1)}\hat{R}_{u3}(q_{i2})\hat{T}_{u1}(l_{g2}) \tag{5.183}$$

$$\hat{H}^{(i0,g_{i3})} = \hat{H}^{(i0,i2)}\hat{R}_{u3}(q_{i3})\hat{T}_{u1}(l_{g3}) \tag{5.184}$$

The final homogeneous transformation matrix with respect to inertial base frame is written as follows;

$$\hat{H}_{g_{ij}} = \hat{H}^{(0,i0)} \hat{H}^{(i0,g_{ij})} \text{ for } i = 1, 2, 3 \text{ and } j = 1, 2, 3 \qquad (5.185)$$

where $\hat{H}_{g_{ij}}$ denotes the homogeneous transformation matrix from inertial base frame to g_{ij}^{th} frame.

By using forward kinematics, velocities of each body can be derived by taking the derivative of $\hat{H}_{g_{ij}}$ with respect to time. The joint velocities are already derived in the kinematic section. Thus, obtaining velocity coefficients is enough to evaluate the velocities of the bodies. In addition, obtaining the homogeneous Jacobian matrices for mass center frames is much more suitable for general representation. Same procedure in the kinematic section can be followed to obtain the homogeneous Jacobian Matrices of the mass centers of the bodies.

$$\frac{\partial \hat{H}_{gij}}{\partial q_{ij}} = \begin{bmatrix} \frac{\partial \hat{R}_{gij}}{\partial q_{ij}} & \frac{\partial \bar{r}_{gij}}{\partial q_{ij}} \\ \bar{0}^T & 1 \end{bmatrix} \qquad (5.186)$$

where $\hat{R}_{gij}$ is the rotation matrix of body and $\bar{r}_{gij}$ is the position column matrix of the body.

Angular velocity coefficients can be obtained by using the derivative of the rotation matrix.

$$\tilde{\lambda}_{ij} = \frac{\partial \hat{R}_{gij}}{\partial q_{ij}} \hat{R}_{gij}^T \qquad (5.187)$$

where $\tilde{\lambda}_{ij}$ is a skew symmetric matrix which contains the angular velocity coefficients of the g_{ij}^{th} frame.

$$\tilde{\lambda}_{ij} = \begin{bmatrix} 0 & -\lambda ij3 & \lambda ij2 \\ \lambda ij3 & 0 & -\lambda ij1 \\ -\lambda ij2 & \lambda ij1 & 0 \end{bmatrix} \qquad (5.188)$$

By using the *col* operator the angular velocity coefficients can be obtained in column matrix form.

$$\bar{\lambda}_{ij} = col(\tilde{\lambda}_{ij}) = \begin{bmatrix} \lambda ij1 \\ \lambda ij2 \\ \lambda ij3 \end{bmatrix} \qquad (5.189)$$

101

Linear velocity coefficients in column matrix form $\bar{\Lambda}_{ij}$ is obtained by differentiating $\bar{r}_{gij}$ with respect to q_{ij}^{th} variable.

$$\bar{\Lambda}_{ij} = \frac{\partial \bar{r}_{gij}}{\partial q_{ij}} \tag{5.190}$$

Homogeneous 6×1 Jacobian column matrix $\bar{\Lambda}_{ij}$ for q_{ij}^{th} variable is formed as follows;

$$\bar{J}_{gij} = \begin{bmatrix} \bar{\Lambda}_{ij} \\ \bar{\lambda}_{ij} \end{bmatrix}_{6 \times 1} \tag{5.191}$$

The homogeneous Jacobian matrix $\hat{J}_{gij}$ for j^{th} body in i^{th} serial chain can be written by using $\bar{J}_{gij}$ and $\bar{J}_{H_{ij}}$ column matrices.

$$\hat{J}_{gi1} = \begin{bmatrix} \bar{J}_{gi1} & \bar{0} & \bar{0} \end{bmatrix}_{6 \times 3} \tag{5.192}$$

$$\hat{J}_{gi2} = \begin{bmatrix} \bar{J}_{s_{i1}} & \bar{J}_{gi2} & \bar{0} \end{bmatrix}_{6 \times 3} \tag{5.193}$$

$$\hat{J}_{gi3} = \begin{bmatrix} \bar{J}_{s_{i1}} & \bar{J}_{s_{i2}} & \bar{J}_{gi3} \end{bmatrix}_{6 \times 3} \tag{5.194}$$

6×1 velocity column matrix of jth body in i^{th} serial chain can be written in generalized coordinates.

$$\bar{V}_{ij} = \begin{bmatrix} \dot{\bar{r}}_{gij} \\ \bar{\omega}_{gij} \end{bmatrix} = \hat{J}_{gij}\dot{\bar{q}}_i \text{ for } j = 1, 2, 3 \tag{5.195}$$

where $\dot{\bar{r}}_{gij}$ and $\bar{\omega}_{gij}$ denote the linear and angular velocities of the mass center of jth body in i^{th} serial chain.

Next, the dynamic model is derived by using the Lagrange's method. Gravitational acceleration is omitted in order to simplify the model for design purpose. In addition, gravitation is a static effect which is considered during the stiffness model derivation. Therefore, the potential energy P_e is 0 and only the kinetic energy K_e is considered for the Lagrange term. The total Lagrange term of the manipulator L and Lagrange term of ith serial chain L_i is shown in below.

$$L = K_e - P_e \tag{5.196}$$

$$L_i = K_{ei} - P_{ei} \tag{5.197}$$

and the kinetic energy is defined in Cartesian space coordinates with respect to base frame as follows;

$$K_{ei} = \frac{1}{2} \sum_{j=1}^{3} \left(\bar{V}_{ij}^T \hat{M}_{ij} \bar{V}_{ij} \right) \text{ for } i = 1, 2, 3 \tag{5.198}$$

where subscript ij denote the ith serial chain and j^{th} body in that serial chain. $\bar{V}_{ij}$ is the velocity of the center of mass of the body. $\hat{M}_{ij}$ is the mass matrix defined in Cartesian space. $\hat{M}_{ij}$ can be obtained by rotating the mass matrix $\hat{M}_{Sj}$ to the Cartesian space where $\hat{M}_{Sj}$ is defined in the body-fixed frame at the center of mass of the jth body. If the body has two planes of symmetry with respect to the body-fixed frame, then, this frame is a principle axes frame and the inertia matrix is a diagonal matrix. Therefore, $\hat{M}_{Sj}$ can be a diagonal matrix shown in Equation 5.199 and the rotation of this matrix to the Cartesian space frame is shown in Equations 5.200.

$$\hat{M}_{Sj} = \begin{bmatrix} m_j & 0 & 0 & 0 & 0 & 0 \\ 0 & m_j & 0 & 0 & 0 & 0 \\ 0 & 0 & m_j & 0 & 0 & 0 \\ 0 & 0 & 0 & I_x^* & 0 & 0 \\ 0 & 0 & 0 & 0 & I_y^* & 0 \\ 0 & 0 & 0 & 0 & 0 & I_z^* \end{bmatrix} \tag{5.199}$$

$$\hat{M}_{ij} = \begin{bmatrix} \hat{R}_{gij} & \hat{0} \\ \hat{0} & \hat{R}_{gij} \end{bmatrix} \hat{M}_{Sj} \begin{bmatrix} \hat{R}_{gij} & \hat{0} \\ \hat{0} & \hat{R}_{gij} \end{bmatrix}^T \tag{5.200}$$

where m_j is the mass of the each body and I_x^*, I_y^*, and I_z^* denote the mass moment of inertia with respect to body fixed frame shown in Figure 5.9. A trivial way to compute the dynamic model of the manipulator is first to obtain the kinetic energy of each serial chain by using Equation 5.198 and then, adding them up to acquire the overall model. The Lagrange equation for i^{th} serial chain is;

$$\bar{\tau}_i = \frac{d}{dt}\left(\frac{\partial L_i}{\partial \dot{\bar{q}}_i}\right) - \frac{\partial L_i}{\partial \bar{q}_i} \tag{5.201}$$

where $\bar{\tau}_i$ is the vector containing torques at the active and passive joints generated by the inertial effects in i^{th} serial chain. Note that passive joints do not carry torques but the torques generated by the inertial effects are distributed among active joints. This relationship can be established as follows.

$$\sum_{i=1}^{3}\left(\hat{J}_i^{-T}\bar{\tau}_i\right) = \bar{F}_{ext} \tag{5.202}$$

$$\hat{J}_m^{-T}\bar{\tau}_m = \bar{F}_{ext} \tag{5.203}$$

$$\bar{\tau}_m = \hat{J}_m^T \sum_{i=1}^{3}\left(\hat{J}_i^{-T}\bar{\tau}_i\right) \tag{5.204}$$

103

$$\Rightarrow \bar{\tau}_{mi} = \hat{J}_m^T \hat{J}_i^{-T} \bar{\tau}_i \tag{5.205}$$

$$\bar{\tau}_{mi} = \hat{J}_i^{\star T} \bar{\tau}_i \text{ where } \hat{J}_i^{\star} = \hat{J}_i^{-1} \hat{J}_m \tag{5.206}$$

where $\bar{\tau}_{mi}$ denotes the distributed torques on active joints generated by the ith serial chain dynamics.

In order to obtain the dynamic model in generalized coordinates, first the $\bar{V}_{ij}$ is substituted in Equation 5.198.

$$K_{ei} = \frac{1}{2} \sum_{j=1}^{3} \left(\dot{\bar{q}}_i^T \hat{J}_{gij}^T \hat{M}_{ij} \hat{J}_{gij} \dot{\bar{q}}_i \right) \tag{5.207}$$

$$\hat{M}_i = \sum_{j=1}^{3} \left(\hat{J}_{gij}^T \hat{M}_{ij} \hat{J}_{gij} \right) \tag{5.208}$$

$$K_{ei} = \frac{1}{2} \dot{\bar{q}}_i^T \hat{M}_i \dot{\bar{q}}_i \tag{5.209}$$

where $\hat{M}_i$ is the lumped mass matrix and defined in the joint space of ith serial chain.

By applying the differentiation operations in Equation 5.201, the dynamic model in joint space can be procured.

$$\bar{\tau}_i = \hat{M}_i \ddot{\bar{q}}_i + \dot{\hat{M}}_i \dot{\bar{q}}_i - \frac{1}{2} \sum_{k=1}^{3} \left(\dot{\bar{q}}_i^T \frac{\partial \hat{M}_i}{\partial q_{ik}} \dot{\bar{q}}_i \bar{e}_k \right) \tag{5.210}$$

where q_{ik} denotes the kth element of $\bar{q}_i$ and $\bar{e}_k$ is direct delta $k \times 1$ column matrix which k^{th} element is 1 and the rest is 0. The above equality is written in terms of active and passive joints. The representation can be modified by using the Equation 5.206 and substituting Equation 5.60 in Equation 5.210. Equation 5.211 can be written in terms of generalized coordinates.

$$\begin{aligned}
\bar{\tau}_{mi} = \hat{J}_i^{\star T} \bar{\tau}_i = &\hat{J}_i^{\star T} \hat{M}_i \hat{J}_i^{-1} \hat{J}_m \ddot{\bar{q}}_m \\
&+ \hat{J}_i^{\star T} \hat{M}_i \hat{J}_i^{-1} \dot{\hat{J}}_m \dot{\bar{q}}_m \\
&+ \hat{J}_i^{\star T} \hat{M}_i \dot{\hat{J}}_i^{-1} \hat{J}_m \dot{\bar{q}}_m \\
&+ \hat{J}_i^{\star T} \dot{\hat{M}}_i \hat{J}_i^{-1} \hat{J}_m \dot{\bar{q}}_m \\
&- \frac{1}{2} \hat{J}_i^{\star T} \sum_{k=1}^{3} \left(\dot{\bar{q}}_m^T \hat{J}_i^{\star T} \frac{\partial \hat{M}_i}{\partial q_{ik}} \hat{J}_i^{\star} \dot{\bar{q}}_m \bar{e}_k \right)
\end{aligned} \tag{5.211}$$

In a more compact form, Equation 5.211 can be written as in Equation 5.212 in generalized coordinates.

$$\bar{\tau}_{mi} = \hat{J}_i^{\star T} \frac{d}{dt} (\hat{M}_i \hat{J}_i^{-1} \hat{J}_m \dot{\bar{q}}_m) - \frac{1}{2} \hat{J}_i^{\star T} \sum_{k=1}^{n} \left(\dot{\bar{q}}_m^T \hat{J}_i^{\star T} \frac{\partial \hat{M}_i}{\partial q_{ik}} \hat{J}_i^{\star} \dot{\bar{q}}_m \bar{e}_k \right) \tag{5.212}$$

Although it is enough to have the Equation 5.212 in order to control the manipulator, it is necessary to obtain the dynamic model in Cartesian space. Since the manipulator is designed to be an impedance type of haptic manipulator, the input is not from the actuators but from the mobile platform by the user. Especially for minimum impedance performance evaluation, the dynamic model in Cartesian space should be evaluated within the performance metrics.

The force/torque interaction between the mobile platform and the actuated joints can be established by using the Jacobian matrix $\hat{J}_m$. The relation can be extended for $\bar{\tau}_{mi}$ to evaluate each serial chain separately. This relation represents how the force input from the platform causes the torques at the joints or vice versa. The relation is written as follows;

$$\bar{\tau}_m = \hat{J}_m^T \bar{F}_{ext} \tag{5.213}$$

$$\bar{F}_{ext} = \hat{J}_m^{-T} \bar{\tau}_m \tag{5.214}$$

$$\bar{F}_{ext} = \hat{J}_m^{-T} \sum_{i=1}^{3} \bar{\tau}_{mi} \tag{5.215}$$

$$\bar{F}_{ext_i} = \hat{J}_m^{-T} \bar{\tau}_{mi} \tag{5.216}$$

where $\bar{F}_{ext_i}$ denotes the relationship between the external force at the mobile platform and the dynamic effects in i^{th} serial chain.

In order to write the dynamic model in Cartesian space with Cartesian space variables, first, the velocity and the acceleration of the mobile platform $\dot{\bar{r}}$ and $\ddot{\bar{r}}$ are obtained in the following Equation set.

$$\frac{\partial \dot{\bar{r}}}{\partial t} = \frac{\partial}{\partial t}(\hat{J}_m \dot{\bar{q}}_m) \tag{5.217}$$

$$\ddot{\bar{r}} = \hat{J}_m \ddot{\bar{q}}_m + \dot{\hat{J}}_m \dot{\bar{q}}_m \tag{5.218}$$

$$\ddot{\bar{q}}_m = \hat{J}_m^{-1} \ddot{\bar{r}} - \hat{J}_m^{-1} \dot{\hat{J}}_m \dot{\bar{q}}_m \tag{5.219}$$

By substituting Equation 5.48 in Equation 5.219 $\ddot{\bar{q}}_m$ is obtained in terms of mobile platform variables in Cartesian space.

$$\Rightarrow \ddot{\bar{q}}_m = \hat{J}_m^{-1} \ddot{\bar{r}} - \hat{J}_m^{-1} \dot{\hat{J}}_m \hat{J}_m^{-1} \dot{\bar{r}} \tag{5.220}$$

Multiplying Equation 5.211 with $\hat{J}_m^{-T}$ from the left and substituting $\dot{\bar{q}}_m$ and $\ddot{\bar{q}}_m$ in Equation 5.211 yields the dynamic model in Cartesian space as shown in Equation 5.221.

$$\bar{F}_{ext_i} = \hat{J}_m^{-T}\bar{\tau}_{mi} = \hat{J}_i^{-T}\hat{M}_i\hat{J}_i^{-1}\ddot{\bar{r}}$$
$$+ \hat{J}_i^{-T}\frac{d}{dt}(\hat{M}_i\hat{J}_{Qi}^{-1})\dot{\bar{r}} \tag{5.221}$$
$$- \frac{1}{2}\hat{J}_i^{-T}\sum_{k=1}^{3}\left(\dot{\bar{r}}^T\hat{J}_i^{-T}\frac{\partial\hat{M}_i}{\partial q_{ik}}\hat{J}_i^{-1}\dot{\bar{r}}\bar{e}_k\right)$$

In simplified form;

$$\bar{F}_{ext_i} = \hat{M}_{Ci}(\bar{q}_i)\ddot{\bar{r}} + \bar{B}_i(\bar{q}_i,\dot{\bar{q}}_i,\dot{\bar{r}}) \tag{5.222}$$

$$\hat{M}_{Ci}(\bar{q}_i) = \hat{J}_i^{-T}\hat{M}_i\hat{J}_i^{-1} \tag{5.223}$$

$$\bar{B}_i(\bar{q}_i,\dot{\bar{q}}_i,\dot{\bar{r}}) = \hat{J}_i^{-T}\frac{d}{dt}(\hat{M}_i\hat{J}_i^{-1})\dot{\bar{r}} - \frac{1}{2}\hat{J}_i^{-T}\sum_{k=1}^{3}\left(\dot{\bar{r}}^T\hat{J}_i^{-T}\frac{\partial\hat{M}_i}{\partial q_{ik}}\hat{J}_i^{-1}\dot{\bar{r}}\bar{e}_k\right) \tag{5.224}$$

Note that $\bar{q}_i$ can be written as a function of $\bar{r}$ by kinematic relations. Therefore, equation of motion of the manipulator is further simplified as presented in Equation 5.226

$$\bar{F}_{ext} = \sum_{i=1}^{3}\bar{F}_{ext_i} \tag{5.225}$$

$$\bar{F}_{ext} = \hat{M}_C^\star(\bar{r})\ddot{\bar{r}} + \bar{B}^\star(\bar{r},\dot{\bar{r}}) \tag{5.226}$$

$$\hat{M}_C^\star(\bar{r}) = \sum_{i=1}^{3}\hat{M}_{Ci}(\bar{q}_i) \tag{5.227}$$

$$\bar{B}^\star(\bar{r},\dot{\bar{r}}) = \sum_{i=1}^{3}\bar{B}_i(\bar{q}_i,\dot{\bar{q}}_i) \tag{5.228}$$

where $\hat{M}_C^\star(\bar{r})$ is the mass matrix of the manipulator in Cartesian space and $\bar{B}^\star(\bar{r},\dot{\bar{r}})$ denotes the nonlinear terms in Cartesian space.

Mass moment of inertia and mass of each link is computed by making use of Figure 5.9 by the following equation.

$$I_z^* = m\left[\frac{l_{ij}^2}{3} + \frac{(\frac{D_{ij}}{2})^2 + (\frac{d_{ij}}{2})^2}{4}\right] \tag{5.229}$$

$$m = \rho\pi l_{ij}\left((\frac{D_{ij}}{2})^2 - (\frac{d_{ij}}{2})^2\right) \tag{5.230}$$

where m is the mass and ρ is the density of the material of the link. I_z^* is sufficient for the dynamics since each link of the manipulator only rotates in their z- axis with respect to Cartesian space.

5.3.1. Verification of the Dynamic Model

In order to verify the dynamic model of modified R-CUBE manipulator, the derived formulation is implemented in MATLAB Simulink environment. Then, Sim-mechanics model of the manipulator is procured in MATLAB Simulink by transferring the CAD data developed in Solidworks. A sinusoidal motion input is given to Sim-mechanics model and derived the model in Simulink environment. The computed torques of both the derived and Sim-mechanics model are compared. The error between the models is observed to be in the range of 10^{-9} N.m for 1 N.m computed torque. This difference is caused by the numerical error or the Simulink.

5.4. Conclusion

In this Chapter, kinematic, stiffness, and dynamic models of the modified R-CUBE mechanism is derived and verified. Forward and inverse kinematic solution of the manipulator has been obtained. Then, the Jacobian matrices which are used in dynamic modeling section and dimensionally homogeneous matrices which are used in stiffness modeling section have been procured. In stiffness modeling, VJM is adopted to derive the stiffness. Both loaded and unloaded modes are investigated and direct/iterative solution algorithms have been introduced. Finally, the dynamic model is obtained by making use of virtual work principle with Lagrange's method. All of the models are derived to generate the performance metric for design purpose.

CHAPTER 6

CASE STUDY: OPTIMIZATION ALGORITHM FOR THE R-CUBE MANIPULATOR DESIGN

In Chapter 5, kinematics, stiffness and dynamics models of the modified R-CUBE manipulator are obtained. In this Chapter, the relationship between the performance metrics of each domain is constructed and the objective functions are obtained. Next, design constraints are determined. Genetic algorithm for Pareto-front approach and particle swarm algorithm for the weighted-sum approach are constructed to procure the optimum values of design parameters. This Chapter divided into the construction of the design optimization problems of kinematics, stiffness, and dynamics. Finally, overall objective functions are constructed.

6.1. Formulation of Kinematics Performance Metrics

There are two main kinematic performance metrics considered in this thesis, manipulability, and condition number. Both use the Jacobian matrix for evaluation. In this section, these performance metrics are procured for the modified R-CUBE mechanism.

6.1.1. Manipulability

Manipulability measure uses the Jacobian matrix. An important note is that it is possible to obtain multiple Jacobian matrices for each serial chain of a parallel mechanism. Most useful choice is to obtain the Jacobian matrix with respect to actuated or controlled joint variables. Hence, $\hat{J}_m$ Jacobian matrix is used for the manipulability measure.

$$\hat{J}_m = \begin{bmatrix} l_1 \cos q_{11} & 0 & 0 \\ 0 & l_1 \cos q_{21} & 0 \\ 0 & 0 & l_1 \cos q_{31} \end{bmatrix} \qquad (6.1)$$

$$\mu_v(\bar{q}_m, l_1) = \det\left(\hat{J}_m\right) = cos(q_{11})cos(q_{21})cos(q_{31})l_1^3 \qquad (6.2)$$

where μ_v is the manipulability measure. When the manipulability measure is evaluated, it is observed that the minimum value $\mu_v = 0$ is obtained when $q_{i1} = \pm\pi/2$ for $i = 1, 2, 3$ which corresponds to singular poses. Such cases are undesired and must be avoided during optimization.

As shown in Equation 6.2, manipulability measure is a function of $\bar{q}_m$ and l_1. Note that, μ_v is pose-dependent. Which brings the requirement of evaluation of μ_v in different poses of the manipulator. The easiest way is to globalize μ_v through the workspace to measure the overall manipulability:

$$k_v = \frac{\int\limits_W \mu_v dw}{W} \tag{6.3}$$

where k_v is the globalized manipulability measure, and W denotes the overall workspace. In the computer environment, the easiest method is to divide the workspace into discrete sections and evaluate the manipulability measure at those discrete points. Finally, by summing them up and dividing to the number of discrete points, a scalar performance metric can be obtained as follows;

$$k_v = \frac{1}{n}\sum_{w=1}^{n} \mu_v(\bar{q}_m, l_1) \tag{6.4}$$

where n is the number of discrete points.

Although k_v is sufficient for manipulability measure, it can be further simplified in order to reduce the computation time. The mechanism has a symmetric topology. Using this symmetry, the number of discrete points can be greatly reduced. Yet, there is an even better way to compute the μ_v thanks to symmetry.

Considering that, the objective is to increase the overall manipulability measure, instead of inspecting the whole workspace, evaluating the performance of the pose where the least performance is expected is sufficient. The reason for this is that if the performance of the worst pose is enhanced, the performance of the rest of the poses is also enhanced with considerably decreased computation time. These poses are the critical poses for the optimization. For the manipulability, the critical pose is the where μ_v is minimum.

μ_v is minimum when the absolute value of joint variables q_{11}, q_{21}, q_{31} are maximized since the inputs get closer to singular poses which are shown in Section 5.1.5. Due to the symmetry, the maximum absolute values of joint variables are all equal.

$$|q_{11max}| = |q_{11min}| \quad |q_{21max}| = |q_{21min}| \quad |q_{31max}| = |q_{31min}| \tag{6.5}$$

$$q_{max} = |q_{11max}| = |q_{21max}| = |q_{31max}| \tag{6.6}$$

109

where q_{max} is the maximum positive value of the joint variable. The updated manipulablity measure μ_v is;

$$\mu_v = \mu_v(q_{max}, l_1) = \cos(q_{max})^3 l_1^3 \qquad (6.7)$$

The cube is just the amplification of the manipulability. Therefore, it can be simplified by taking the cube root.

$$\mu_v = \cos(q_{max})l_1 \qquad (6.8)$$

When q_{max} approaches to 0 or l_1 approaches to ∞, the manipulability measure increases. Yet, due to the prescribed workspace, they are related to each other. The constraint between q_{max} and l_1 is given in Section 6.1.3.

A side note should be given for passive joints and links. $\hat{J}_m$ is a matrix constructed by assuming that the passive joints do not go to a singular pose. There are also passive joint variables which are constrained by the active ones. Hence, the design parameters must include constraints between the active links/joints and passive links/joints. Therefore, closeness to singular poses for passive joints should also be investigated. Evaluation of the determinant of the Jacobian matrices of each serial chain might seem a reasonable solution to consider the passive joints since Equation 5.56 holds the same for forward kinematics.

$$\hat{J}_i \dot{\bar{q}}_i = \hat{J}_m \dot{\bar{q}}_m \qquad (6.9)$$

However, remember that the manipulability measure μ_v is the indication of the volume of velocity/force ellipsoids. The ellipsoids are based on the fact that there is a unit input from active joints variables. However, passive joint variables do not experience unit change since they are constrained by the active joints. Using these constraints, $\dot{\bar{q}}_i$ can be found for a unit change of active joints $\dot{\bar{q}}_m$ as shown below.

$$\dot{\bar{q}}_i = \hat{J}_i^{-1} \hat{J}_m \dot{\bar{q}}_m \text{ if } \det\left(\hat{J}_i\right) \neq 0 \qquad (6.10)$$

Then, it is substituted in Equation 6.9.

$$\Rightarrow \hat{J}_i \hat{J}_i^{-1} \hat{J}_m \dot{\bar{q}}_m = \hat{J}_m \dot{\bar{q}}_m \qquad (6.11)$$

$$\hat{I} = \hat{J}_i \hat{J}_i^{-1} \qquad (6.12)$$

where $\hat{I}$ is the identity matrix.

Determinant of $\hat{J}_i \hat{J}_i^{-1} \hat{J}_m$ includes the effect of passive joints. Yet, $\hat{J}_i \hat{J}_i^{-1}$ results as identity matrix if the manipulator is not in a singular pose. Determinant of $\hat{J}_i \hat{J}_i^{-1} \hat{J}_m$

110

is always equal to determinant of $\hat{J}_m$ in non-singular poses. Which concludes that the closeness to singularity cannot be measured in terms of passive joints by using Jacobian matrices.

There is a simple solution to prevent the passive joints getting close to singularity by making use of design constraints related with the size of the workspace. Manipulators are desired to have a certain workspace dimension. In a general case, boundaries of the workspace are the singular poses of the mechanism. Of course this is valid if the mechanism is not constrained mechanically. In R-CUBE manipulator, boundary is determined by two singular poses. One is if the active joints in singular pose which can be avoided by making use of $\hat{J}_m$. The other one is if the passive joints are in a singular pose which is to be avoided by a proper design.

As the distance between the mobile platform and the boundary increases, the dexterity also increases. The solution is acquired by using this fact. The manipulator can be designed for a larger workspace and then the dexterous subpart of it can be extracted which is the originally desired objective dimensions of the workspace. The required constraints are shown in Section 6.1.3.

6.1.2. Condition number

The condition number is used to compute the motion/force resolution of the mobile platform. The ratio of maximum and minimum Euclidean norms of Jacobian matrix is investigated for the condition number metric.

The problem to use one of the Jacobian matrix ($\hat{J}_m$ or $\hat{J}_i$) has already been explained in the previous Section. As in the manipulability measure, evaluation of the condition number of the Jacobian matrix is based on the assumption of that there are unit inputs from active joints. Therefore, $\hat{J}_m$ is used for the condition number. The norm operation is given below.

$$c_v = \|\hat{J}_m\| \|\hat{J}_m^{-1}\| \tag{6.13}$$

where c_v denotes the measure of the condition number. Normally, the condition number also must be globalized. Similar to the worst manipulability poses, if the worst location of condition number is known the performance of the worst pose may be increased to enhance the overall performance of the manipulator. Due to the special topology of the manipulator, these poses can easily be determined. To do that, analytical form of the norms must be calculated.

Since the components of the Jacobian matrix are known, norms can be analytically calculated. Later, they can be evaluated in the critical poses.

$$\|\hat{J}_m\| = \max(\left|\cos^2(q_{i1})\right|l_1^2) \tag{6.14}$$

$$\|\hat{J}_m^{-1}\| = \max\left(\frac{1}{\left|\cos^2(q_{i1})\right|l_1^2}\right) \text{ for } i = 1, 2, 3 \tag{6.15}$$

The norms are computed for an arbitrary pose of q_{i1} and the maximum values of $\|\hat{J}_m\|$ and $\|\hat{J}_m^{-1}\|$ are obtained. First, the maximum values for $\|\hat{J}_m\|$ and $\|\hat{J}_m^{-1}\|$ correspond to 2 distinct joint variables of the manipulator. $\|\hat{J}_m\|$ is maximum when the $\left|\cos^2(q_{i1})\right|$ is maximum. Since the maximum value of cosine function is 1, the only pose is when one of the $q_{i1} = 0$ within the operation range. Second, the maximum value of $\|\hat{J}_m^{-1}\|$, on the other hand, occurs when one of the serial chains of the manipulator is fully folded or fully extended. Those poses correspond to $q_{i1} = q_{max}$ and $q_{i1} = q_{min}$ (both results same value for cosine function). The most critical pose of the manipulator is when one of the arms is at the home position $q_{i1} = 0$ and the other one is when it is fully extended $q_{i1} = q_{max}$. This being said, norms can be updated for the critical pose.

$$\|\hat{J}_m\| = \max(\left|\cos^2(0)\right|l_1^2) = l_1^2 \tag{6.16}$$

$$\|\hat{J}_m^{-1}\| = \max\left(\frac{1}{\left|\cos^2(q_{max})\right|l_1^2}\right) = \frac{1}{\cos^2(q_{max})l_1^2} \tag{6.17}$$

Now, c_v the condition number can be written in analytical form.

$$c_v = l_1^2 \frac{1}{\cos^2(q_{max})l_1^2} = \frac{1}{\cos^2(q_{max})} \tag{6.18}$$

As shown in Equation 6.18, c_v is independent of the link length and it is a function of maximum operating range. As the operation range increases, the cosine function approaches to 0 and increases the value of c_v meaning that the resolution is decreasing. In order to increase the resolution, q_{max} must be decreased. The minimum value of c_v might be 1.

6.1.3. Implementation of Kinematic Design Constraints

The kinematic performance metrics are derived for the manipulator. Yet, the metrics must be minimized considering the kinematic constraints in order to obtain the optimum solution and the aimed design, simultaneously.

First, the dimensions of the desired workspace are defined as follows;

Dimensions of the Workspace: 120mm $\times$ 120mm $\times$ 120mm

The dimensions of the workspace depend on the maximum and minimum value of q_{i1} and the link length l_1. This can be shown by using Equation 5.29.

$$r_i = d + l_1 \sin q_{i1} \text{ for } i = 1, 2, 3 \tag{6.19}$$

$$\Delta r_i = r_{imax} - r_{imin} \tag{6.20}$$

$$\Rightarrow \Delta r_i = l_1(\sin(q_{max}) - \sin(q_{min})) \tag{6.21}$$

$$\Delta r_i = 120\text{mm} \tag{6.22}$$

Since $|q_{max}| = |q_{min}|$ and $q_{max} = -q_{min}$, the following simplification can be made.

$$2l_1 \sin(q_{max}) = 120\text{mm} \Rightarrow l_1 \sin(q_{max}) = 60\text{mm} \tag{6.23}$$

Notice that l_1 can be written as a function of q_{max}.

$$\textbf{Constraint 1: } l_1 = \frac{60}{\sin(q_{max})}\text{mm} \tag{6.24}$$

Due to the workspace constraint, the manipulability measure now has only one input variable which is q_{max}.

$$\mu_v = 60\frac{\cos(q_{max})}{\sin(q_{max})} \tag{6.25}$$

Note that, $60mm$ is only a scaling factor for the manipulability measure μ_v. Hence, the μ_v can be modified as follows.

$$\mu_v = \frac{\cos(q_{max})}{\sin(q_{max})} = \cot(q_{max}) = \frac{1}{\tan(q_{max})} \tag{6.26}$$

Depending on whether the optimization algorithm is maximization or minimization of the values of the objective function, $\mu_v = \cot(q_{max})$ or $\mu_v^{-1} = \tan(q_{max})$ can be chosen.

Another constraint comes up due to the denominator of μ_v. In order to have a solution, the condition $\sin(q_{max}) \neq 0$ must be sustained. Also $\mu_v = 0$ when $\cos(q_{max}) = 0$ which corresponds to a singular position. Therefore, $\cos(q_{max}) \neq 0$ must be ensured. Hence the input range for q_{max} is defined as follows.

$$0 < q_{max} < \pi/2 \tag{6.27}$$

In a numerical computation study, choosing close numbers to constraints may cause computational difficulties due to the closeness to the singularity where the solution algorithm may fail. In order to avoid the problem, the input range of q_{max} is slightly modified.

$$\textbf{Constraint 2: } 0.07 < q_{max} < 1.5 \tag{6.28}$$

113

The secondary desired objective is to achieve the workspace with the shortest link lengths. In terms of kinematics, longer link lengths cause higher footprint area for the manipulator which is not desired for desktop type haptic manipulators. The other benefits of having short links are discussed in stiffness and dynamics performance metric sections.

To have the minimum link length, l_1, l_2, and l_3 should be minimized. Up to now, the design constraints of l_1 has already been specified in terms of manipulability measure, condition number, workspace dimension, and the minimum link length. l_2, and l_3, on the other hand, are not constrained yet. Minimization of the link lengths of l_2, and l_3 must have these two constraints; singularity free manipulation, and ergonomy. Both can be inspected via inverse kinematics in position and velocity level.

Only singular pose for the passive joints occurs when $q_{i3} = 0$ or $q_{i3} = \pm\pi$. In order to avoid the singularity, the possible range for q_{i3} for the '$-$' configuration is defined as follows.

$$-\pi < q_{i3} < 0 \tag{6.29}$$

The constraint for q_{i3} is extended by virtue of inverse kinematic to constrain the link lengths l_2 and l_3.

$$\sin(q_{i3}) = -\sqrt{1 - \cos^2(q_{i3})} \neq 0 \tag{6.30}$$

$$\Rightarrow 0 < 1 - \cos^2(q_{i3}) \tag{6.31}$$

By using the notation in inverse kinematic solution section, substitute $\cos(q_{i3})$ as $\cos(q_{a3})$ in Equation 6.31.

$$0 < 1 - \frac{[(r_c - l_1 \cos q_{a1})^2 + (-r_b)^2 - l_2^2 - l_3^2]^2}{[2l_2 l_3]^2} \tag{6.32}$$

The desired workspace dimensions can be implemented as a constraint for 2R passive mechanism to avoid the singularity by making use of the terms $r_c - l_1 \cos q_{a1}$ and $-r_b$ in Equation 6.32. $r_c - l_1 \cos q_{a1}$ and $-r_b$ terms can be written in open form and modified to denote the mobile platform frame with respect to $(i2)$ frame. This modification is shown in Equations 6.33 and 6.34 with the terms r_x and r_y which denote the $\vec{u}_1^{(i2)}(\vec{x})$ and $\vec{u}_2^{(i2)}(\vec{y})$ position components of the mobile platform with respect to $(i2)$ frame. Figure 6.1 shows axes x- and y- axes.

$$-r_b \rightarrow r_x = d + l_1 \sin q_{b1} \tag{6.33}$$

$$r_c - l_1 \cos q_{a1} \rightarrow r_y = d + l_1 \sin q_{c1} - l_1 \cos q_{a1} \tag{6.34}$$

$$0 < 1 - \frac{[(d + l_1 \sin q_{c1} - l_1 \cos q_{a1})^2 + (d + l_1 \sin q_{b1})^2 - l_2^2 - l_3^2]^2}{[2l_2 l_3]^2} \tag{6.35}$$

114

Due to the symmetry, determining the constraints for the passive links of a single serial chain is sufficient. For that, $a = 1$ is chosen. Then, $b = 2$ and $c = 3$.

$$0 < 1 - \frac{[(d + l_1 \sin q_{31} - l_1 \cos q_{11})^2 + (d + l_1 \sin q_{21})^2 - l_2^2 - l_3^2]^2}{[2l_2 l_3]^2} \qquad (6.36)$$
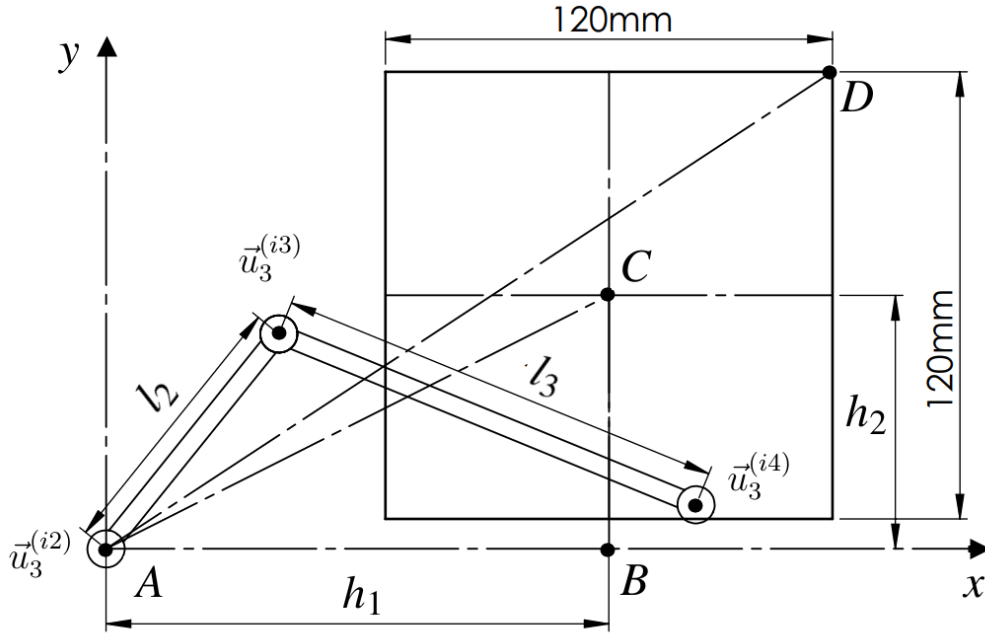
Figure 6.1. Placement of the workspace with respect to $(i2)$ frame. Point C is the center of the workspace.

The critical poses of the manipulator has already been discussed. These poses can be substituted in Equation 6.36 as active joint variables. However, constant distance d has not been discussed yet. In order to determine the term d, first r_x and r_y should be determined. In Figure 6.1, maximum reach $\vec{AD}$ and center of the workspace with respect to $(i2)$ frame $\vec{AC}$ are shown. It is obvious that, if the maximum reach $\vec{AD}$ is as close as possible to $(i2)$ frame, the required link lengths l_2 and l_3 are minimized. $(i2)$ frame cannot be inside of the workspace otherwise the workspace includes a singular pose. Therefore, the x- component of $\vec{AC}$ vector must be $h_1 > 60$ mm. Secondly, $\vec{AD}$ is minimized when $h_2 = 0$. Now, the center C is positioned along x- axis. Also, recall that the center C corresponds to the home pose of the manipulator when $q_{i1} = 0$ for $i = 1, 2, 3$. Then, by substituting the $q_{i1} = 0$ in r_x and r_y the following Equation set is obtained.

$$r_x = d \qquad (6.37)$$

$$r_y = d - l_1 = 0 \tag{6.38}$$

$$\Rightarrow d = l_1 = h_1 \tag{6.39}$$

Since the center is positioned on the x- axis, $r_y = 0$. Then, the distance d is equal to l_1.
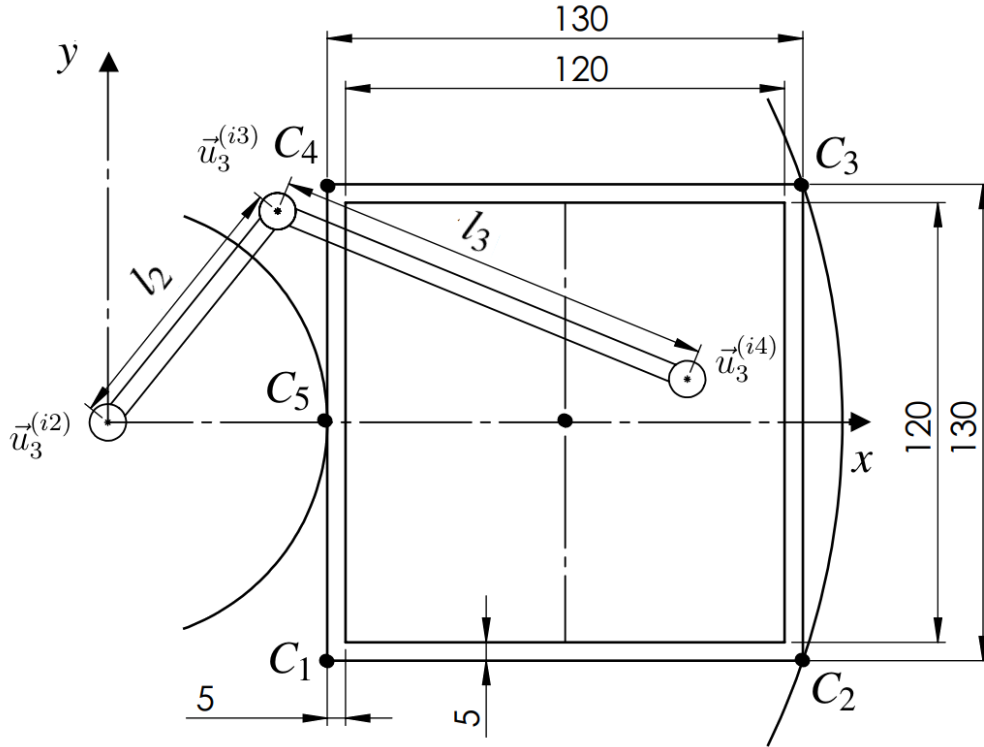
Figure 6.2. The workspace placement when $q_{11} = 0$.

Figure 6.2 shows the placement of the workspace with respect to $(i2)$ frame when $q_{11} = 0$ and Figure 6.3 shows the placement when $q_{11} = q_{max}$. Note that, $q_{11} = q_{max} = -q_{min}$ for the sketched Figures 6.2 and 6.3. The points C_2, C_3, B_3 are coincident with the outer boundary of the workspace which can be achieved by the passive links. The points C_5, B_5 are coincident with the inner boundary. The points also correspond the singular and critical poses for passive links. Hence, evaluation of the constraints in those poses is sufficient.

In order to avoid getting closer to the singularity, these points are located on a larger workspace which has the dimensions of 130mm $\times$ 130mm. Then, the dexterous subspace which is the desired workspace is taken. Note that, 130mm $\times$ 130mm workspace is a virtual workspace. Therefore, actuator angles which affect the position of the last frame in the workspace are also virtual. The angles are denoted by superscript $*$. The

Figure 6.3. The workspace placement when $q_{11} = q_{max}$. $\Delta y = l_1 - l_1 \cos q_{max}$.

critical poses for $i = 1$ are listed as follows.

$$q_{11} = 0 \rightarrow q_{21} = q_{min}^*, q_{31} = q_{min}^* \text{ the point } C_1$$

$$q_{11} = 0 \rightarrow q_{21} = q_{max}^*, q_{31} = q_{min}^* \text{ the point } C_2$$

$$q_{11} = 0 \rightarrow q_{21} = q_{max}^*, q_{31} = q_{max}^* \text{ the point } C_3$$

$$q_{11} = 0 \rightarrow q_{21} = q_{min}^*, q_{31} = q_{max}^* \text{ the point } C_4$$

$$q_{11} = 0 \rightarrow q_{21} = q_{min}^*, q_{31} = 0 \text{ the point } C_5$$

$$q_{11} = q_{max} \rightarrow q_{21} = q_{min}^*, q_{31} = q_{min}^* \text{ the point } B_1$$

$$q_{11} = q_{max} \rightarrow q_{21} = q_{max}^*, q_{31} = q_{min}^* \text{ the point } B_2$$

$$q_{11} = q_{max} \rightarrow q_{21} = q_{max}^*, q_{31} = q_{max}^* \text{ the point } B_3$$

$$q_{11} = q_{max} \rightarrow q_{21} = q_{min}^*, q_{31} = q_{max}^* \text{ the point } B_4$$

$$q_{11} = q_{max} \rightarrow q_{21} = q_{min}^*, q_{31} = 0 \text{ the point } B_5$$

The position components of the points C_2, C_3, B_3, C_5, B_5 with respect to $\vec{u}_3^{(i3)}$ can be written by virtue of Figures 6.2 and 6.3. Hence, $l_1 \sin q_{max}^*$, $l_1 \sin q_{min}^*$, and $l_1 \cos q_{max}^*$

117

can be numerically computed. The joint variables and the distance d are substituted in position components r_x and r_y and computed as follows.

$$C_2 \rightarrow r_x = l_1 + l_1 \sin q_{max}^* = l_1 + 65, r_y = l_1 \sin q_{min}^* = -65 \tag{6.40}$$

$$C_3 \rightarrow r_x = l_1 + l_1 \sin q_{max}^* = l_1 + 65, r_y = l_1 \sin q_{max}^* = 65 \tag{6.41}$$

$$C_5 \rightarrow r_x = l_1 + l_1 \sin q_{min}^* = l_1 - 65, r_y = 0 \tag{6.42}$$

$$B_3 \rightarrow r_x = l_1 + l_1 \sin q_{max}^* = l_1 + 65, r_y = l_1 + l_1 \sin q_{max}^* - l_1 \cos q_{max} = \Delta y + 65 \tag{6.43}$$

$$B_5 \rightarrow r_x = l_1 + l_1 \sin q_{min}^* = l_1 - 65, r_y = l_1 - l_1 \cos q_{max} = \Delta y \tag{6.44}$$

Note that, l_1 has already been defined as a variable of q_{max} which is substituted in the following constraint set. Hence, the final form of constraints for passive links by making use of Equation 6.36.

$$\textbf{Constraint 3: } 1 > \frac{[(60/\sin q_{max} + 65)^2 + (-65)^2 + \xi_1]^2}{\xi_2} \tag{6.45}$$

$$\textbf{Constraint 4: } 1 > \frac{[(60/\sin q_{max} + 65)^2 + (65)^2 + \xi_1]^2}{\xi_2} \tag{6.46}$$

$$\textbf{Constraint 5: } 1 > \frac{[(60/\sin q_{max} - 65)^2 + (0)^2 + \xi_1]^2}{\xi_2} \tag{6.47}$$

$$\textbf{Constraint 6: } 1 > \frac{[(60/\sin q_{max} + 65)^2 + (60/\sin q_{max} + 60 \cot q_{max} + 65)^2 + \xi_1]^2}{\xi_2} \tag{6.48}$$

$$\textbf{Constraint 7: } 1 > \frac{[(60/\sin q_{max} - 65)^2 + (60/\sin q_{max} - 60 \cot q_{max})^2 + \xi_1]^2}{\xi_2} \tag{6.49}$$

where $\xi_1 = -l_2^2 - l_3^2$ and $\xi_2 = [2l_2 l_3]^2$

One final constraint for passive links is the constraint of ergonomics. Since the manipulator is a haptic manipulator and in contact with the user's hand, it is necessary to have obstacle free workspace for the users hand during the haptic interaction. The foreseen interaction range is shown in Figure 6.4.

The collision with the user's hand can only be avoided if the horizontal x- location of $(i3)$ frame is equal or less than the horizontal location of $(i4)$ frame. Again, by using the critical poses for passive links, the constraint equation can be constructed as follows.

$$-l_2 \sin q_{i2} \leq -l_2 \sin q_{i2} - l_3 \sin(q_{i2} + q_{i3}) \tag{6.50}$$

$$0 \geq l_3 \sin(q_{i2} + q_{i3}) \tag{6.51}$$

$$\textbf{Constraint 8: } \Rightarrow 0 \geq \sin(q_{i2} + q_{i3}) \geq -1 \tag{6.52}$$
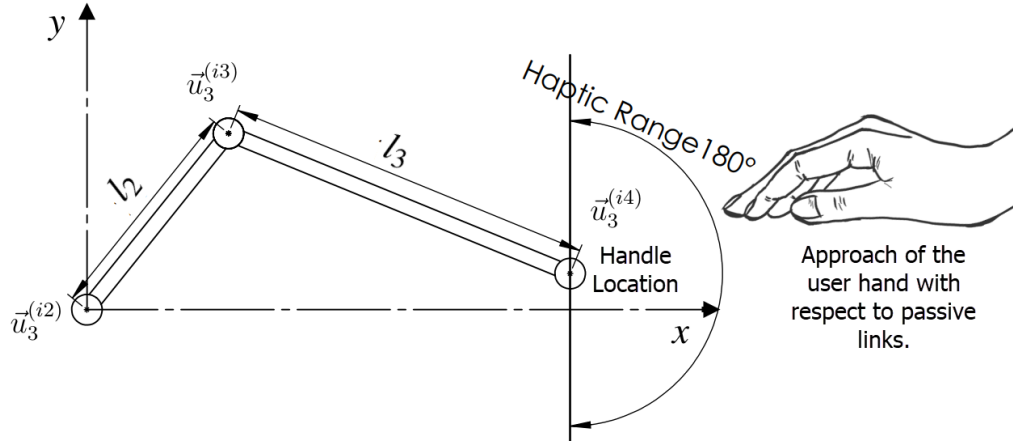
Figure 6.4. Location of the user hand with respect to origin of x- and y- axes.

If the condition in constraint 8 is achieved for C_1 and B_1 locations of the workspace, the validity of the constraint Equation for an arbitrary pose of the manipulator is sustained.

6.2. Formulation of Stiffness Performance Metrics

The evaluation of stiffness performance is inspected in accordance with the performance metrics introduced in Section 4.2.5. The material properties and cross-section dimensions are assumed to be constant. Hence, the purpose is to investigate the effect of kinematic properties on stiffness performance. It is shown that some stiffness performance metrics are related to the kinematic ones.

6.2.1. Stiffness Condition Number

Stiffness condition number S_e gives the ratio of the maximum singular value to the minimum singular value of $\hat{K}_C$.

$$S_e = \|\hat{K}_C\| \|(\hat{K}_C)^{-1}\| \tag{6.53}$$

Minimizing S_e makes the maximum and minimum singular values of $\hat{K}_C$ closer to each other which increases the stiffness uniformity. However, there is one problem in the using S_e with $\hat{K}_C$. $\hat{K}_C$ contains both translational and rotational DoF. S_e compares the translational stiffness with the torsional stiffness which causes a homogeneity problem.

119

A solution to homogeneity problem is to evaluate the translational part and torsional part of the stiffness matrix separately. $\hat{K}_C$ has been divided into 3×3 matrices as shown in Equation 6.54.

$$\hat{K}_C = \begin{bmatrix} \hat{K}_{CA} & \hat{K}_{CB} \\ \hat{K}_{CC} & \hat{K}_{CD} \end{bmatrix} \tag{6.54}$$

where $\hat{K}_{CA}$, $\hat{K}_{CB}$, $\hat{K}_{CC}$, and $\hat{K}_{CD}$ are sub-matrices of $\hat{K}_C$ and have the units of N/m, N/rad, N/rad, and Nm, respectively. Now, $\hat{K}_{CA}$ and $\hat{K}_{CD}$ can be used to obtain the norms without any mixing in translational and torsional stiffness values. Moreover, since the manipulator has only the translational motion at the mobile platform, $\hat{K}_{CA}$ should be focused on. S_e for translational and rotational DoF is computed as follows;

$$S_{et} = \|\hat{K}_{CA}\|\|(\hat{K}_{CA})^{-1}\| \tag{6.55}$$

$$S_{er} = \|\hat{K}_{CD}\|\|(\hat{K}_{CD})^{-1}\| \tag{6.56}$$

where S_{et} and S_{er} denote the stiffness condition number for translational and rotational deflections.

It has already been shown that matrix $\hat{K}_C$ is a combination of the Jacobian matrices $\hat{J}_{\theta_i}$ and the local stiffness matrices $\hat{K}_{\theta_i}$ of each serial chain. Since each serial chain is identical, stiffness condition number evaluation of a single serial chain is sufficient only if the applied forces cause small deflections at the end-effector and this approach shortens the computation time. By applying similar separation as in Equation 6.54, $\hat{K}_{Ci}$ is shown as follows;

$$\hat{K}_{Ci} = \begin{bmatrix} \hat{K}_{CiA} & \hat{K}_{CiB} \\ \hat{K}_{CiC} & \hat{K}_{CiD} \end{bmatrix} \tag{6.57}$$

However, when $\hat{K}_{Ci}$ is used for stiffness condition number, it cannot be inverted and stiffness condition number for a single serial chain cannot be computed due to the rank deficiency (caused by the passive joints). Hence, pseudo-inverse is used to obtain the inverse of sub-parts of $\hat{K}_{Ci}$.

$$S_{eti} = \|\hat{K}_{CiA}\|\|(\hat{K}_{CiA})^{+}\| \tag{6.58}$$

$$S_{eri} = \|\hat{K}_{CiD}\|\|(\hat{K}_{CiD})^{+}\| \tag{6.59}$$

where super-script $+$ denotes the pseudo-inverse. S_{eti} and S_{eri} represent the stiffness condition number for translational and rotational DoF of the ith serial chain. Since the metric is computed for $\hat{K}_{Ci}$, it only gives the performance along the $\vec{u}_i^{(0)}$ axis.

For the stiffness condition number, it is assumed that the components of the external wrench acting on end-effector either '0' or have the same magnitude and directions along the motion axes. Then, the stiffness condition number of $\hat{K}_C$ is affected by the pose and link lengths changes of the manipulator, only. The Euclidean norms of $\hat{K}_C$ and $\hat{K}_C^{-1}$ have equal values for given link lengths and for the poses where all active joints have the same angle $q_{11} = q_{21} = q_{31}$. As the active joints angle diverges from the equality between each other, the stiffness condition number increases in the same way as the condition number in kinematics. For a given pose in the workspace, the condition number c_v and the stiffness condition number S_e is proportionally related. However, when the whole workspace is investigated via globalizing of both metrics, their maximum and minimum values highly diverge from each other. For the stiffness matrix, the most and the least stiff poses are where the manipulator is fully extended and folded. Between these poses $S_e > 1$ whereas $c_v = 1$.

The relation between the condition number and stiffness condition number is shown in the following Equation set. In order to simplify the analytic approach, $\hat{K}_C$ is constructed by excluding the DoF caused by the passive joints.

$$\hat{K}_{Ci}^* = (\hat{J}_{\theta_i} \hat{K}_{\theta_i}^{-1} \hat{J}_{\theta_i}^T)^{-1} \tag{6.60}$$

$$\hat{K}_C^* = \sum_{i=1}^{3} \hat{K}_{Ci}^* \tag{6.61}$$

$$S_e = \|\hat{K}_C^*\| \|\hat{K}_C^{-*}\| \tag{6.62}$$

$$S_{ei} = \|\hat{K}_{Ci}^*\| \|\hat{K}_{Ci}^{-*}\| \tag{6.63}$$

$$\Rightarrow S_e = \sum_{i=1}^{3} S_{ei} \tag{6.64}$$

$$S_{ei} = \|\hat{J}_{\theta_i}^{-T} \hat{K}_{\theta_i} \hat{J}_{\theta_i}^{-1}\| \|\hat{J}_{\theta_i}^T \hat{K}_{\theta_i}^{-1} \hat{J}_{\theta_i}\| \tag{6.65}$$

$$\Rightarrow S_{ei} \leq \|\hat{J}_{\theta_i}^{-T}\| \|\hat{K}_{\theta_i}\| \|\hat{J}_{\theta_i}^{-1}\| \|\hat{J}_{\theta_i}^T\| \|\hat{K}_{\theta_i}^{-1}\| \|\hat{J}_{\theta_i}\| \tag{6.66}$$

$$\|\hat{J}_{\theta_i}^{-T}\| = \|\hat{J}_{\theta_i}^{-1}\| \text{ and } \|\hat{J}_{\theta_i}^T\| = \|\hat{J}_{\theta_i}\| \tag{6.67}$$

$$\Rightarrow S_{ei} \leq (\|\hat{J}_{\theta_i}^{-1}\| \|\hat{J}_{\theta_i}\|)^2 \|\hat{K}_{\theta_i}\| \|\hat{K}_{\theta_i}^{-1}\| \tag{6.68}$$

Due to the topology: $\hat{K}_{\theta_m} = \hat{K}_{\theta_1} = \hat{K}_{\theta_2} = \hat{K}_{\theta_3} \tag{6.69}$

$$\Rightarrow S_e \leq \left(\sum_{i=1}^{3} (\|\hat{J}_{\theta_i}^{-1}\| \|\hat{J}_{\theta_i}\|)^2 \right) \|\hat{K}_{\theta_m}\| \|\hat{K}_{\theta_m}^{-1}\| \tag{6.70}$$

where $\hat{K}_{Ci}^*$ is the stiffness matrix of ith serial chain for which the effect passive joints on stiffness computation is excluded. $\hat{K}_{\theta_m}$ indicates the common stiffness matrix in joints space for all serial chains. Notice that, $\|\hat{J}_{\theta_i}^{-1}\| \|\hat{J}_{\theta_i}\|$ is the condition number of ith se-

rial chain which contains the passive links and joints. Therefore, fully folded and fully expanded poses results different between the globalized S_e and c_v. Yet, increasing the performance of c_v still increases the performance of S_e.

Note that, the difference between the stiffness condition number and the kinematic condition number is caused by the passive links. If there were no passive links or the passive links' poses were not changing with respect to active joints, then the stiffness condition number would be proportionally related with the condition number. The condition number reduces the maximum deviation angle. As the deviation angle is reduced, the change in pose of the passive links is also decreased. Hence, the relation between the condition number and stiffness condition number becomes linear.

6.2.2. Volume of Stiffness Ellipsoids

The determinants of the stiffness matrices are inspected in order to comprehend the volume of the stiffness ellipsoids which indicate how stiff the manipulator is for the given pose and link lengths.

$$S_d = \det\left(\hat{K}_C\right) \tag{6.71}$$

Note that, S_d requires the computation of the stiffness matrix $\hat{K}_{Ci}$ of every serial chain to construct the matrix $\hat{K}_C$ which has relatively longer computation time with respect to $\hat{K}_{Ci}$. Therefore, $\hat{K}_{Ci}$ may be used to reduce the computation time. Yet, $\hat{K}_{Ci}$ is rank deficient and determinant always results in 0. If the passive joints are excluded in the computation of $\hat{K}_{Ci}$ only for the external forces which are applied along the $\vec{u}_i^{(0)}$ axis, $\hat{K}_{Ci}$ may be modified as $\hat{K}_{Ci}^*$. The determinant of $\hat{K}_{Ci}^*$ gives intuition about the physical provision of the manipulator along the $\vec{u}_i^{(0)}$ axis.

$$S_{di} = \det\left(\hat{K}_{Ci}^*\right) = \det\left(\hat{J}_{\theta_i}\hat{K}_{\theta_i}^{-1}\hat{J}_{\theta_i}^T\right)^{-1} = \frac{\det\left(\hat{K}_{\theta_i}\right)}{\det\left(\hat{J}_{\theta_i}\hat{J}_{\theta_i}^T\right)} \tag{6.72}$$

It can be concluded that S_{di} can be increased by increasing the determinant of local stiffness matrix $\hat{K}_{\theta_i}$ and/or decreasing the determinant of $\hat{J}_{\theta_i}\hat{J}_{\theta_i}^T$. The magnitude of the determinant of the local stiffness matrix depends on material properties, the geometric properties of the cross-section profile, and the link length. The components of local stiffness matrix in Equation 4.59 are inversely related to the link length. Hence, shorter links enhance the stiffness. This also reduces the value of the denominator supplying an extra enhancement in stiffness. On the other hand, the denominator which is also the definition

of manipulability, should be increased. Therefore, maximizing the stiffness by reducing the link lengths makes the manipulator closer to the singularity. In the singularity, the stiffness becomes infinite but one of the DoF is lost.

The volume of the stiffness ellipsoids of $\hat{K}_C$ and $\hat{K}_{Ci}$ is related with the force ellipsoids in kinematic level. Notice $\det\left(\hat{J}_{\theta_i}\hat{J}_{\theta_i}^T\right)$ in the denominator of S_{di} denotes the volume of velocity ellipsoids of a single serial chain. Since the inverse of $\det\left(\hat{J}_{\theta_i}\hat{J}_{\theta_i}^T\right)$ is used in S_{di}, it represents the volume of force ellipsoids. Hence, if the volume of the force ellipsoids is increased, the volume stiffness ellipsoids are also increased. Therefore, the following statement can be made;

$$S_{di} \sim \det\left(\hat{J}_{\theta_i}\hat{J}_{\theta_i}^T\right)^{-1} \tag{6.73}$$

Although this enhances the stiffness, it also makes the manipulator closer to a singular pose. What is important here is whether singularity occurs by reducing the link lengths or by adjusting the joint variables close to singular joint values. For instance, passive joint q_{i3} has two singular poses which correspond to $q_{i3} = 0$ and $q_{i3} = \pm\pi$. Both of them increases the volume of force ellipsoids. However, only $q_{i3} = 0$ generates the minimum link length. The focus in here is to enhance the performance of stiffness of the manipulator through the link lengths. Therefore, the standalone usage of $\det\left(\hat{J}_{\theta_i}\hat{J}_{\theta_i}^T\right)^{-1}$ is not appropriate. Fortunately, $\det\left(\hat{K}_{\theta_i}\right)$ at the nominator, ensures that the volume of stiffness ellipsoids are decreased via decreasing the link lengths.

Same homogeneity problem in stiffness condition number is also valid for the determinant operation of stiffness matrices $\hat{K}_C$. Therefore, sub-matrices $\hat{K}_{CA}$ and $\hat{K}_{CD}$ which are introduced in Equation 6.54 are investigated for the computation of S_d. $\hat{K}_{Ci}$ is not considered due to rank deficiency. The formulation of determinant of translational stiffness $\hat{K}_{CA}$ and rotational stiffness $\hat{K}_{CD}$ are;

$$S_{da} = \det\left(\hat{K}_{CA}\right) \tag{6.74}$$

$$S_{dd} = \det\left(\hat{K}_{CD}\right) \tag{6.75}$$

where S_{da} and S_{dd} denote the volume of translational and rotational stiffness ellipsoids. S_{da} and S_{dd} are computed for fully extended pose which has the maximum moment arm.

6.3. Formulation of Dynamics Performance Metrics

Evaluation of the dynamic properties of the R-CUBE mechanism is achieved via inertia matrix defined in joint space and Cartesian space. The first evaluation is conducted

by taking the determinant of the generalized inertia matrices shown in Equations 5.227 and 5.223. The following operation indicates the volume of the inertia ellipsoids;

$$I_m = \det\left(\hat{M}_C\right) \tag{6.76}$$

where I_m is the determinant of the generalized inertia matrix of the whole manipulator. Unlike the stiffness matrices, inertia matrices are faster to compute. Since the above inertia matrix is defined in Cartesian space, the input is from the Cartesian space for I_m. Hence, I_m is the scalar indication of the felt dynamic effects by the user.

The open form of I_m is shown below;

$$\det\left(\hat{M}_C\right) = \det\left(\sum_{i=1}^{3} \hat{M}_{Ci}\right) \tag{6.77}$$

$$\Rightarrow \det\left(\hat{M}_C\right) = \det\left(\sum_{i=1}^{3} \hat{J}_i^{-T} \hat{M}_i \hat{J}_i^{-1}\right) \tag{6.78}$$

where $\hat{M}_{Ci}$ is the inertia matrix of a single link. Above equality indicates that I_m is reduced by increasing the manipulability and/or decreasing the inertia of the manipulator. Therefore, there is an analogy between μ_v and I_m. I_m may be stated as a version of μ_v amplified by $\hat{M}_i$. Hence, μ_v may be used to increase the dynamic performance. However, μ_v does not include the effect of passive links on dynamics.

When the determinants are computed, it can be seen that the order of the link length variables at the nominator is greater than the denominator. This means small loss in $\hat{M}_i$ has a greater effect on I_m. Hence, μ_v should accompany with the multipliers which include the effect of passive links.

Dynamic manipulability is computed as follows;

$$I_d = \det\left(\hat{M}_C^{-1}\right) \tag{6.79}$$

$$I_d = \det\left(\sum_{i=1}^{3} \hat{J}_i \hat{M}_i^{-1} \hat{J}_i^T\right) \tag{6.80}$$

where I_d is the dynamic manipulability index. Note that, it is proportional with the inverse of I_m. The objective is to increase the dynamic manipulability. A similar relation between μ_v with I_m can also be established for I_d.

A simplification can be made for both I_d and I_m by investigating only one of the serial chains. The objectives of I_d or I_m is to decrease the link length and increase the manipulability. μ_v has its minimum value when $q_{11} = q_{21} = q_{31} = q_{max} = |q_{min}|$ which is also the poses where dynamic manipulability is minimum.

124

Although it is important to reduce the inertial effects, it is also vital to achieve an equal distribution to obtain the same impedance performance for all of the workspace. This effect is measured by taking the ratio of maximum and minimum Euclidean norm of $\hat{M}_C$. $\hat{M}_{Ci}$ should not be used in here because the purpose is not the reduce the inertia of a single link but to maintain the equal inertial distribution of the whole manipulator. The performance metric is shown in Equation 6.81.

$$I_e = \|\hat{M}_C\|\|(\hat{M}_C)^{-1}\| \tag{6.81}$$

This metric is proportional with the condition number c_v. As c_v is decreased, the variation of inertial effects are also decreased. Hence, I_e is decreased.

6.4. Construction of the Objective Functions

In this section objective functions for optimization are determined by considering the relations of the performance metrics. All of the objective functions are constructed to be minimized, so some of the performance metrics are inverted.

First the relation is between manipulability in Equation 6.26 and condition number in Equation 6.18 is investigated. The objective for manipulability is to increase it. Hence, the objective function for manipulability O_1 is the inverse of the manipulability metric $(\tan(q_{max}))^{-1}$. Condition number $\cos^2(q_{max})^{-1}$ is needed to be decreased so no inversion is required. However, there is also no needed to construct a separate objective function for condition number since O_1 already includes $\cos(q_{max})$ in its denominator. To separate the usage of the metrics in the weighted-sum approach would increase the weight of the condition number. In Pareto-front approach it is not needed. Moreover, the condition number and O_1 have their minimum value when q_{max} is minimized. Therefore, O_1 ensures that the manipulability and condition number performance is enhanced simultaneously.

$$O_1 = \tan(q_{max}) \tag{6.82}$$

The relation of the condition number with the dynamics and stiffness has already stated. Optimizing O_1 also ensures the equal distribution of dynamic and stiffness properties in the workspace.

Objective functions considering the dynamics and stiffness performance metrics are constructed by employing the metrics I_m and S_{da}. Desired objective for I_m is to decrease and for S_{da} is to increase the numerical value. The objective functions O_2 and

O_3 are given in the following equation set. S_{dd} is not included since the focal point of the optimization is to increase translational stiffness.

$$O_2 = \det\left(\hat{M}_C\right) \tag{6.83}$$

$$O_3 = \det\left(\hat{K}_{CA}\right)^{-1} \tag{6.84}$$

Note that, O_2 and O_3 both reduces the link lengths. O_2 is evaluated 2 of the active links are fully folded and the other one is at home position. O_3 is only evaluated in fully expanded pose which has the maximum moment arm. While O_2 enhances the manipulability including the passive links, O_3 tries to get close to a singular pose. The condition number for dynamics and stiffness is not included in optimization since c_v ensures that kinematic, stiffness, and dynamic variations in manipulator are decreased.

6.5. Construction of Objective Function for Optimization of Cross-Section Profile

In above Sections, dynamics and stiffness are evaluated in terms of link lengths. However, the dimensional evaluation of cross-section profile of the hollow tube links is not discussed. Since the cross-section dimensions do not affect the kinematic properties, a separate design of the dimensions of the cross-section is conducted. The purpose in here is to obtain the ratio of the outer diameter to the inner diameter which provides best dynamic performance with the highest possible stiffness. Then, the real values of the diameters are determined in terms of required strength.

The relation of dynamic and stiffness properties in terms of cross-section dimensions are conducted via using the Equations 5.162 to 5.166 for stiffness and Equations 5.229 and 5.230 for dynamics by making use of Figure 5.9.

The inertia of a single link with respect to rotation along the z- axis;

$$I_l = I_z^* + m\frac{l_{ij}^2}{4} \tag{6.85}$$

$$I_l = \rho\pi l_{ij}\left(\left(\frac{D_{ij}}{2}\right)^2 - \left(\frac{d_{ij}}{2}\right)^2\right)\left(\frac{l_{ij}^2}{3} + \frac{\left(\frac{D_{ij}}{2}\right)^2 + \left(\frac{d_{ij}}{2}\right)^2}{4} + \frac{l_{ij}^2}{4}\right) \tag{6.86}$$

where I_l is the inertia of a single rotating link. Since the link lengths are determined in the previous section, the remaining optimization is conducted on the inner and outer diameters. The outer diameter is given unit value to obtain the inner diameter as a ratio of the outer diameter.

In the evaluation of the stiffness, only the elements of the stiffness matrix which are affected by the bending forces are considered since the bending is the most effective action on deformation. Hence, stiffness is indicated with a scalar value S_l.

$$S_l = \frac{12E_y I_z}{l_{ij}^3} = \frac{12E_y \pi}{4l_{ij}^3}((\frac{D_{ij}}{2})^4 - (\frac{d_{ij}}{2})^4) \tag{6.87}$$

Since S_l and I_l determined, they can be used in multi objective optimization where d_{ij} is the design parameter. $\rho = 1$, $l_{ij} = 1$, $D_{ij} = 1$, and $E_y = 1$ are taken as unit values. Hence, the objective functions to be minimized for genetic algorithm are

$$CS_1 = S_l^{-1} \tag{6.88}$$

$$CS_2 = I_l \tag{6.89}$$

where CS_1 and CS_2 are the cross-section profile related objective functions. After determining the ratio, the optimized dimensions of the cross-section may be determined in terms of eligible products in the market, required strength and/or maximum deformation under load. The optimum result is called d_{op} to be used in next section and shown as follows;

$$d_{op} = \frac{d_{ij}}{D_{ij}} \tag{6.90}$$

6.6. Construction of Objective Function for Optimization of Composite Fiber Orientations

The orientation of plies are determined in accordance with the maximum deflections and applied wrenches. Deflections at the end-effector are computed by using the stiffness matrix $\hat{K}_{Ci}^*$ for a single serial chain. The stiffness matrix, however, is modified as described in Section 5.2.4.

$$\Delta\bar{\kappa}_i^* = (\hat{K}_{Ci}^*)^{-1}\bar{F}_{ext} \tag{6.91}$$

$\Delta\bar{\kappa}_i^*$ is computed in the fully extended pose where the maximum deflections occur. The corresponding pose for 1st serial chain is $q_{11} = q_{21} = q_{31} = q_{max}$. Hence, the ply orientations of the composite link are optimized in this pose. Next, the norm of displacements in Cartesian space is used as a performance metric. Since the displacement contains translational and rotational deflections, each displacement type is evaluated separately.

$$CF_1 = \|(\Delta\bar{\kappa}_i^*)_{1-3}\| \tag{6.92}$$

$$CF_2 = \|(\Delta\bar{\kappa}_i^*)_{4-6}\| \qquad (6.93)$$

where CF_1 and CF_2 denote the norms of translational and rotational deflections, respectively. Subscript $1-3$ and $4-6$ denote the evaluated components of $\Delta\bar{\kappa}_i^*$.

Stiffness matrix in Cartesian space is also a function of composite fiber orientations. The objective is to obtain the number of minimum required composite layers. Therefore, the maximum number of each ply in 0°, 90°, 45°, and -45° is limited by 10. 0° and 90° orientation enhances the stiffens against bending and crushing stiffness. 45° and -45° orientation, on the other hand, increases the stiffness against the torsional loads. The applied forces on the manipulator are along the $\vec{u}_i^{(0)}$ axis. 0° and 90° ensure the stiffness is increased for both $\pm$ directions along the $\vec{u}_i^{(0)}$ axis. However, torsional load is also compensated by 45° and -45° oriented composites. Since the analysis is conducted for a single direction, the number of 45° and -45° plies are taken equal to reduce the required analysis number.

In the market, each ply has a thickness about 0.15mm. This value is adopted in this thesis. Due to the ratio of inner and outer diameter, the number of layers also determines the cross-section dimensions. The relation is shown as follows;

$$t = \frac{D_{ij} - d_{ij}}{2} \qquad (6.94)$$

$$t = 0.15(a_{ij} + b_{ij} + c_{ij} + d_{ij})/1000 \text{ m} \qquad (6.95)$$

$$\frac{D_{ij}}{2} = 0.15(a_{ij} + b_{ij} + c_{ij} + d_{ij})/1000 + \frac{d_{ij}}{2} \qquad (6.96)$$

where a_{ij}, b_{ij}, c_{ij}, and d_{ij} denote the number of layers of each respective body and orientation which are used as optimization parameter. t denote the thickness of the hollow tube.

The links are designed under 20 N external force along the motion axis of the inspected serial chain which is 4 times of the foreseen force in order to ensure the failure safety.

6.7. Conclusion

In this Chapter performance metrics of modified R-CUBE mechanism is obtained and constraint functions are determined. The relation between the kinematics, stiffness, and dynamics performance metrics has been shown. Due to the long computation time of stiffness matrices, the performance metrics related to stiffness has been simplified. 3 objective functions are constructed to optimize the kinematic dimensions of the manipulator

by virtue of kinematics, stiffness, and dynamics performance metrics. Since the cross-section profile and the material type do not affect the kinematics, the design of these domains is achieved only by evaluating their stiffness and dynamics performance. After determining the optimum inner and outer diameter ratio, the composite material design optimization has been conducted to obtain the diameter and the ply numbers with their orientations. As a result, kinematic, cross-section profile, and composite link properties are determined.

CHAPTER 7

CASE STUDY: RESULT OF OPTIMAL DESIGN OF R-CUBE

In this Chapter, results of the optimization algorithm are presented. First, the Pareto-front solution set is listed. Then, the selection approach of the one of the optimum solutions is discussed. After determining the kinematic synthesis results, the optimization result of cross-section profile dimension of the hollow tube is presented. Finally, by determining the composite material design parameters, the optimal design of modified R-CUBE mechanism is achieved.

7.1. Optimal Solution Results of Kinematic Synthesis

The optimization is conducted for 3 sets of boundary conditions of input parameters. The inputs of the kinematic optimization are determined to be the maximum deviation angle q_{max}, and the lengths of l_2 and l_3. The lengths are minimum of 1 mm. The upper boundaries, however, are given a number of values to ensure that the Pareto-front solution set is not constrained by these limitations. First, higher upper boundaries are given for inputs (Set 1). Then, they have been reduced at each set depending on the outputs of the previous set of genetic algorithm solution. The lower and upper boundaries are given in Table 7.1.

Table 7.1. Lower-upper boundaries of q_{max}, l_2, and l_3.

	Set 1	Set 2	Set 3
q_{max} (rad)	0.07-1.5	0.07-1.5	0.07-1.5
l_2 (mm)	1-500	1-250	1-100
l_3 (mm)	1-500	1-250	1-150

O_1, O_2, and O_3 objective functions are evaluated at each iteration of genetic algorithm. Among the Pareto front solutions, the solutions with $l_1 + l_2 + l_3 < 400$ mm total link length are preserved and listed in Table 7.2 in descending order with respect to natural frequency index. 40 optimal solutions are shown in total with the determined link

lengths for l_1, l_2, and l_3 and maximum deviation angle from home position q_{max}. Notice that, as l_1 increases, maximum deviation angle q_{max} decreases due to the constraint equation of prescribed workspace. Since the increment in l_1 also increases the footprint of the manipulator, passive links also increase to cope with the dimensional change.

A post evaluation is conducted for obtained kinematic design parameters. Inertia index I_f, stiffness index S_f, natural frequency index ω_n which are the Frobenius norm of corresponding matrices are computed. All indices are computed at home position of the manipulator for a single serial chain. In order to compare only the link lengths and joint angles effect on optimization, above matrices are computed for the following design parameters of links;

$$D_{ij} = 20 \text{ mm}, d_{ij} = 10 \text{ mm}$$

$$q_{11} = q_{21} = q_{31} = 0 \text{ rad}$$

$$\rho = 2000 \text{ kg/m}^3.$$

Next, manipulability index μ_v and condition number c_v are computed as kinematic performance metrics for the angle of q_{max} where the manipulability and the condition number have their minimum value. Table 7.3 shows the computed indices. Notice that, as the total link length increases, both the inertia and stiffness performance of the manipulator decreases. Higher I_f indicates that total mass of the manipulator increase which decreases the dynamic performance. Low S_f shows that the manipulator is more compliant against to applied forces. Both are mainly affected by increased link lengths since this adds extra mass to the system and makes it more vulnerable to reaction moments due to the increased moment arm. Hence, the maximum natural frequency index is obtained when the total link length is at its minimum value because in this design parameter inertia has its minimum value and the stiffness has its maximum value. Manipulability and condition number performance on the other hand increases as the total link length is increased. Higher μ_v shows that manipulator is more manipulable at $q_{i1} = q_{max}$. Lower c_v, on the other hand, means that the motioning resolution is enhanced since q_{max} is minimized.

In order to compare the performance of the design with respect to each other, every performance metric is normalized. The normalization is conducted in accordance with the following equation;

$$p_i = \frac{p_i - p_{i-min}}{p_{i-max} - p_{i-min}} \tag{7.1}$$

where p_i is the inspected performance metric, p_{i-max} and p_{i-min} denote the maximum and minimum values among the all p_i performance metric values. Normalized values of performance metrics are listed in Table 7.4.

Table 7.2. Optimal design solutions.

	l_1 (mm)	l_2 (mm)	l_3 (mm)	Total Link Length (mm)	Max. Deviation Angle (Deg)
Sol. 1	111.7	74.1	121.8	307.6	32.5
Sol. 2	113.3	74.4	123.4	311.1	32.0
Sol. 3	114.3	75.9	122.5	312.8	31.6
Sol. 4	115.1	76.9	123.3	315.3	31.4
Sol. 5	117.0	79.4	124.2	320.5	30.9
Sol. 6	117.8	76.8	126.4	321.0	30.6
Sol. 7	115.4	82.0	129.6	327.0	31.3
Sol. 8	117.7	80.0	124.3	322.1	30.7
Sol. 9	118.9	81.0	124.6	324.5	30.3
Sol. 10	119.3	82.1	125.7	327.0	30.2
Sol. 11	119.7	81.8	124.9	326.4	30.1
Sol. 12	120.0	80.5	126.3	326.7	30.0
Sol. 13	120.2	82.8	125.8	328.9	29.9
Sol. 14	120.9	81.1	126.0	328.1	29.7
Sol. 15	120.6	82.6	125.2	328.4	29.8
Sol. 16	121.7	80.7	126.4	328.8	29.5
Sol. 17	121.6	83.7	125.9	331.2	29.6
Sol. 18	121.0	84.6	127.5	333.1	29.7
Sol. 19	120.9	85.8	131.5	338.3	29.7
Sol. 20	121.5	86.3	129.3	337.1	29.6
Sol. 21	122.4	84.3	128.5	335.2	29.3
Sol. 22	123.9	81.8	128.9	334.6	29.0
Sol. 23	122.6	87.0	129.2	338.9	29.3
Sol. 24	123.1	88.2	130.4	341.7	29.2
Sol. 25	124.3	86.6	134.4	345.3	28.9
Sol. 26	126.3	83.7	128.7	338.6	28.4
Sol. 27	127.1	84.5	129.9	341.5	28.2
Sol. 28	125.3	90.0	130.8	346.1	28.6
Sol. 29	128.6	83.1	131.5	343.3	27.8
Sol. 30	127.2	88.2	135.9	351.2	28.2
Sol. 31	132.3	90.0	135.2	357.5	27.0
Sol. 32	136.1	89.1	132.4	357.7	26.2
Sol. 33	135.7	93.2	130.6	359.5	26.2
Sol. 34	142.2	88.5	134.5	365.2	25.0
Sol. 35	143.7	90.2	136.0	370.0	24.7
Sol. 36	144.5	92.4	136.9	373.8	24.5
Sol. 37	143.3	98.2	144.8	386.3	24.8
Sol. 38	145.2	97.1	136.9	379.2	24.4
Sol. 39	146.8	99.0	143.7	389.5	24.1
Sol. 40	149.8	97.4	134.8	382.0	23.6

Table 7.3. Performance metrics of optimal design solutions.

	I_f Inertia Index	S_f Stiffness Index	ω_n Natural Freq. Index	μ_v Manipulability	c_v Condition Number
Sol. 1	0.0051	1133587	331525202	0.094	1.406
Sol. 2	0.0052	1095177	309517709	0.096	1.390
Sol. 3	0.0053	1063707	294630402	0.097	1.380
Sol. 4	0.0054	1038044	282566624	0.098	1.373
Sol. 5	0.0056	980515	256584886	0.100	1.357
Sol. 6	0.0060	987725	254949706	0.101	1.351
Sol. 7	0.0058	959458	254866276	0.099	1.370
Sol. 8	0.0057	963351	248468428	0.101	1.351
Sol. 9	0.0058	936780	236081279	0.103	1.342
Sol. 10	0.0059	918266	228926771	0.103	1.339
Sol. 11	0.0059	917414	227370239	0.104	1.336
Sol. 12	0.0060	921158	227146646	0.104	1.333
Sol. 13	0.0060	898470	219944260	0.104	1.332
Sol. 14	0.0063	903387	218884106	0.105	1.326
Sol. 15	0.0060	897399	218494136	0.105	1.329
Sol. 16	0.0064	895673	214137002	0.106	1.321
Sol. 17	0.0061	873352	208464185	0.106	1.322
Sol. 18	0.0061	867702	208227605	0.105	1.326
Sol. 19	0.0062	846651	201671000	0.105	1.326
Sol. 20	0.0062	842196	199110533	0.106	1.322
Sol. 21	0.0063	850286	198806113	0.107	1.316
Sol. 22	0.0064	851172	194619964	0.108	1.306
Sol. 23	0.0063	824031	190995639	0.107	1.315
Sol. 24	0.0064	806462	184749162	0.107	1.312
Sol. 25	0.0065	794454	177467489	0.109	1.304
Sol. 26	0.0069	809640	177425742	0.111	1.292
Sol. 27	0.0070	790620	170172711	0.112	1.287
Sol. 28	0.0067	767734	168598210	0.110	1.297
Sol. 29	0.0070	779350	163501606	0.114	1.278
Sol. 30	0.0069	749162	158652698	0.112	1.286
Sol. 31	0.0077	689390	133924533	0.118	1.259
Sol. 32	0.0078	666764	122645426	0.122	1.241
Sol. 33	0.0080	652238	120334590	0.122	1.243
Sol. 34	0.0088	614608	102680374	0.129	1.217
Sol. 35	0.0089	591610	96112347	0.131	1.211
Sol. 36	0.0089	574595	91835797	0.131	1.208
Sol. 37	0.0092	543219	86551622	0.130	1.213
Sol. 38	0.0094	549336	86229458	0.132	1.206
Sol. 39	0.0097	519280	78579104	0.134	1.201
Sol. 40	0.0098	522482	76977545	0.137	1.191

Table 7.4. Normalized performance metrics of optimal design solutions.

	I_{fn} Normalized Inertia Index	S_{fn} Normalized Stiffness Index	ω_{nn} Normalized Natural Freq.Index	μ_{vn} Normalized Manipulability	c_{vn} Normalized Condition Number
Sol. 1	0.000	1.000	1.000	0.000	1.000
Sol. 2	0.040	0.937	0.914	0.045	0.924
Sol. 3	0.061	0.886	0.855	0.073	0.880
Sol. 4	0.079	0.844	0.808	0.094	0.847
Sol. 5	0.121	0.751	0.706	0.144	0.773
Sol. 6	0.194	0.763	0.699	0.166	0.743
Sol. 7	0.163	0.717	0.699	0.102	0.836
Sol. 8	0.138	0.723	0.674	0.164	0.745
Sol. 9	0.164	0.680	0.625	0.196	0.702
Sol. 10	0.175	0.649	0.597	0.207	0.688
Sol. 11	0.183	0.648	0.591	0.218	0.673
Sol. 12	0.192	0.654	0.590	0.226	0.663
Sol. 13	0.197	0.617	0.562	0.232	0.655
Sol. 14	0.262	0.625	0.557	0.251	0.631
Sol. 15	0.205	0.616	0.556	0.242	0.642
Sol. 16	0.275	0.613	0.539	0.272	0.605
Sol. 17	0.228	0.576	0.517	0.268	0.610
Sol. 18	0.220	0.567	0.516	0.253	0.628
Sol. 19	0.230	0.533	0.490	0.251	0.630
Sol. 20	0.241	0.526	0.480	0.267	0.611
Sol. 21	0.253	0.539	0.479	0.292	0.582
Sol. 22	0.283	0.540	0.462	0.331	0.536
Sol. 23	0.268	0.496	0.448	0.296	0.576
Sol. 24	0.282	0.467	0.423	0.308	0.562
Sol. 25	0.312	0.448	0.395	0.341	0.525
Sol. 26	0.382	0.473	0.395	0.393	0.468
Sol. 27	0.418	0.442	0.366	0.416	0.444
Sol. 28	0.337	0.404	0.360	0.368	0.495
Sol. 29	0.405	0.423	0.340	0.456	0.404
Sol. 30	0.382	0.374	0.321	0.417	0.444
Sol. 31	0.564	0.277	0.224	0.551	0.316
Sol. 32	0.584	0.240	0.179	0.650	0.233
Sol. 33	0.613	0.216	0.170	0.639	0.242
Sol. 34	0.784	0.155	0.101	0.807	0.118
Sol. 35	0.800	0.118	0.075	0.846	0.093
Sol. 36	0.816	0.090	0.058	0.866	0.080
Sol. 37	0.863	0.039	0.038	0.834	0.100
Sol. 38	0.917	0.049	0.036	0.884	0.068
Sol. 39	0.968	0.000	0.006	0.924	0.044
Sol. 40	1.000	0.005	0.000	1.000	0.000

7.2. Selection of Optimum Solution

The selection of an optimum solution requires engineering approach depending on the requirements of the design objective. In terms of mathematical approach, all of the solutions are optimum yet each solution has its own trade-off with respect to performance metrics. In order to study in a common framework, all performance metrics are normalized as shown in Table 7.4. Since the values in the table are normalized with respect to their minimum and maximum values, they represent the proportional gain or loss for the chosen design points. For instance, in the solution set 1, I_{fn} and μ_{vn} equals to 0 means that solution set 1 has the least amount of inertia and the lowest manipulability among all the solutions. While 0 indicates a better performance for I_{fn}, the performance of μ_{vn} equals 0 indicates the vice versa. In order to prevent the dilemma between the numerical values, the following indices are updated as follows;

$$S_{fn}^* = 1 - S_{fn} \tag{7.2}$$

$$\omega_{nn}^* = 1 - \omega_{nn} \tag{7.3}$$

$$\mu_{vn}^* = 1 - \mu_{vn} \tag{7.4}$$

With this modification, the performance is maximum when all of the indices equal to 0.

The evaluation to select an optimum solution may be conducted between any of the metrics. However, note that natural frequency index already contains the relation of stiffness and inertia indices. Similarly, as the manipulaiblity increases, the performance of condition number also increases. Therefore, it is sufficient to evaluate the natural frequency with respect to manipulability. Of course, inertia and manipulability or stiffness and condition number comparison may be conducted which is up to designer and desired objectives of the design.

First, the relation of natural frequency ω_{nn}^* with manipulability μ_{vn}^* is investigated. The evaluation is conducted by root mean square (RMS) of the indices. Since the desired objective for both metrics is 0, lowest RMS value indicates the design point which is closest to 0. Figure 7.1 shows the distribution of ω_{nn}^* with respect to μ_{vn}^*. In Figure 7.2 the RMS value of ω_{nn}^* and μ_{vn}^* is indicated. The minimum RMS value in Figure 7.2 corresponds to the solution set 29.

It is important to highlight that in terms of engineering, 32.5^o maximum deviation angle for active links is already a good value. However, due to the normalization approach adopted for Table 7.4, it is indicated as if it is an angle close to singularity but it is not. Note that, singularity constraints are already defined in the optimization algo-
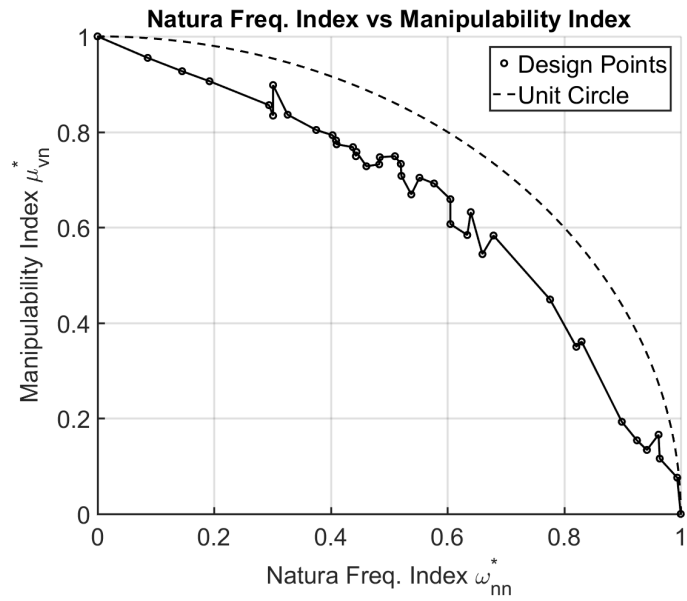
Figure 7.1. Natural Frequency Index vs Manipulability Index.
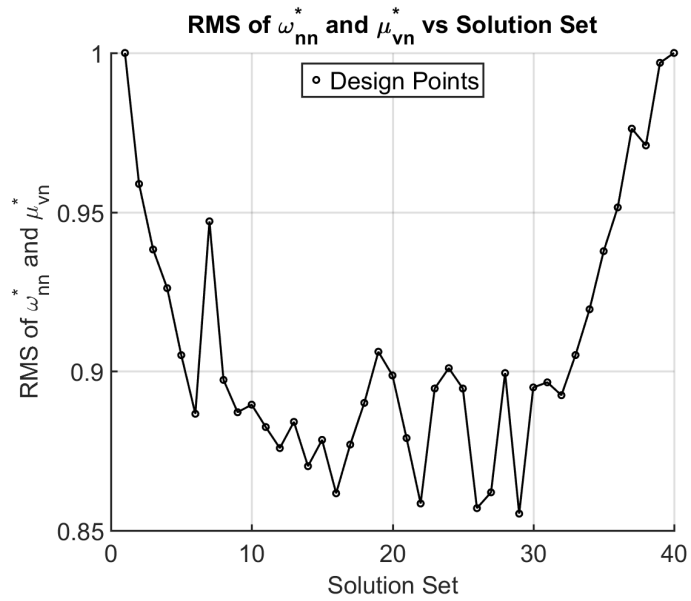
Figure 7.2. RMS value vs the number of solution sets.

rithm. Hence, any solution set has a dexterous workspace. In addition, the maximum difference in angle for obtained solution sets is 8.9^o. On the other hand, the gain in total link length for the increment in manipulability performance is 74 mm. Since the order of inertia and stiffness in terms of link length is higher than the manipulability, it is logical to give weight to manipulability in RMS computation. Figure 7.3 shows the computed RMS values with respect to the number of the solution set. The optimum solution sets which correspond to a minimum of weighted RMS values are given in Table 7.5. Since the objective of the thesis is to enhance the impedance performance, the selected solution set is 1 which has the highest natural frequency index.
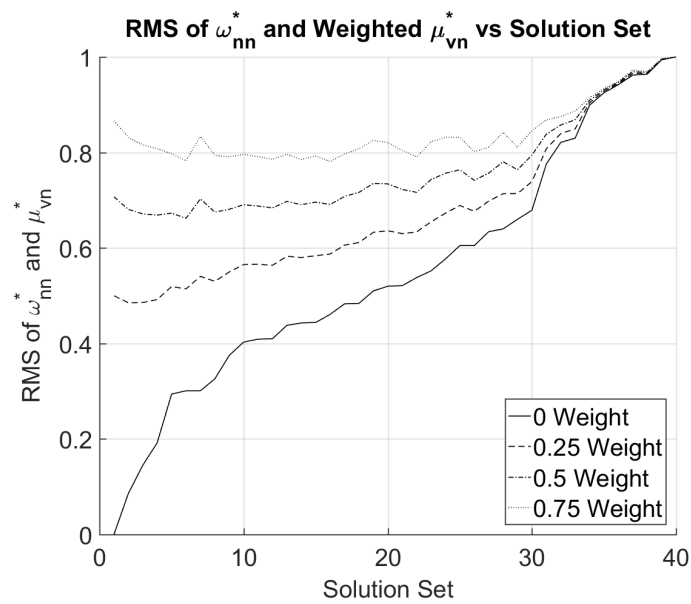

Figure 7.3. Weighted RMS value vs the number of solution sets.

Table 7.5. Solution sets for weighted RMS.

	0 Weight μ^*_{vn}	0.25 Weight μ^*_{vn}	0.5 Weight μ^*_{vn}	0.75 Weight μ^*_{vn}
Solution Set	1	2	6	16

7.3. Results of Hollow Link Cross-Section Optimization

The optimization is conducted to obtain the best inertia/stiffness ratio. The optimum solution is where the objective functions CS_1 and CS_2 have their minimum value. The obtained values of objective functions are normalized using Equation 7.1. Next, the RMS values of CS_1 and CS_2 are computed to obtain the minimum value and its corresponding inner and outer diameter ratio. Figure 7.4 shows the computed RMS value and CS_1 values with respect to CS_2. Selected data points on the Figure denotes the minimum RMS curve and its corresponding diameter ratios on the left, and the closest data point to 0 on the right. Hence, the obtained ratio is;

$$d_{op} = \frac{d_{ij}}{D_{ij}} = 0.768 \tag{7.5}$$
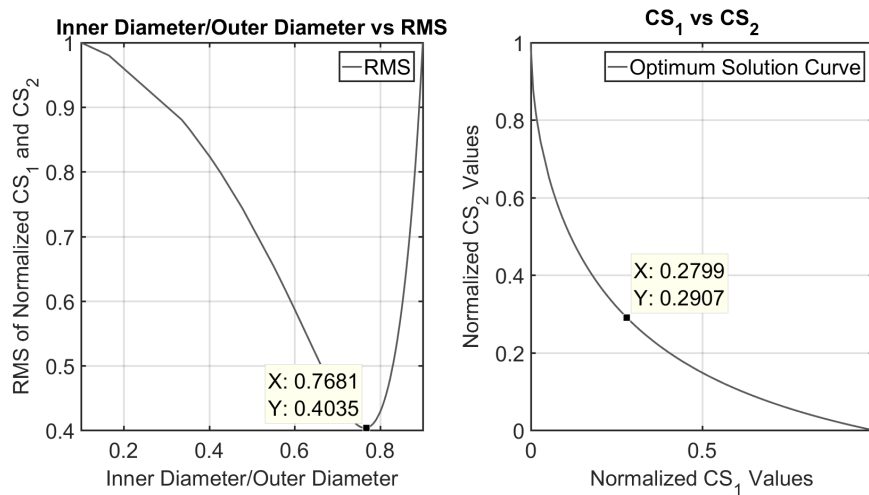
Figure 7.4. Computed RMS vs diameter ratio (on the left), and Pareto-front curve (on the right).

7.4. Results of Composite Link Optimization

Composite link optimization is conducted to minimize the translational and rotational deflection at the end-effector and required a number of composite layers. Since both objectives are contradictive, less number of composite layers result in higher deflections. The obtained results are shown in Table 7.6 and their corresponding link diameters

in Table 7.7. Note that, the deflections are computed for 20 N external force which is 4 times of the foreseen force output of the haptic device. In this thesis, solution set 29 chosen as link dimensions.

7.5. Performance Evaluation of Designed Manipulator

In this Section, obtained design parameters and graphical illustration of performance metrics for optimized design are presented. A summary of preferred design parameters is presented in Table 7.8. Depending on the designated design parameters, estimated specifications of the manipulator are given in Table 7.9.

Computed inertia and stiffness matrices in Cartesian space for home position under no external wrenches are given in Equations 7.6 and 7.7. Simplified version of only the translational deflection sub-part of the Cartesian stiffness matrix is given in Equation 7.8.

$$\hat{M}_C = \begin{bmatrix} 0.0429 & -0.0039 & -0.0039 \\ -0.0039 & 0.0429 & -0.0039 \\ -0.0039 & -0.0039 & 0.0429 \end{bmatrix} \text{(kg)} \tag{7.6}$$

$$\hat{K}_C = \begin{bmatrix} 209110 & 0 & 0 & 0 & -80 & 6495 \\ 0 & 209110 & 0 & 6495 & 0 & -80 \\ 0 & 0 & 209110 & -80 & 6495 & 0 \\ 0 & 6495 & -80 & 727 & -2 & -2 \\ -80 & 0 & 6495 & -2 & 727 & -2 \\ 6495 & -80 & 0 & -2 & -2 & 727 \end{bmatrix} \tag{7.7}$$

$$\hat{K}_C^* = \begin{bmatrix} 209110 & 0 & 0 \\ 0 & 209110 & 0 \\ 0 & 0 & 209110 \end{bmatrix} \text{(N/m)} \tag{7.8}$$

Using $\hat{M}_C$ and $\hat{K}_C^*$, the dynamic matrix $\hat{D}_C = \hat{M}_C^{-1} \hat{K}_C^*$ and the Frobenius norm is computed as shown in Equation 7.9 and 7.10. Equations 7.11 to 7.13 give the natural frequencies 'e' and corresponding modal vectors '$\bar{m}$'.

$$\hat{D}_C = \begin{bmatrix} 4.9664 & 0.5002 & 0.5002 \\ 0.5002 & 4.9664 & 0.5002 \\ 0.5002 & 0.5002 & 4.9664 \end{bmatrix} 10^6 \text{ N/(kg.m)} \tag{7.9}$$

Table 7.6. Number of composite plies for each link and orientation. Translational deflections (Tr. Def.) and rotational deflections (Rot. Def.) denote the end-effector compliant displacement for given composite design.

	Tr. Def. (mm)	Rot. Def. (deg)	1st link 0°	1st link 90°	1st link 45°	2nd link 0°	2nd link 90°	2nd link 45°	3rd link 0°	3rd link 90°	3rd link 45°
Sol. 1	0.048	0.011	9	9	9	9	9	9	8	9	9
Sol. 2	0.049	0.012	9	9	9	9	9	9	7	9	8
Sol. 3	0.050	0.012	9	9	9	8	9	9	6	9	8
Sol. 4	0.052	0.013	9	9	9	8	9	9	8	9	4
Sol. 5	0.053	0.014	9	9	9	7	9	9	8	9	4
Sol. 6	0.056	0.015	9	9	9	6	8	9	6	9	5
Sol. 7	0.057	0.015	9	9	9	5	8	9	8	9	5
Sol. 8	0.059	0.016	8	9	9	6	9	9	7	9	3
Sol. 9	0.060	0.017	8	9	9	6	9	9	6	9	3
Sol. 10	0.062	0.018	8	9	9	7	8	9	4	8	4
Sol. 11	0.065	0.019	8	9	9	5	8	9	7	9	2
Sol. 12	0.070	0.020	8	9	9	4	7	9	5	9	3
Sol. 13	0.078	0.023	9	8	9	3	8	8	6	9	2
Sol. 14	0.081	0.023	8	8	9	4	7	8	6	9	3
Sol. 15	0.087	0.025	7	8	9	3	8	8	6	9	2
Sol. 16	0.091	0.026	5	9	9	5	7	8	5	9	2
Sol. 17	0.099	0.031	8	7	9	6	7	7	6	8	1
Sol. 18	0.103	0.032	4	9	9	5	7	8	4	8	2
Sol. 19	0.112	0.033	6	8	9	4	5	8	5	8	2
Sol. 20	0.119	0.035	3	8	9	3	8	8	4	7	3
Sol. 21	0.125	0.037	5	7	9	3	8	7	4	8	2
Sol. 22	0.138	0.039	4	7	9	3	7	7	3	8	3
Sol. 23	0.152	0.045	4	7	9	3	6	7	4	9	1
Sol. 24	0.171	0.053	4	8	8	3	8	6	4	8	1
Sol. 25	0.178	0.056	3	6	9	2	6	8	3	8	1
Sol. 26	0.228	0.068	3	6	9	3	5	6	3	6	3
Sol. 27	0.242	0.065	2	4	9	2	5	8	2	8	2
Sol. 28	0.244	0.074	3	7	8	2	6	6	3	8	1
Sol. 29	0.291	0.095	4	7	7	2	6	6	2	6	2
Sol. 30	0.343	0.098	2	6	8	2	4	6	3	8	1
Sol. 31	0.359	0.106	3	6	7	2	5	6	3	7	1
Sol. 32	0.472	0.149	5	5	6	5	4	5	4	5	1
Sol. 33	0.491	0.148	2	5	7	3	5	5	3	6	1
Sol. 34	0.600	0.169	2	5	6	3	8	4	3	6	1
Sol. 35	0.717	0.211	3	3	7	3	3	5	2	6	1

Table 7.7. Inner and outer diameters of each respective link for chosen solution set.

	D_{i1} (mm)	d_{i1} (mm)	D_{i2} (mm)	d_{i2} (mm)	D_{i3} (mm)	d_{i3} (mm)
Sol. 1	21.6	16.2	21.6	16.2	21	15.75
Sol. 2	21.6	16.2	21.6	16.2	19.2	14.4
Sol. 3	21.6	16.2	21	15.75	18.6	13.95
Sol. 4	21.6	16.2	21	15.75	15	11.25
Sol. 5	21.6	16.2	20.4	15.3	15	11.25
Sol. 6	21.6	16.2	19.2	14.4	15	11.25
Sol. 7	21.6	16.2	18.6	13.95	16.2	12.15
Sol. 8	21	15.75	19.8	14.85	13.2	9.9
Sol. 9	21	15.75	19.8	14.85	12.6	9.45
Sol. 10	21	15.75	19.8	14.85	12	9
Sol. 11	21	15.75	18.6	13.95	12	9
Sol. 12	21	15.75	17.4	13.05	12	9
Sol. 13	21	15.75	16.2	12.15	11.4	8.55
Sol. 14	20.4	15.3	16.2	12.15	12.6	9.45
Sol. 15	19.8	14.85	16.2	12.15	11.4	8.55
Sol. 16	19.2	14.4	16.8	12.6	10.8	8.1
Sol. 17	19.8	14.85	16.2	12.15	9.6	7.2
Sol. 18	18.6	13.95	16.8	12.6	9.6	7.2
Sol. 19	19.2	14.4	15	11.25	10.2	7.65
Sol. 20	17.4	13.05	16.2	12.15	10.2	7.65
Sol. 21	18	13.5	15	11.25	9.6	7.2
Sol. 22	17.4	13.05	14.4	10.8	10.2	7.65
Sol. 23	17.4	13.05	13.8	10.35	9	6.75
Sol. 24	16.8	12.6	13.8	10.35	8.4	6.3
Sol. 25	16.2	12.15	14.4	10.8	7.8	5.85
Sol. 26	16.2	12.15	12	9	9	6.75
Sol. 27	14.4	10.8	13.8	10.35	8.4	6.3
Sol. 28	15.6	11.7	12	9	7.8	5.85
Sol. 29	15	11.25	12	9	7.2	5.4
Sol. 30	14.4	10.8	10.8	8.1	7.8	5.85
Sol. 31	13.8	10.35	11.4	8.55	7.2	5.4
Sol. 32	13.2	9.9	11.4	8.55	6.6	4.95
Sol. 33	12.6	9.45	10.8	8.1	6.6	4.95
Sol. 34	11.4	8.55	11.4	8.55	6.6	4.95
Sol. 35	12	9	9.6	7.2	6	4.5

Table 7.8. Determined optimum design of modified R-CUBE manipulator.

	D (mm)	d (mm)	**Link Length** (mm)	**Composite** 0°	**Composite** 90°	**Composite** 45°	**Composite** -45°
l_1	15	11.25	111.7	4	7	7	7
l_2	12	9	74.1	2	6	6	6
l_3	7.2	5.4	121.8	2	6	2	2

Table 7.9. Estimated specs of modified R-CUBE mechanism

Workspace	$(120 \times 120 \times 120)$ mm^3
Footprint	< 120 mm^2 (Fully Folded) < 170 mm^2 (Fully Expanded)
DoF	3 Translation
Continious Force Output	> 5 N
Maximum Deflection	< 0.07 mm
Total Mass of Composite Links	77.7g

$$\|\hat{D}_C\|_f = (8.6888)10^6 \text{ N/(kg.m)} \tag{7.10}$$

$$e_1 = (2.1133)10^3 \, , \bar{m}_1 = \begin{bmatrix} 0.7071 & -0.7071 & 0 \end{bmatrix}^T \tag{7.11}$$

$$e_2 = (2.1133)10^3 \, , \bar{m}_2 = \begin{bmatrix} 0.4082 & 0.4082 & -0.8165 \end{bmatrix}^T \tag{7.12}$$

$$e_3 = (2.4427)10^3 \, , \bar{m}_3 = \begin{bmatrix} 0.5774 & 0.5774 & 0.5774 \end{bmatrix}^T \tag{7.13}$$

Computed performance metrics are illustrated on the planes which are located at $\bar{f}_p(-60)$, $\bar{f}_p(0)$, and $\bar{f}_p(60)$ where $\bar{f}_p$ is a function which defines the planes at given Cartesian space position with respect to home position.

In Figures 7.5, 7.6, and 7.7 manipulability index is illustrated depending on the pose of the manipulator. Figures 7.5 and 7.7 show the manipulability measure on the boundaries of the workspace. Since the boundaries are close to singular poses the values obtained on the boundaries are smaller than the given values in Figure 7.6 given in $\bar{f}_p(0)$. Also notice that the corners of the workspace in Figures 7.5 and 7.7 have the lowest values since all of the 3 axes are close to singularity simultaneously. On the other hand, in Figure 7.6, highest manipulability is located at the middle of the workspace. Therefore, this pose is the most manipulable pose.

Figures 7.8, 7.9, and 7.10 show the condition number performance. Notice that the highest performance for condition number is obtained in the middle of the workspace similar to the manipulability. The boundaries of the workspace given in Figures 7.8 and 7.10 is dominated by the worst values. However, unlike manipulability, the condition number performance increases at the corners of the workspace. This is observed since the active joint angles are close/same with each other. Even at the corners, if the active joint angles are equal the condition number is equal to 1 since the number computes the directional motion resolution ratio for a given pose.

Figures 7.11, 7.12, and 7.13 show the maximum positioning error in the workspace. Notice that, this metric is inversely related with the manipulability index. If the manipulator is highly manipulable for the given pose, it means that even with a small joint input

the mobile platform may experience high displacement. Even though this enhances the back-drivability, it also reduces the positioning resolution since a small amount of joint input is amplified. Hence, the highest value of the positioning is observed on the poses which are close to the singularity. In fact in singularity, even high joint inputs do not change the mobile platform position which makes it highly robust in positioning.

In Figures 7.14, 7.15, and 7.16, inertia index is computed as the determinant of generalized inertia matrix defined in Cartesian space. Unlike the above-mentioned figures, the trend of distribution of inertia matrix is nonlinear. Inertia index gets its maximum value on the boundaries where only one of the arms is fully folded and the other one is at home position which is shown in Figure 7.14. This effect is caused by the change in passive links. In these poses, passive links are close to singularity and almost folded on each other. However, the cause in a high output on inertia index is not the closeness to singularity but the rotational motion experienced by the passive links. If the manipulator is given motion in this pose, the rotation at the passive links is relatively higher. Since the linear motion of the mass centers is low, the inertial effect in pose is caused by the rotation. Hence, in Figure 7.16, this effect is not observed on fully expanded poses which are also close to the singularity. However, this effect instantly dies out when the mobile platform is moved from these poses as shown in Figure 7.15. Therefore, a smooth distribution of inertia is observed throughout the workspace.

Finally, Figures 7.17, 7.18, and 7.19 show the stiffness performance of the manipulator for the boundaries and the home position of the manipulator. In Figures 7.17, it can be clearly observed that the stiffest pose is when the manipulator is fully folded. The reason for this is because the moment arm with respect to active joints has its minimum value. Thus, applied external wrenches on the mobile platform cause small deflections in this pose. Similarly, in extended poses, as shown in Figure 7.19 the compliance has its highest value due to increased moment arm. Although, there is a high difference between the highest and lowest stiffness indices, the generality of the workspace exhibit smooth transitions in stiffness and this makes it easier to linearize the stiffness model to use it in control algorithm as shown in Figure 7.18.
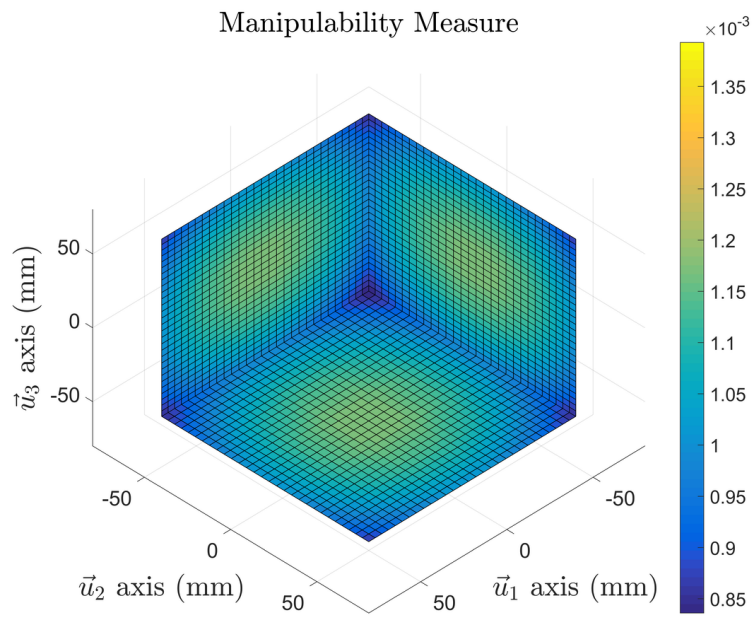
Figure 7.5. Manipulability index at $-60, -60, -60$.
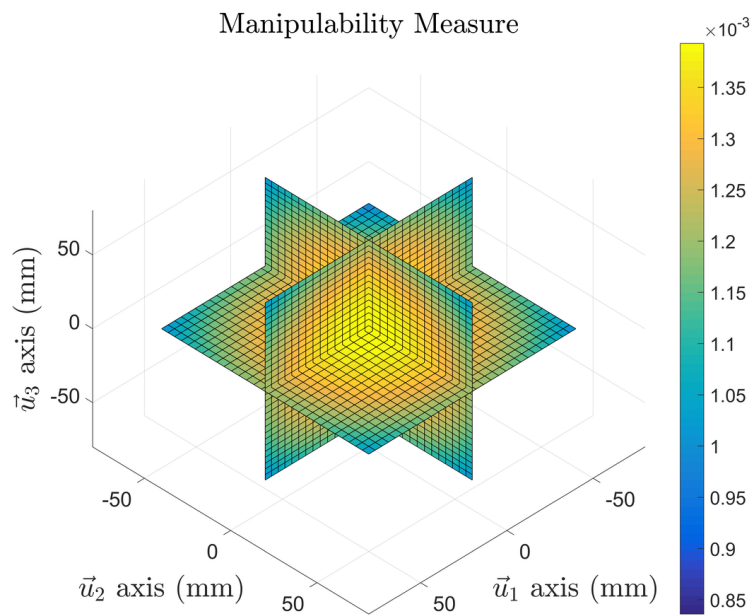

Figure 7.6. Manipulability index at $0, 0, 0$.
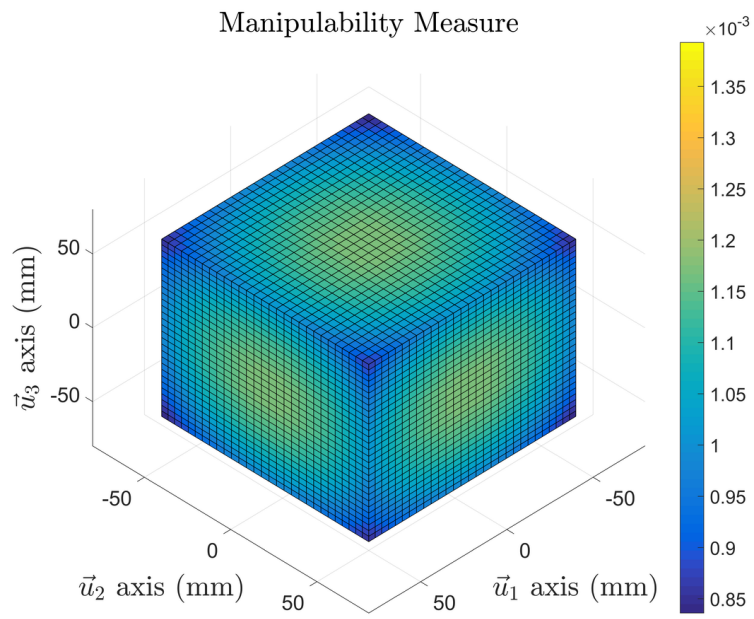
Figure 7.7. Manipulability index at $60, 60, 60$.
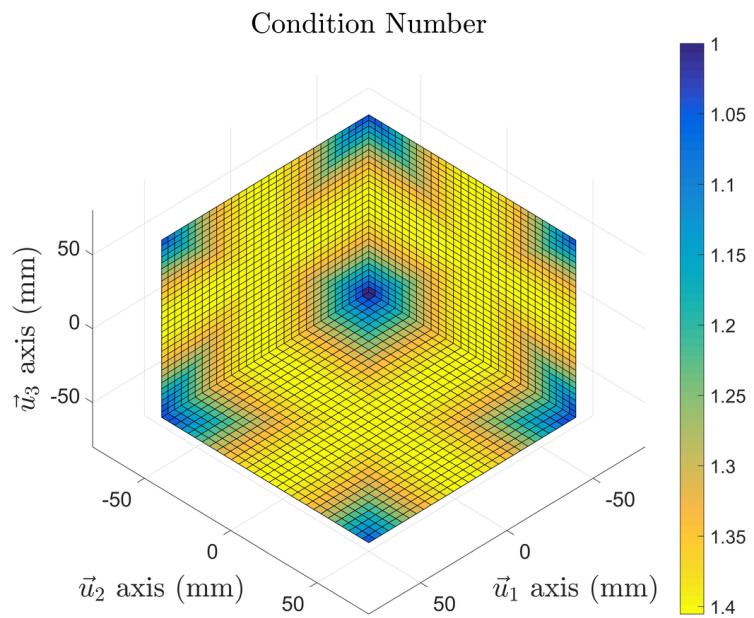
Figure 7.8. Condition number index at $-60, -60, -60$.
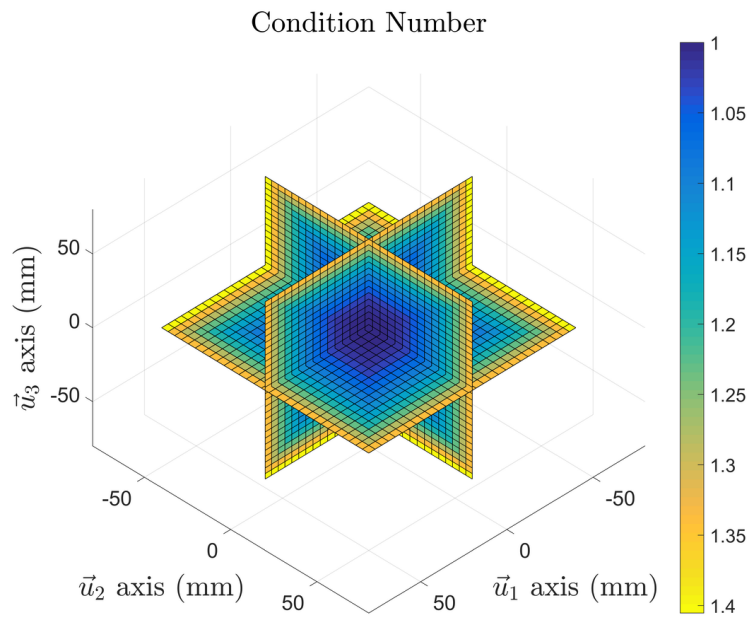
Figure 7.9. Condition number index at $0, 0, 0$.
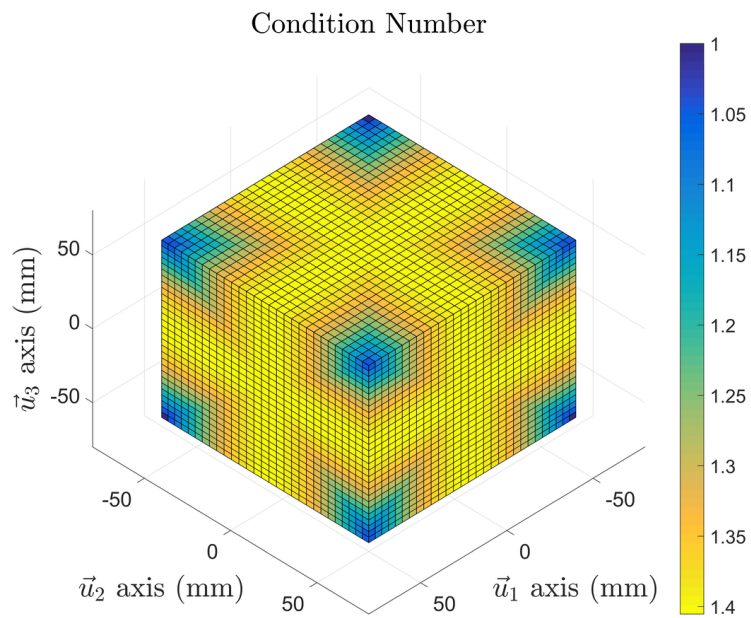

Figure 7.10. Condition number index at $60, 60, 60$.
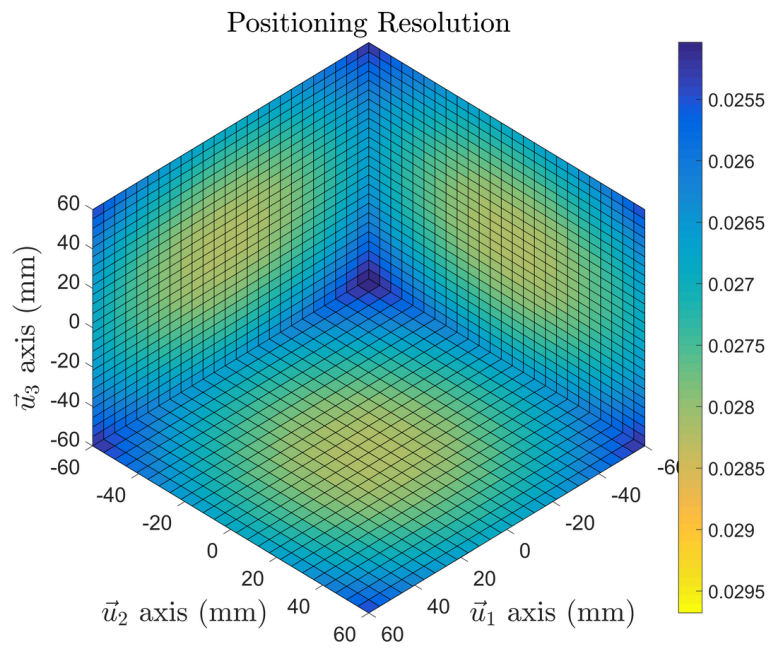
Figure 7.11. Positioning resolution at $-60, -60, -60$.
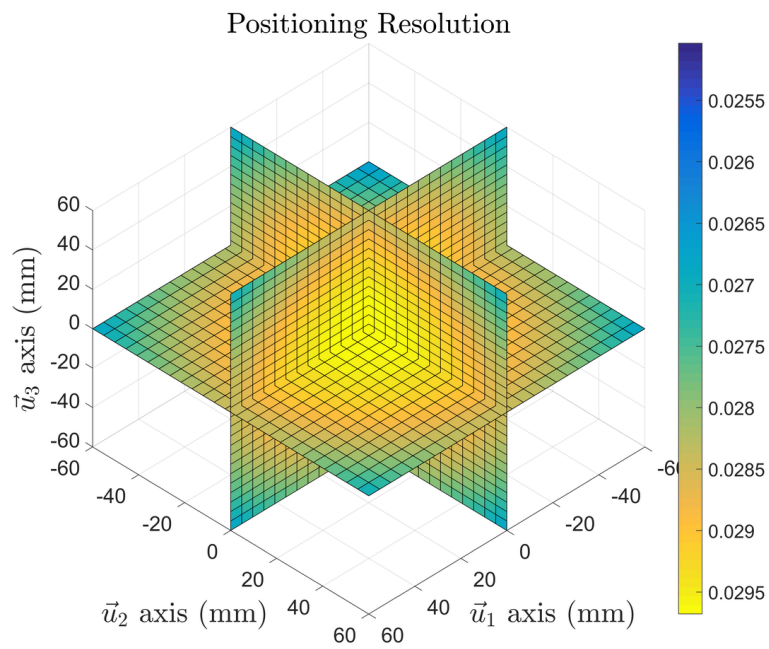

Figure 7.12. Positioning resolution at $0, 0, 0$.
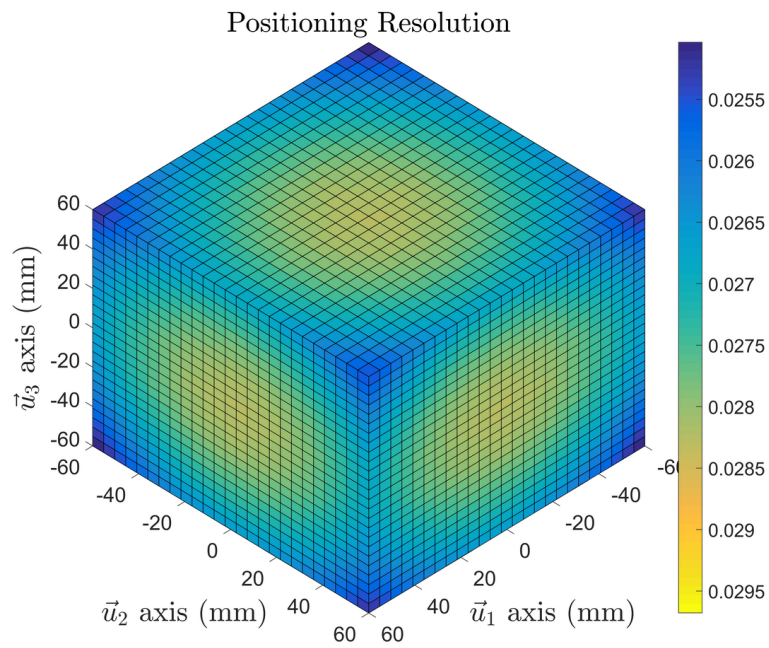
Figure 7.13. Positioning resolution at $60, 60, 60$.
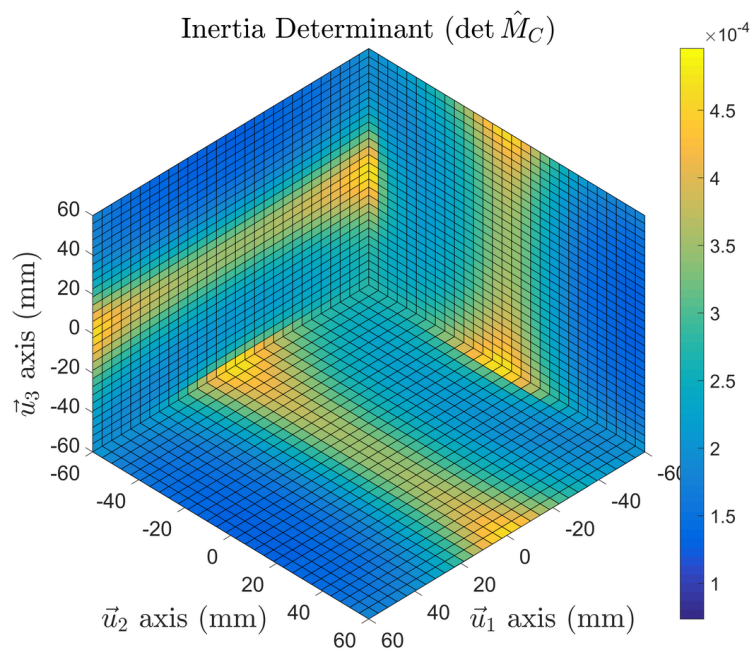
Figure 7.14. Inertia index at $-60, -60, -60$.
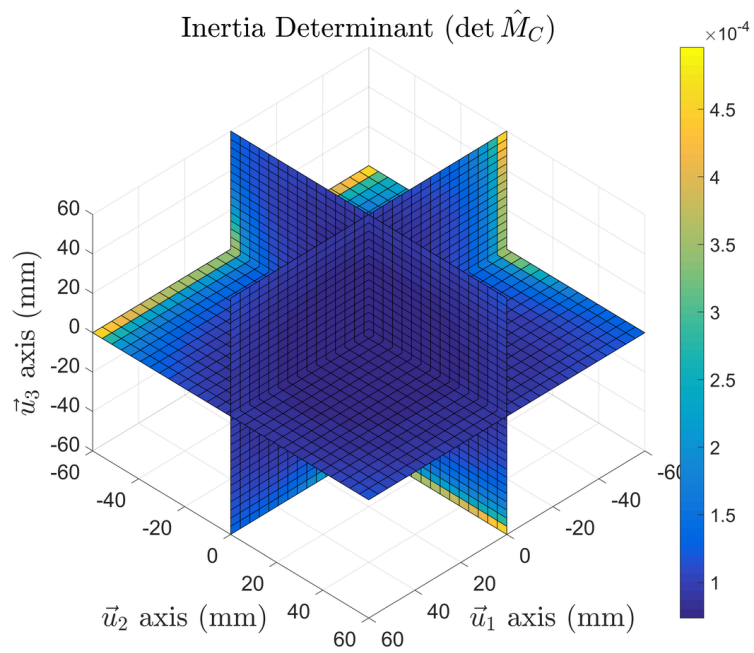
Figure 7.15. Inertia index at $0, 0, 0$.
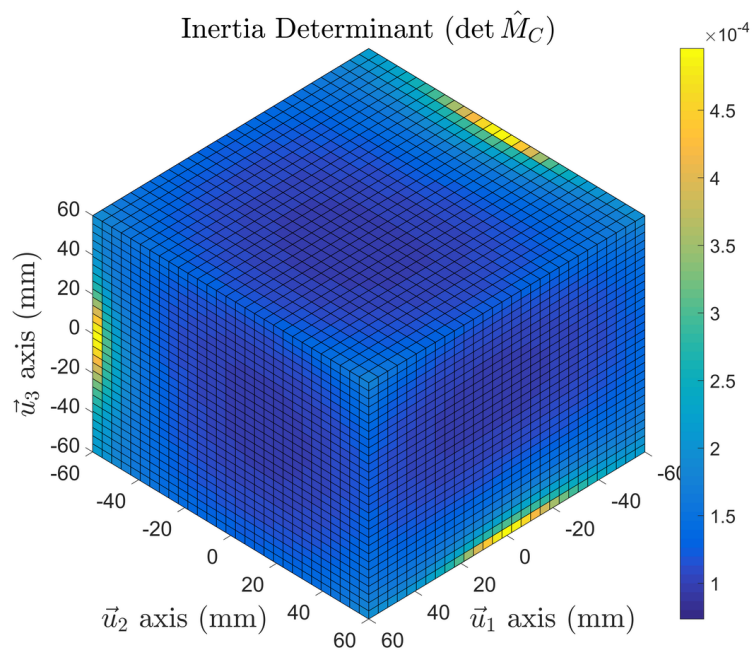


Figure 7.16. Inertia index at $60, 60, 60$.
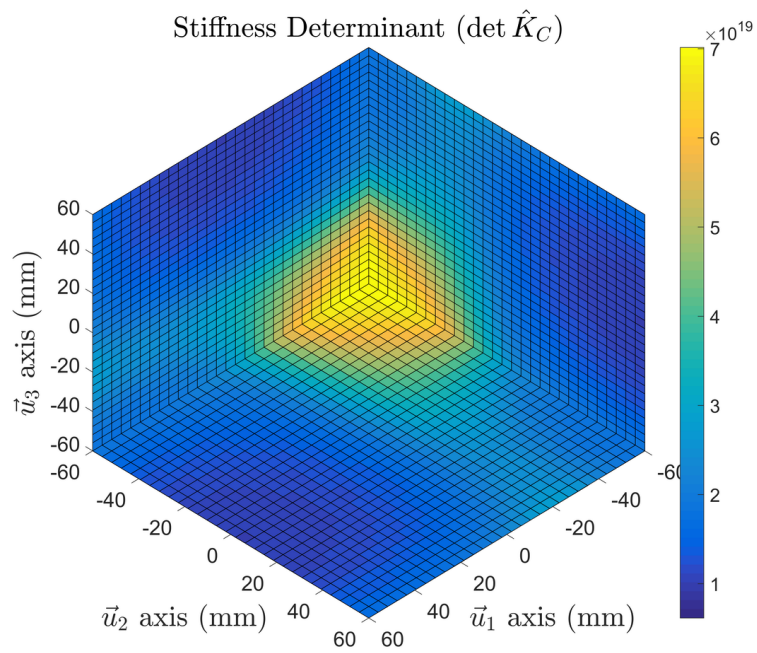
Figure 7.17. Stiffness index at $-60, -60, -60$.
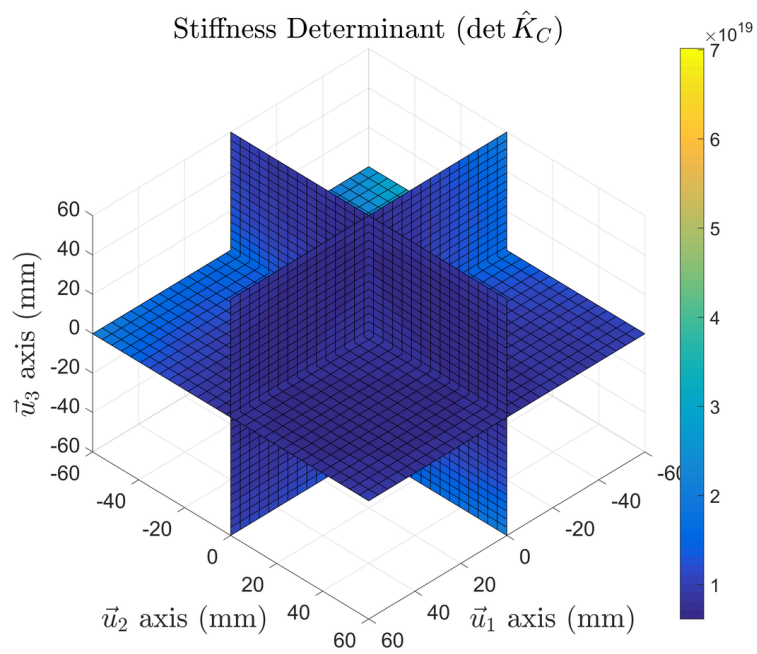
Figure 7.18. Stiffness index at $0, 0, 0$.
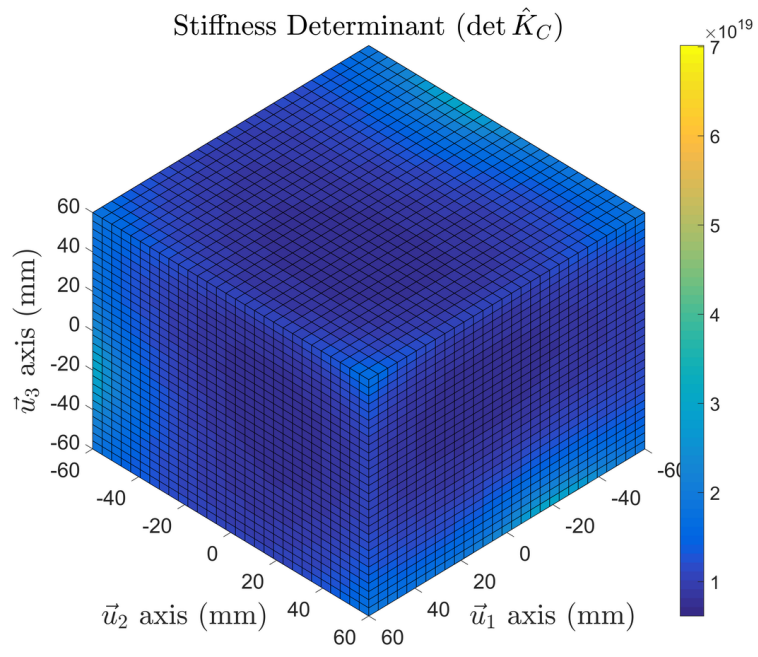
Figure 7.19. Stiffness index at $60, 60, 60$.

CHAPTER 8

CONCLUSION

In this thesis, multi-objective optimization of modified R-CUBE mechanism for haptic applications is conducted in order to enhance the impedance performance of the mechanism. First, the un-powered system properties are reviewed in order to reveal the design domains which are kinematics, stiffness, and dynamics. Next, a literature review is conducted to understand the design approach to haptic manipulators. In the literature, the majority of the researches have focused on kinematics oriented optimization. Although kinematics affects the dynamics and stiffness properties, the impedance performance of a haptic manipulator is not only dependent on kinematics but also on dynamics and stiffness and their relation is non-linear. Due to the non-linearity, evolutionary or artificial intelligence based solution algorithm is adopted by the researchers. However, they prefer to use weighted-sum approach to construct the objective functions. Nevertheless, this approach requires iterative solutions to adjust the weight of each objective function but the global optima are not guaranteed. In some studies, all performance metrics are used simultaneously by adopting multi-objective optimization methods with the Pareto-front approach. However, the number of these studies is relatively small. This thesis has focused on the use of multi-objective haptic manipulator design optimization by using genetic algorithm with the Pareto-front approach. A modified version of R-CUBE mechanism is used for optimization. Composite tubes are preferred for the links.

Initially, the performance metrics are reviewed and investigated to understand the relation between the metrics including their physical intuitions. First, velocity and force ellipsoids are investigated to procure the manipulability and condition number. It has been observed that condition number contributes to all performance indices regardless if it is kinematics, stiffness, or dynamics related. While the manipulability contributes to the dynamic performance as it increases, decreasing the value of it contributes to stiffness performance. Other performance metrics are derived by taking the determinant, Euclidean, and Frobenius norms of the stiffness and inertia matrices which are represented in Cartesian space. While the determinant is a scalar representation of the total magnitude of the matrices, Frobenius norm only deals with the trace of the matrices which is a fast and effective approach to evaluate the performance. Euclidean norm, on the other hand, measures the ratio of the directional quality of the matrices. A final evaluation is conducted

by making use of the dynamic matrix to obtain the natural frequencies. Since the natural frequency denotes the ratio of the stiffness to inertia, higher value implies the high impedance performance and also high-frequency range.

In order to construct the objective functions, first the forward and inverse kinematics are formulated. Then, Jacobian matrices are procured. Obtained model is validated by CAD programs. Next, the stiffness model is obtained by using the virtual joint method. The stiffness matrix is modified to construct the composite material based stiffness matrices. Since the orientations and the number of the plies of composite links affect the stiffness performance, these are also modeled and optimized. The model is verified by making use of ADAMS and ANSYS Workbench simulation environments. Finally, the dynamic model is obtained with Lagrange's method and verified in MATLAB Simulink.

After obtaining the models, the objective functions are constructed by making use of the performance metrics. The optimization is conducted by using the most critical poses of the manipulator in order to reduce the computation time. In the kinematic evaluation, the relation between the condition number and manipulability is discussed and it has been concluded that evaluation of only one of them is sufficient due to the symmetric structure of the manipulator. Next, kinematic constraints are introduced to the optimization procedure to prevent the singularity and achieve the ergonomy by hindering the collision of the user's body part with the links of the manipulator. A discussion on the evaluation of the stiffness matrix is conducted to simplify the performance metrics since the stiffness consumes relatively higher computation time and power compared to kinematics and dynamics performance metrics. Minimization of reaction forces/torques on virtual joints is preferred to enhance the stiffness performance. Finally, dynamics oriented performance metrics are procured and the determinant of generalized inertia matrix is evaluated. Since the enhancement in the performance of condition number also enhances the norm related performance metrics of stiffness and dynamics, these metrics are not evaluated. The performance metrics are included in the objective function such that the minimization of these functions enhances the performance of related metrics. Next, the objective functions to determine the best inner/outer diameter ratio, stiffness and dynamic oriented objective functions are constructed. The composite links are optimized to minimize the maximum deflection at the mobile platform by adjusting the number of plies and their orientations in each link, separately.

Finally, the optimization results are presented and discussed. Among the number of Pareto-front solution sets, 40 best results are given in the solution set. In order to compare the values of different performance metrics, computed metrics are normalized.

153

Since the main objective is to enhance the impedance performance, the result with the minimum link length is chosen which is $l_1 = 111.7$ mm, $l_2 = 74.1$ mm, and $l_3 = 121.8$ mm with the maximum deviation angle for 32.5^o from home position. The best ratio of the inner diameter to outer diameter is obtained as 0.768. Finally, the composite link design is chosen where the maximum estimated mobile platform deflection is less than 0.07 mm. After that, the evaluation of the manipulator is conducted for the obtained design parameters. The generalized inertia and stiffness matrices are denoted in Cartesian space and computed for home position. Next, the dynamic matrix is procured and modal vectors and eigenvalues are computed. Finally, the graphical illustration of the performance metrics is shown. It is shown that a uniform distribution in stiffness and inertia within the workspace is achieved which is crucial for equal impedance distribution to feel the equal amount of forces in an arbitrary pose of the manipulator.

As a future work, sensitivity of the manipulator should be investigated for possible dimensional errors which may occur in manufacturing process. This post process is crucial to ensure that the manufactured links does not cause any self collision or singularity. Later, the stiffness model may be updated by including the joint and connection elements such as bearings. Since the shapes of the connection elements may not be represented with analytical formulations, finite element method may be used to enhance the accuracy of the virtual joint method.

REFERENCES

3D SYSTEMS, P. O. (2018). https://www.3dsystems.com/haptics-devices/.

Agboh, W. C., M. Yalcin, and V. Patoglu (2016). A six degrees of freedom haptic interface for laparoscopic training. In *Intelligent Robots and Systems (IROS), 2016 IEEE/RSJ International Conference on*, pp. 1107–1112. IEEE.

Ahmad, A., K. Andersson, and U. Sellgren (2014). A model-based and simulation-driven methodology for design of haptic devices. *Mechatronics 24*(7), 805–818.

Alici, G. and B. Shirinzadeh (2005). Enhanced stiffness modeling, identification and characterization for robot manipulators. *IEEE transactions on robotics 21*(4), 554–564.

Angeles, J. (2002). *Fundamentals of robotic mechanical systems*, Volume 2. Springer.

Arata, J., H. Kondo, N. Ikedo, and H. Fujimoto (2011). Haptic device using a newly developed redundant parallel mechanism. *IEEE Transactions on robotics 27*(2), 201–214.

Asada, H. (1983). A geometrical representation of manipulator dynamics and its application to arm design. *Journal of dynamic systems, measurement, and control 105*(3), 131–142.

Banala, S. K., S. H. Kim, S. K. Agrawal, and J. P. Scholz (2009). Robot assisted gait training with active leg exoskeleton (alex). *IEEE transactions on neural systems and rehabilitation engineering 17*(1), 2–8.

Barbosa, M. R., E. S. Pires, and A. M. Lopes (2005). Design optimization of a parallel manipulator based on evolutionary algorithms.

Bilgincan, T., E. Gezgin, and M. I. C. Dede (2010). Integration of the hybrid-structure haptic interface: Hiphad v1. 0. In *Proceedings of the International Symposium of Mechanism and Machine Theory*, pp. 18.

Birglen, L., C. Gosselin, N. Pouliot, B. Monsarrat, and T. Laliberté (2002). Shade, a new 3-dof haptic device. *IEEE Transactions on Robotics and Automation 18*(2), 166–175.

Borro, D., J. Savall, A. Amundarain, J. J. Gil, A. Garcia-Alonso, and L. Matey (2004). A large haptic device for aircraft engine maintainability. *IEEE Computer Graphics and Applications 24*(6), 70–74.

Carbone, G. and M. Ceccarelli (2010). Comparison of indices for stiffness performance evaluation. *Frontiers of Mechanical Engineering in China 5*(3), 270–278.

Chablat, D. and P. Wenger (2006). A six degree-of-freedom haptic device based on the

orthoglide and a hybrid agile eye. In *ASME 2006 International Design Engineering Technical Conferences and Computers and Information in Engineering Conference*, pp. 795–802. American Society of Mechanical Engineers.

Chiu, S. L. (1988). Kinematic characterization of manipulators: an approach to defining optimality. In *Robotics and Automation, 1988. Proceedings., 1988 IEEE International Conference on*, pp. 828–833. IEEE.

Ciblak, N. and H. Lipkin (1999). Synthesis of cartesian stiffness for robotic applications. In *Robotics and Automation, 1999. Proceedings. 1999 IEEE International Conference on*, Volume 3, pp. 2147–2152. IEEE.

Colgate, J. E. and J. M. Brown (1994). Factors affecting the z-width of a haptic display. In *Robotics and Automation, 1994. Proceedings., 1994 IEEE International Conference on*, pp. 3205–3210. IEEE.

Connor, J. J. (1976). *Analysis of structural member systems*. Ronald Press Co.

Dimensions, F. (2018). Haptic device, http://www.forcedimension.com.

Duffy, J. (2007). *Statics and kinematics with applications to robotics*. Cambridge University Press.

El Saddik, A. (2007). The potential of haptics technologies. *IEEE Instrumentation & Measurement Magazine 10*(1), 10–17.

Ergin, M. A. and A. Peer (2013). Development of a new 6 dof parallel haptic interface for the rendering of elements and interior equipment in a car. In *RO-MAN, 2013 IEEE*, pp. 238–244. IEEE.

Ergin, M. A., A. C. Satici, and V. Patoglu (2011). Design optimization, impedance control and characterization of a modified delta robot. In *Mechatronics (ICM), 2011 IEEE International Conference on*, pp. 737–742. IEEE.

Faulring, E. L., J. E. Colgate, and M. A. Peshkin (2006). The cobotic hand controller: design, control and performance of a novel haptic display. *The International Journal of Robotics Research 25*(11), 1099–1119.

Frisoli, A., F. Rocchi, S. Marcheschi, A. Dettori, F. Salsedo, and M. Bergamasco (2005). A new force-feedback arm exoskeleton for haptic interaction in virtual environments. In *Eurohaptics Conference, 2005 and Symposium on Haptic Interfaces for Virtual Environment and Teleoperator Systems, 2005. World Haptics 2005. First Joint*, pp. 195–201. IEEE.

Gao, Z., D. Zhang, and Y. Ge (2010). Design optimization of a spatial six degree-of-freedom parallel manipulator based on artificial intelligence approaches. *Robotics and Computer-Integrated Manufacturing 26*(2), 180–189.

Gosselin, C. (1990). Stiffness mapping for parallel manipulators. *IEEE Transactions on*

Robotics and Automation 6(3), 377–382.

Gosselin, C. (2002). Stiffness analysis of parallel mechanisms using a lumped model. *Int. J. Robotics Automat. 17*, 17–27.

Gosselin, C. and J. Angeles (1991). A global performance index for the kinematic optimization of robotic manipulators. *Journal of Mechanical design 113*(3), 220–226.

Gosselin, F., C. Bidard, and J. Brisset (2005). Design of a high fidelity haptic device for telesurgery. In *Robotics and Automation, 2005. ICRA 2005. Proceedings of the 2005 IEEE International Conference on*, pp. 205–210. IEEE.

Gosselin, F., J.-P. Martins, C. Bidard, C. Andriot, and J. Brisset (2005). Design of a new parallel haptic device for desktop applications. In *Eurohaptics Conference, 2005 and Symposium on Haptic Interfaces for Virtual Environment and Teleoperator Systems, 2005. World Haptics 2005. First Joint*, pp. 189–194. IEEE.

Graettinger, T. J. and B. H. Krogh (1988). The acceleration radius: a global performance measure for robotic manipulators. *IEEE Journal on Robotics and Automation 4*(1), 60–69.

Griffis, M. and J. Duffy (1993). Global stiffness modeling of a class of simple compliant couplings. *Mechanism and machine theory 28*(2), 207–224.

Haption (2018). Haptic devices, https://www.haption.com.

Howard, S., M. Zefran, and V. Kumar (1998). On the 6×6 cartesian stiffness matrix for three-dimensional motions. *Mechanism and machine theory 33*(4), 389–408.

Huang, C., W.-H. Hung, and I. Kao (2002). New conservative stiffness mapping for the stewart-gough platform. In *Robotics and Automation, 2002. Proceedings. ICRA'02. IEEE International Conference on*, Volume 1, pp. 823–828. IEEE.

Hung, V. M. and U. J. Na (2011). Optimal design of a new 6-dof haptic device. In *Control, Automation and Systems (ICCAS), 2011 11th International Conference on*, pp. 849–852. IEEE.

Iwata, H. (1993). Pen-based haptic virtual environment. In *Virtual Reality Annual International Symposium, 1993., 1993 IEEE*, pp. 287–292. IEEE.

Jones, R. M. (1975). *Mechanics of composite materials*, Volume 193. Scripta Book Company Washington, DC.

Kang, S. G., H. Iqbal, and D. Y. Lee (2012). Multi-criteria optimization of the 4 links of an 8 dof haptic master device for a surgical robot. In *Control, Automation and Systems (ICCAS), 2012 12th International Conference on*, pp. 1756–1761. IEEE.

Kern, T. A. (2009). *Engineering haptic devices: a beginner's guide for engineers*. Springer Publishing Company, Incorporated.

Khan, S., A. Ahmad, and K. Andersson (2011). Design optimization of the tau haptic device. In *Ultra Modern Telecommunications and Control Systems and Workshops (ICUMT), 2011 3rd International Congress on*, pp. 1–8. IEEE.

Khan, W. A. and J. Angeles (2006). The kinetostatic optimization of robotic manipulators: the inverse and the direct problems. *Journal of mechanical design 128*(1), 168–178.

Khatib, O. and J. Burdick (1987). Optimization of dynamics in manipulator design: The operational space formulation. *INT. J. ROBOTICS AUTOM. 2*(2), 90–98.

Kim, J.-O. and K. Khosla (1991). Dexterity measures for design and control of manipulators. In *Intelligent Robots and Systems' 91.'Intelligence for Mechanical Systems, Proceedings IROS'91. IEEE/RSJ International Workshop on*, pp. 758–763. IEEE.

Klimchik, A. (2011). *Enhanced stiffness modeling of serial and parallel manipulators for robotic-based processing of high performance materials*. Ph. D. thesis, Ecole Centrale de Nantes (ECN); Ecole des Mines de Nantes.

Kövecses, J. and J. Angeles (2007). The stiffness matrix in elastically articulated rigid-body systems. *Multibody System Dynamics 18*(2), 169–184.

Kumar, A. and K. Waldron (1981). The workspaces of a mechanical manipulator. *Journal of Mechanical Design 103*(3), 665–672.

Lab, D. H. (2018). Haptic master, http://www.delfthapticslab.nl/device/hapticmaster/.

Lambert, P. and J. Herder (2015). A novel parallel haptic device with 7 degrees of freedom. In *World Haptics Conference (WHC), 2015 IEEE*, pp. 183–188. IEEE.

Lee, J. H., K. S. Eom, and I. I. Suh (2001). Design of a new 6-dof parallel haptic device. In *Robotics and Automation, 2001. Proceedings 2001 ICRA. IEEE International Conference on*, Volume 1, pp. 886–891. IEEE.

Lee, S. S. and J. M. Lee (2003). Design of a general purpose 6-dof haptic interface. *Mechatronics 13*(7), 697–722.

Lee, S.-U. and S. Kim (2006). Analysis and optimal design of a new 6 dof parallel type haptic device. In *Intelligent Robots and Systems, 2006 IEEE/RSJ International Conference on*, pp. 460–465. IEEE.

Li, W., F. Gao, and J. Zhang (2005). R-cube, a decoupled parallel manipulator only with revolute joints. *Mechanism and Machine Theory 40*(4), 467–473.

Li, Y., Z. Yan, H. Wang, Z. Du, and Y. Zhang (2012). Design and optimization of a haptic manipulator using series-parallel mechanism. In *Mechatronics and Automation (ICMA), 2012 International Conference on*, pp. 2140–2145. IEEE.

Lopes, A. M., E. S. Pires, and M. R. Barbosa (2012). Design of a parallel robotic ma-

nipulator using evolutionary computing. *International Journal of Advanced Robotic Systems 9*(1), 27.

López M., J., J. M. Breñosa Martínez, I. Galiana Bujanda, M. Ferre Pérez, A. Giménez Fernández, and J. Barrio Gragera (2012). Mechanical design optimization for multi-finger haptic devices applied to virtual grasping manipulation. *Strojniki vestnik-Journal of Mechanical Engineering 58*(7-8), 431–443.

Majou, F., C. Gosselin, P. Wenger, and D. Chablat (2007). Parametric stiffness analysis of the orthoglide. *Mechanism and Machine Theory 42*(3), 296–311.

Martin, H. C. (1966). *Introduction to matrix methods of structural analysis*. McGraw-Hill.

Merlet, J.-P. (2006). *Parallel robots*, Volume 128. Springer Science and Business Media.

MPB, T. (2018). Haptic interfaces, http://www.mpb-technologies.ca.

Novint, F. (2011). Haptic device.

Pashkevich, A., D. Chablat, and P. Wenger (2009). Stiffness analysis of overconstrained parallel manipulators. *Mechanism and Machine Theory 44*(5), 966–982.

Pashkevich, A., A. Klimchik, and D. Chablat (2011). Enhanced stiffness modeling of manipulators with passive joints. *Mechanism and machine theory 46*(5), 662–679.

Patel, Y. and P. George (2012). Parallel manipulators applications—a survey. *Modern Mechanical Engineering 2*(03), 57.

Paul, R. P. and C. N. Stevenson (1983). Kinematics of robot wrists. *The International journal of robotics research 2*(1), 31–38.

Peng, L., Z.-G. Hou, L. Peng, and W. Wang (2015). Design of casia-arm: A novel rehabilitation robot for upper limbs. In *Intelligent Robots and Systems (IROS), 2015 IEEE/RSJ International Conference on*, pp. 5611–5616. IEEE.

Qin, H., A. Song, Y. Liu, G. Jiang, and B. Zhou (2015). Design and calibration of a new 6 dof haptic device. *Sensors 15*(12), 31293–31313.

QUANSER (2018). Parallel haptic device, https://www.quanser.com/products/hd2-high-definition-haptic-device/.

Sabater, J. M., J. M. Azorin, R. Aracil, and R. J. Saltaren (2005). Magister-p; a 6-urs parallel haptic device with open control architecture. *Robotica 23*(2), 177–187.

Sabater, J. M., R. J. Saltarén, and R. Aracil (2004). Design, modelling and implementation of a 6 urs parallel haptic device. *Robotics and Autonomous Systems 47*(1), 1–10.

Salcudean, S. and L. Stocco (2000). Isotropy and actuator optimization in haptic interface design. In *Robotics and Automation, 2000. Proceedings. ICRA'00. IEEE International Conference on*, Volume 1, pp. 763–769. IEEE.

Salisbury, J. K. (1980). Active stiffness control of a manipulator in cartesian coordinates. In *Decision and Control including the Symposium on Adaptive Processes, 1980 19th IEEE Conference on*, Volume 19, pp. 95–100. IEEE.

Salisbury, J. K. and J. J. Craig (1982). Articulated hands: Force control and kinematic issues. *The International journal of Robotics research 1*(1), 4–17.

Samur, E. (2012). *Performance metrics for haptic interfaces*. Springer Science & Business Media.

Stocco, L., S. Salcudean, and F. Sassani (1998). Matrix normalization for optimal robot design. In *Robotics and Automation, 1998. Proceedings. 1998 IEEE International Conference on*, Volume 2, pp. 1346–1351. IEEE.

Stocco, L. J., S. E. Salcudean, and F. Sassani (2001). Optimal kinematic design of a haptic pen. *IEEE/ASME Transactions on Mechatronics 6*(3), 210–220.

Systems, C. (2018). Haptic device, http://www.cyberglovesystems.com/.

Taner, B. and M. I. C. Dede (2017). Image processing based stiffness mapping of a haptic device. In *New Advances in Mechanisms, Mechanical Transmissions and Robotics*, pp. 447–454. Springer.

Tsumaki, Y., H. Naruse, D. N. Nenchev, and M. Uchiyama (1998). Design of a compact 6-dof haptic interface. In *Robotics and Automation, 1998. Proceedings. 1998 IEEE International Conference on*, Volume 3, pp. 2580–2585. IEEE.

Ueberle, M. and M. Buss (2002). Design, control, and evaluation of a new 6 dof haptic device. In *Intelligent Robots and Systems, 2002. IEEE/RSJ International Conference on*, Volume 3, pp. 2949–2954. IEEE.

Ueberle, M., N. Mock, and M. Buss (2004). Vishard10, a novel hyper-redundant haptic interface. In *Haptic Interfaces for Virtual Environment and Teleoperator Systems, 2004. HAPTICS'04. Proceedings. 12th International Symposium on*, pp. 58–65. IEEE.

Unal, R., G. Kiziltas, and V. Patoglu (2008). A multi-criteria design optimization framework for haptic interfaces. In *Haptic interfaces for virtual environment and teleoperator systems, 2008. haptics 2008. symposium on*, pp. 231–238. IEEE.

Unal, R. and V. Patoglu (2008). Optimal dimensional synthesis of a dual purpose haptic exoskeleton. In *International Conference on Human Haptic Sensing and Touch Enabled Computer Applications*, pp. 529–535. Springer.

Vulliez, M. and S. Zeghloul (2016). Multi-objective design optimization of the delthap-

tic, a new 6-dof haptic device. In *Industrial Informatics (INDIN), 2016 IEEE 14th International Conference on*, pp. 248–253. IEEE.

Wagner, C. R., S. J. Lederman, and R. D. Howe (2002). A tactile shape display using rc servomotors. In *Haptic Interfaces for Virtual Environment and Teleoperator Systems, 2002. HAPTICS 2002. Proceedings. 10th Symposium on*, pp. 354–355. IEEE.

Winfield, L., J. Glassmire, J. E. Colgate, and M. Peshkin (2007). T-pad: Tactile pattern display through variable friction reduction. In *EuroHaptics Conference, 2007 and Symposium on Haptic Interfaces for Virtual Environment and Teleoperator Systems. World Haptics 2007. Second Joint*, pp. 421–426. IEEE.

Yoon, J. and J. Ryu (2001). Design, fabrication, and evaluation of a new haptic device using a parallel mechanism. *IEEE/ASME Transactions on mechatronics 6*(3), 221–233.

Yoon, J. W., J. Ryu, and Y.-K. Hwang (2010). Optimum design of 6-dof parallel manipulator with translational/rotational workspaces for haptic device application. *Journal of mechanical science and technology 24*(5), 1151–1162.

Yoshikawa, T. (1985a). Dynamic manipulability of robot manipulators. In *Robotics and Automation. Proceedings. 1985 IEEE International Conference on*, Volume 2, pp. 1033–1038. IEEE.

Yoshikawa, T. (1985b). Manipulability and redundancy control of robotic mechanisms. In *Robotics and Automation. Proceedings. 1985 IEEE International Conference on*, Volume 2, pp. 1004–1009. IEEE.

Zhao, C., X. Luo, F. Ma, and H. Zhang (2011). Transparency design of a new haptic interface. In *Electrical and Control Engineering (ICECE), 2011 International Conference on*, pp. 6193–6197. IEEE.

Zoss, A. B., H. Kazerooni, and A. Chu (2006). Biomechanical design of the berkeley lower extremity exoskeleton (bleex). *IEEE/ASME Transactions On Mechatronics 11*(2), 128–138.

APPENDIX A

6K M55J COMPOSITE MATERIAL DATA SHEET

TORAYCA®
M55J DATA SHEET

MJ type high modulus fiber with enhanced tensile and compressive strength over **M** series fibers. Mainly used for premium sporting goods, aerospace, and industrial applications.

FIBER PROPERTIES

	English	Metric	Test Method
Tensile Strength	583 ksi	4,020 MPa	TY-030B-01
Tensile Modulus	78.2 Msi	540 GPa	TY-030B-01
Strain	0.8 %	0.8 %	TY-030B-01
Density	0.069 lbs/in^3	1.91 g/cm^3	TY-030B-02
Filament Diameter	2.0E-04 in.	5 µm	
Yield 6K	6,833 ft/lbs	218 g/1000m	TY-030B-03
Sizing Type 50B & Amount		1.0 %	TY-030B-05
Twist	Untwisted		

FUNCTIONAL PROPERTIES

CTE	-1.1 α·10^{-6}/°C	
Specific Heat	0.17 Cal/g·°C	
Thermal Conductivity	0.372 Cal/cm·s·°C	
Electric Resistivity	0.8 x 10^{-3} Ω·cm	
Chemical Composition: Carbon	>99 %	
Na + K	<50 ppm	

COMPOSITE PROPERTIES *

	English	Metric	
Tensile Strength	290 ksi	2,010 MPa	ASTM D-3039
Tensile Modulus	49.0 Msi	340 GPa	ASTM D-3039
Tensile Strain	0.6 %	0.6 %	ASTM D-3039
Compressive Strength	130 ksi	880 MPa	ASTM D-695
Flexural Strength	180 ksi	1,230 MPa	ASTM D-790
Flexural Modulus	40.5 Msi	280 GPa	ASTM D-790
ILSS	10.0 ksi	7 kgf/mm^2	ASTM D-2344
90° Tensile Strength	5.0 ksi	34 MPa	ASTM D-3039

* Toray 250°F Epoxy Resin. Normalized to 60% fiber volume.

TORAY CARBON FIBERS AMERICA, INC.

162